UC Berkeley
Research Reports

Title
Methods to Address Headlight Glare

Permalink

Authors
Christianson, Kent B.
Greenhouse, Daniel S.
Barton, Joseph E.
et al.

Publication Date
2009-03-01

Methods to Address Headlight Glare

Kent B. Christianson, Daniel S. Greenhouse,
Joseph E. Barton, Christina Chow
University of California, Berkeley

This work was performed as part of the California PATH Program of the University of California, in cooperation with the State of California Business, Transportation, and Housing Agency, Department of Transportation, and the United States Department of Transportation, Federal Highway Administration.

The contents of this report reflect the views of the authors who are responsible for the facts and the accuracy of the data presented herein. The contents do not necessarily reflect the official views or policies of the State of California. This report does not constitute a standard, specification, or regulation.

Final Report for Task Order 6603

CALIFORNIA PARTNERS FOR ADVANCED TRANSIT AND HIGHWAYS

Final Report

Methods to Address Headlight Glare

Prepared for

California PATH

TO#6603

by

Visual Detection Laboratory
University of California, Berkeley
360 Minor Hall
Berkeley, CA 94720

Kent B. Christianson
Daniel S. Greenhouse
Joseph E. Barton
Christina Chow

February 27, 2008

Methods to Address Headlight Glare
California PATH Task Order 6603
Final Report

I. Abstract

The goal of this project was to design, implement, and validate a computerized Glare Meter Tool that could be used in the field to assess the level of glare from headlights of opposing vehicles in a variety of situations, without relying on subjective reports of observers. Both disability glare and discomfort glare were addressed. The net result is an instrument that is capable of acquiring an image of a scene with glare, then analyzing the image to output a number on the standard, widely-used De Boer Rating Scale for Evaluation of Discomfort Glare, and also an equivalent veiling luminance that can be used to assess the level of disability glare. The Glare Meter Tool has been demonstrated to provide accurate results in both laboratory and field experiments, but at the current level of development, its practical use in the field is compromised by dynamic range limitations and exposure time requirements.

Keywords:

headlight glare, discomfort glare, disability glare, De Boer scale, equivalent veiling luminance

II. Executive Summary

Glare from headlights of opposing vehicles is a frequent problem in nighttime driving, and in some instances can reduce visibility or cause distraction to the extent that an accident can occur. Glare can be classified into two general categories, disability glare and discomfort glare.

Disability glare is caused by scattering of light within the optical media of the eye. This reduces overall contrast and can be characterized by an equivalent veiling luminance which adds to, and is superimposed upon, the scene. The magnitude of the equivalent veiling luminance is a function of several factors, including the intensity of the glare source, the angular distance between the glare source and the visual target of interest, and the age of the observer. Disability glare can be measured experimentally in a particular scenario by determining the contrast thresholds for a visual task, with and without the presence of glare.

Discomfort glare, on the other hand, is a subjective response of the observer, and can occur independently of the reduction in task performance associated with disability glare. The mechanism of discomfort glare is still undetermined but some researchers believe that a physiological correlate is facial muscle tension in the vicinity of the eyes. It is also claimed by some researchers that discomfort glare is related to the scotopic luminosity function of the visual system, and thus might be mediated by rods. The magnitude of discomfort glare is often specified on the De Boer Rating Scale for Evaluation of Discomfort Glare, in which a number is specified from 1 ("unbearable") to 9 ("unnoticeable").

The general consensus among researchers is that disability glare is the more important factor in traffic safety, since task performance (i.e. driving) can be directly affected, while pure discomfort glare results only in annoyance to the driver. Of course many glare sources, including headlights from an opposing vehicle, will result in both kinds of glare.

The Visual Detection Laboratory at UC Berkeley has developed an objective glare measurement device with which we can measure the disability glare and discomfort glare levels that will be experienced by a driver in nighttime driving. This Glare Meter Tool is based on images acquired by a full-color video photometer. The images are analyzed by two separate computer programs, one for disability glare and one for discomfort glare.

The disability glare program performs a pixel by pixel analysis, determining each pixel's contribution to the equivalent veiling luminance on the basis of the standard Vos equation and then summing the results. We tested and validated the Glare Meter Tool in a series of laboratory experiments in which observers performed an increment threshold task. The observer gradually increased the contrast of a disc presented within a small, black annulus in the center of a large gray background until he or she could just see the disc with respect to the annulus. We had observers perform this task with and without the presence of glare, which we introduced by use of a high-intensity white LED placed in front of the computer screen. We could measure the contrast threshold under various conditions of eccentricity and/or intensity of the glare source (LED). We performed this experiment for observers over a wide range of ages. We then showed that the equivalent veiling luminance predicted by the Glare Meter Tool was in agreement with the experimentally determined number.

In the case of discomfort glare, we again analyzed the image, this time to implement the method of Vos and Baer to estimate a Discomfort Glare Index score, then using a conversion described by Vos to estimate the equivalent score on the De Boer scale. The results of this computer analysis were found to agree with the scores given by observers in a series of laboratory experiments in which we presented photographs of nighttime driving scenes on a computer monitor while presenting varying intensities and locations of glare from an LED (simulating the headlights of an opposing vehicle). Having tested and validated the Glare Meter Tool in the laboratory we then ran some field tests in which observers rated glare from headlights of an actual opposing (stationary) vehicle under various conditions of intensity of the headlights, ambient illumination (mainline lighting), presence or absence of a glare screen, and condition of the windshield of the observer's (stationary) vehicle. Again, the scores produced objectively by the Glare Meter Tool closely matched the subjective scores of the observers.

Thus we have successfully developed an objective Glare Meter Tool that can acquire an image of a scene in which glare is present and estimate the equivalent veiling luminance of disability glare and the severity of discomfort glare. However, while the Glare Meter Tool functions well in principle, the prototype has proven impractical in the field for a number of reasons. While the video photometer we employed is the most advanced and capable currently on the market, it still has insufficient dynamic range to encompass in a *single* exposure the wide range of luminance found in typical nighttime scenes in which glare from headlights is present. This then results in the need to make multiple exposures and then combine the results in order to avoid saturation from intense sources and/or quantization noise for the darker objects in the scene. In addition,

some exposures require very lengthy acquisition times. Finally, optical scattering within the optics of the photometer itself, along with pattern recognition difficulties in the case of multiple glare sources, results in the requirement of some special image processing techniques that would need further development in order to be applicable to a wide variety of field situations. The result is that the Glare Meter Tool, at its present stage of development, can only be used for static scenes, and requires a labor-intensive and time-consuming amount of image processing, thus limiting its utility. It is believed, however, that with advances in video photometry and additional software evolution, an instrument can be produced that allows development of a Glare Meter Tool that is practical for field use. We are nevertheless very pleased to have taken this important initial step toward that goal.

Table of Contents

Note on Figures and Tables

Many of the figures in this report contain important color information which is not reproduced in the printed version of this document. To view the figures in color, please see the PDF format available online.

Figures, tables, and equations are numbered consecutively starting with 1 within each major section or appendix heading, except in Appendix A (Literature Review) where the original captions are reproduced.

III. Introduction

Headlight glare is a significant safety problem, both in reality and perception, and has been the subject of a considerable body of research (for a thorough review of the literature, see Appendix A). Glare is caused by scenes in the visual world that contain relatively small luminous elements with high photometric intensity compared to their surroundings. Through logbooks and focus groups, researchers have found that 29% of older drivers perceive headlight glare as their primary nighttime driving concern[1]. This will continue to be a problem, as the number of elderly drivers continues to increase: In 1991, 45% of males eighty-five and over were licensed to drive. By 2000, 78% in this age group had a license. Similarly, the percentage of females eighty-five and over who had licenses increased from 13.5% in 1991 to 36.3% in 2000.[1,2] Older drivers are particularly susceptible to glare due to cataracts, cataract surgery and other age-related issues with contrast sensitivity. Additionally, it is widely acknowledged that glare is underreported in state and national accident and fatality data.[2,3]

An additional observation is that while 30% of VMT (vehicle miles traveled) occurs at night, over 50% of all fatalities occur during that time[4] – a fatality rate of 4.63 per 100 million VMT, 4.4 times the national average. Given the above, one of the contributing factors must be glare.

Glare from headlights can be a factor anywhere, but can be an especially severe problem when ambient light is low, as in rural environments. Glare is characterized, alternatively or in combination, as disability glare and discomfort glare. Both are problems, but care must be taken in separating the two when determining countermeasures.

---

[1] Mace, Garvey, Porter, Schwab, Adrian, *Countermeasures for Reducing Effects of Headlight Glare*, AAA Foundation for Traffic Safety (New York: December, 2001)

[2] Rosenbloom, Sandra. The Mobility Needs of Older Americans: Implications for Transportation Reauthorization. Brookings Institute Series on Transportation Reform. July, 2003.
http://www.brookings.org/dybdocroot/es/urban/publications/20030807_Rosenbloom.pdf
Accessed 2/20/04.

[3] Mortimer, R.G., "Headlamp Performance Factors Affecting the Visibility of Older Drivers in Night Driving", in *Transportation in an Aging Society, Special Report 218*, Vol 2, pp. 379-403, Transportation Research Board, 1988.

[4] U.S. Department of Transportation, National Highway Traffic Safety Administration, *Traffic Safety Facts 2001*, DOT-HS-809-484 (Washington, DC: 2002).

More specifically, disability glare results in short reductions in contrast sensitivity and from perception, and is caused by scattering of light within the optical media of the eye. This reduces overall contrast and can be characterized by an equivalent veiling luminance which adds to, and is superimposed upon, the scene. The magnitude of the equivalent veiling luminance is a function of several factors, including the intensity of the glare source, the angular distance between the glare source and the visual target of interest, and the age of the observer. Disability glare reduces the effective contrast of objects in the scene relative to their background, and thus might impair the ability of drivers to detect or recognize road hazards.

Discomfort glare, a subjective response of the observer, is a distraction but may not impair a driver's ability to perform visual tasks assuming it does not cause the driver to avert his gaze. Thus discomfort glare can occur independently of the reduction in task performance associated with disability glare. The mechanism of discomfort glare is still undetermined but some researchers believe that a physiological correlate is facial muscle tension in the vicinity of the eyes, and that discomfort glare is related to the scotopic luminosity function of the visual system, thus mediated by rods[5]. Discomfort glare is often rated on the De Boer Rating Scale for Evaluation of Discomfort Glare, in which a number is specified from 1 ("unbearable") to 9 ("unnoticeable").

The general consensus among researchers is that disability glare is the more important factor in traffic safety, since task performance can be directly affected, while pure discomfort glare results only in annoyance to the driver. Of course many glare sources, including headlights from an opposing vehicle, will result in both kinds of glare.

Thus glare from headlights of opposing vehicles is a known contributing factor to nighttime accidents, is recognized by drivers, and is an ever-increasing problem as the population of older drivers increases. In an effort to allow effective countermeasures to glare to be developed, this project had as its goal the development of a Glare Meter Tool, a computerized instrument that can assess levels of disability and discomfort glare without need for human observers. This instrument would be capable of acquiring an image of a scene with glare, then analyzing the image to output a number on the standard De Boer scale, and also an equivalent veiling luminance that can be used to assess the level of disability glare. With the Glare Meter Tool, countermeasures such as mainline lighting or glare screens could be tested in the field to assess their effectiveness in reducing disability glare and discomfort glare.

---

[5] Berman, Bullimore, Jacobs, Bailey, and Gandhi, *An Objective Measure of Discomfort Glare*, Journal of the Illuminating Engineering Society (Summer, 1994)

IV. Laboratory Experiments

1. Overview

Our strategy was to measure disability glare and discomfort glare in separate experiments under carefully controlled laboratory conditions with human observers, and simultaneously to develop, test, and assess the accuracy of our objective glare measurement device, the Glare Meter Tool.

The Glare Meter Tool is based on images acquired by a full-color video photometer of a scene containing glare sources. Analysis is done by two separate computer programs, one for disability glare and one for discomfort glare, but both programs operate on the same set of photometer images. Our objective with the Glare Meter Tool is to be able to measure the disability glare and discomfort glare levels with a physical instrument such that the values obtained are in agreement with the results of the psychophysical experiments or subjective assessments. In this way, we can have confidence that the Glare Meter Tool is accurate and will have predictive power.

2. Disability Glare Experimental Methods

In a darkened room, we presented observers with an evenly-illuminated gray background presented on a computer monitor at a viewing distance of 77.5 centimeters, and at the center of which was an increment threshold task. The observer gradually increased the contrast of a disc presented within a small annulus until he or she could just see the disc with respect to the annulus. The task can be seen in Figure 1.

Figure 1. Photograph of the disability glare experiment task, showing the computer monitor with glare source illuminated. The observer adjusted the intensity of the disc within the annulus to threshold.

Observers could press either of two buttons on a computer keyboard, one of which raised the intensity of the disc in discrete amounts, the other of which decreased the intensity[6]. The display was calibrated through use of the Radiant Imaging PR-1613F-2 video photometer, with results confirmed by use of a Spectra Pritchard 1980A photometer. The luminance values of the gray background, annulus, and disc at each of its possible discrete levels of intensity are found in Appendix B, along with a complete methodology concerning use of the video photometer for luminance mapping.

We employed a modified method of adjustment routine whereby observers were asked to fixate the center of the annulus, then raise the intensity until the disc was first seen, then decrease the disc luminance until it was no longer seen, then raise the intensity one notch, the value thus achieved representing the threshold contrast condition. First, observers set the contrast threshold with the glare source off. Then the observers performed the task with and without the presence of glare, which we introduced by use of a high-intensity white LED placed in front of the computer screen. The glare source could be positioned at any location horizontally with respect to the disc. Experiments were performed at three different eccentricities[7] of the glare source, and at three different intensities for each position. Thus there were ten measurements in all for each observer[8].

The methodology for determining the luminance of the glare source at each intensity level and for specifying the eccentricity of the glare source is fully described in appendices B and C, but, in brief, the net up/down button pushes at threshold contrast for each trial were recorded and turned into the associated grayscale values that were showing on the monitor. There were 256 possible grayscale values on the display and a single button push corresponded to changing the disc's grayscale value by one unit, unless the subject reached the lowest possible grayscale value of "pure black" in which case a beep sounded to alert the subject and further attempts at decrease had no effect. The grayscale values were then converted into luminance levels using the calibration curve obtained in Appendix B. This was necessary because equal grayscale step sizes were **not** equivalent to equal luminance changes.

The complete set of this data is shown in Appendix G.

3. Disability Glare Analysis and Results

Since the data analysis is informed by the results of previous work, a little more background information is in order.

An excellent summary reference on glare is a 2003 paper by Johannes J Vos.[9] He details the long effort to distinguish the different types of glare and to quantify them, beginning with what

---

[6] The monitor settings, and the background and annulus grayscale (luminance) values were always constant throughout the experiments; only disc intensity was varied to change contrast.
[7] *Eccentricity* here is the angle the LED location makes with the observer's line-of-sight.
[8] Three observers made additional observations corresponding to two new positions of the LED after the original set of runs, with all other observers having completed their trials; this was in order to generate additional data points for curve-fitting purposes, as explained later in the report and discussed in appendix E.
[9] **Reflections on Glare**, *Johannes J Vos* in **Lighting Res. Technol.** 35, 2 (2003).

appears to be the first mention of glare in the scientific literature almost 100 years ago. The consensus according to Vos seems to be that glare falls into basically three categories: disability glare, discomfort glare and dazzling glare. The latter does not concern us here[10] and discomfort glare is discussed in the next section of this report.

Holladay[11] did the first quantitative work on disability glare in the 1920's. His work and that of his contemporary Stiles[12] developed an expression for an equivalent veiling luminance that was proportional to the glare illuminance and inversely proportional to the square of the glare angle (eccentricity). It is the direct ancestor to equation (1) shown below.

Vos himself has probably made the biggest contribution to understanding disability glare since that time. Through a series of clever experiments in the early 1960's he not only managed to show that disability glare is, indeed, due to the veiling luminance being produced by scattering within the optical media of the eye, but he was actually able to quantify that scattering. He found the cornea scattering about 30% of total glare veil[13], 40% scattering from the fundus[14] and, by subtraction of the retinal and corneal contributions, about 30% from the lens.[15]

Thus disability glare, defined by the CIE[16] as "glare that impairs the vision of objects without necessarily causing discomfort", has its physical origins in the scattering of the light from the glare source by the eye itself. This scattering causes some portion of the light from the glare source to fall on the retina where the rest of the field of view is being imaged, much like shining a broad, diffuse flashlight beam onto a movie theater screen while a film is being shown. The stray light from the glare source casts this "veiling luminance" onto the imaged scene and contrast is thereby reduced. Objects thus become harder to distinguish than if the glare source was not there.

Since scattering of light in the lens of the eye typically increases with age, it is not surprising that quantification of disability glare includes a factor depending on age. According to Vos, this age dependence was not made precise until the work of IJspeert *et al*.[17] This group also found a pigmentation (eye-color) dependence for disability glare, but the dependence was not as strong as for the other factors mentioned above and it only became a factor at larger angles than concern us here.

---

[10]The CIE (*Commission Internationale de l'Eclairage* or the *International Commission on Illumination*) defines dazzling glare as a type of discomfort glare, but it is phenomenologically distinct enough from "ordinary" discomfort glare that it should be treated differently. It does not appear in the types of situations considered here (i.e. headlight glare). The interested reader should consult Vos' paper and the references therein. CIE's website is at http://www.cie.co.at/index_ie.html.

[11] **The Fundamentals of Glare and Visibility,** *LL Holladay* in **J. Opt. Soc. Am.** 12 (1926), and **Action of a Light Source in the Field of View in Lowering Visibility,** *LL Holladay* in **J. Opt. Soc. Am.** 14 (1927).

[12] **The Effect of Glare on the Brightness Difference Threshold**, *WS Stiles* in **Proc. Roy. Soc. London** 104B (1929).

[13] **Contribution of the Cornea to Entoptic Scatter,** *JJ Vos* and *J Boogaard* in **J. Opt. Soc. Am.** 53 (1963).

[14] **Contribution of the Retina to Entoptic Scatter,** *JJ Vos* and *MA Bouman* in **J. Opt. Soc. Am.** 54 (1964).

[15] **Contribution of the Fundus Oculi to Entoptic Scatter,** *JJ Vos* in **J. Opt. Soc. Am.** 53 (1963).

[16] **International Lighting Vocabulary**, CIE #17.4 (1987).

[17] **The Intraocular Stray Light Function in 129 Healthy Volunteers; Dependence on Angle, Age and Pigmentation**, *JK IJspeert, et al.* in **Vision Res.** 27 (1987).

Reviewing this previous work and that of many others, a CIE committee[18] on disability glare, chaired by Vos, produced a series of related[19] equations on disability glare. The relevant one for this series of experiments, called the *CIE Small Angle Disability Glare Equation*, is given by

$$\left[L_{veil} \middle/ E_{glare} \right]_{small\ angle} = \frac{10}{\theta^3} + \left[1 + \left(\frac{Age}{62.5} \right)^4 \right] \times \frac{5}{\theta^2} \qquad (1)$$

where the glare angle (eccentricity), θ, is between 0.1º and 30º. Since the photometer's field of view is only about 20º on either side of its center, larger angles are not needed.

Here L_{veil} is the equivalent luminance that would (directly) produce the same veiling effect on the eye as the glare source does (indirectly through scattering). E_{glare} is the *illuminance* at the eye created by the glare source. Since the imaging photometer produces luminance "images" (two dimensional maps of luminance) and the illuminance at the eye cannot be measured by the imaging photometer, our use of this formula is modified slightly (see below).

To proceed further and connect the disability glare equation to our experimental data requires some definitions:

$L_T = $ Luminance of the target (disc) at threshold contrast *as measured by*

    a "perfect" photometer $\left[cd/m^2 \right]$

$L_B = $ Luminance of the background (annulus) *as measured by a "perfect"*

    photometer $\left[cd/m^2 \right]$

$L_T' = $ Luminance of the target at threshold contrast *as perceived by the*

    eye in the presence of a glare source $\left[cd/m^2 \right]$

$L_B' = $ Luminance of the background *as perceived by the eye in the*

    presence of a glare source $\left[cd/m^2 \right]$

$L_V = $ "Veiling" Luminance $\left[cd/m^2 \right]$

$L_P = $ Output number from the computer program $\left[arbitrary\ units \right]$.

These definitions require some elaboration to avoid confusion. Here "as measured by a 'perfect' photometer" should more properly be "if the glare source were removed or switched off *after* threshold contrast was reached and a measurement was immediately taken with nothing else changed until the measurement was complete", but that is too wordy. The problem here is that, *just like the eye*, the photometer's optics scatters light and creates its own veiling luminance!

---

[18] **CIE TC I-50 Report CIE Equations for Disability Glare,** CIE #146 (2002) in **CIE Collection on Glare 2002**.
[19] That is, the equations are progressively more complicated depending on the number of factors used, the domain of validity, and the precision needed.

(<u>See the discussion below</u>.) Furthermore the dynamic range of the photometer scales to the brightest light in its field of view or the photometer *saturates*.[20] Suffice it to say that only an *ideal* instrument could get a proper reading on the luminance of the disc at threshold contrast while the glare source remained on.

In practice, we of course neither had an ideal instrument, nor did we turn the glare source off to directly measure the threshold contrast luminance, but rather we recorded the button pushes as outlined above and converted those into the luminance of the disc. The luminance of the background annulus, however, *was* measured without the glare source on since the annulus luminance was constant under all the experimental conditions.

Such definitions might seem to the casual reader to be a pedantic attention to details, but a moment's reflection will show that such difficulties as just mentioned do, in fact, greatly impede the development of a practical glare meter. One can't say, except in a theoretical way, "luminance of the disc at threshold contrast" without specifying how it is measured in practice. A *real photometer*, affected as it is by its own internal scattering and dynamic range issues, *will typically give the wrong value for the disc luminance while the glare source is active*. Furthermore, in the field a glare source might, depending on location, have some sidescatter or backscatter, which will change the illumination on a target.[21]

If we had said "luminance of the disc at threshold contrast with the glare source removed" that definition could give the false impression that the experimental run was done with the glare source off; hence, we used the somewhat involved definition above. *It is thus important to keep in mind the distinctions between what a real photometer measures, what an observer actually sees, and what a perfect photometer would measure.*

Now under the assumption that the veiling luminance in the eye caused by a glare source is *uniform*, or at least uniform over the area constituting the target and "nearby" background, we get

$$L'_T = L_T + L_V$$
$$L'_B = L_B + L_V .$$

(2)

In other words, we assume that the observer experiences an effective target luminance that is the combination of the true target luminance (ideal photometer) and a constant luminance that washes over the retina's image of the target due to glare source scatter in the observer's eyes. The background luminance is considered in the same way.

---

[20] The problems of saturation and dynamic range are discussed in much more detail in the section on *discomfort glare*.
[21] This did not seem to be an issue in our laboratory experiments since the LED had little backscatter and was mounted far enough forward of the monitor screen. It also seems unlikely in the case of headlight glare too barring, say, fog, but in some situations there is the potential for it to occur.

Now we make two further assumptions. The first is that, over a wide range of photopic situations, *but without any glare source present*,[22] Weber's law of just noticeable difference (in vision, the ratio of the increment threshold to the background intensity) will hold:

$$c = \frac{L_T - L_B}{L_B} . \tag{3}$$

Here c represents (threshold) contrast. Equation (3) goes from merely being a definition of contrast to a psychophysical statement about subjects[23] when *we assume that c is a constant.* Here, other than having a threshold contrast, the eyes are taken to behave like ideal photometers when no glare source is around. Our assumption is reasonable given that Weber's Law is known to hold in the range of luminance employed in these experiments (or to be found in nighttime driving, given that the headlights of the driver's automobile are illuminating the roadway ahead and thus adapting the eye to low photopic levels, even without the benefit of ambient mainline lighting).

The second assumption is that this equation continues to hold in the presence of a glare source provided that unprimed quantities are replaced by primed quantities. Thus, with the replacements $L_T \rightarrow L_T', L_B \rightarrow L_B'$:

$$\frac{L_T' - L_B'}{L_B'} = c . \tag{4}$$

Putting equation (2) into equation (4) gives,

$$\frac{L_T' - L_B'}{L_B'} = \frac{(L_T + L_V) - (L_B + L_V)}{L_B + L_V} = \frac{L_T - L_B}{L_B + L_V} = c . \tag{5}$$

In order to connect this with our experimental data, we need something akin to equation (1). Consider the following expression,

$$L_P = \frac{\sum_{i=0}^{1019} \sum_{j=0}^{1019} L_{ij} \left(\frac{10}{\theta_{ij}^3} + \left[1 + \left(\frac{age}{62.5} \right)^4 \right] \cdot \frac{5}{\theta_{ij}^2} \right)}{(1020 \times 1020)} . \tag{6}$$

This is what our computer program yielded after giving it the photometer luminance "image" as input.

---

[22] In this instance we really do simply mean that no glare source is around, nothing to do with the instrumental measurement issues just discussed.

[23] It is understood that c will likely be different for different observers (i.e. individual variability). Thus this equation is to be interpreted in a statistical sense.

Our Radiant Imaging PR-1613F-2 digital video photometer, or imaging photometer, can export a luminance "image" as an ASCII data table consisting of a 1020 x 1020 array of numbers. The numbers are space delimited (separated by single spaces) and each number in the x-y table represents the luminance value at that x-y or row and column position in the image formed on the photometer's CCD detector, which consists of, not surprisingly, a square 1020 x 1020 grid of pixels.[24]

With such a data table as input, our program calculated equation (6) as follows. The row and column indexing used C programming conventions where the row number (i) and the column number (j) both run from 0 to 1019 rather than 1 to 1020. At each pixel point or array entry (i, j) the luminance value at that point, namely L_{ij}, was used to weight the expression in large parentheses in equation (6). This was in lieu of E_{glare} in equation (1) since that was not easily available.

The expression in large parentheses is, of course, the right-hand side of equation (1) with the glare angle or eccentricity θ replaced by its discrete version, the glare angle at position (i, j) or θ_{ij}. This means the angle of the pixel at (i, j) with respect to the center of the photometer's CCD. (The center of the luminance image was set to be the same as the subject's line-of-sight.) The details of just what that angle is and how it is actually computed are relegated to Appendix D. (Equation (6), being directly related to equation (1), uses degrees rather than radians when computations are made.)

The denominator in equation (6) [1,020 x 1,020 = 1,040,400] is just a normalization factor to keep the computed numbers at a reasonable value (i.e. not gigantic in comparison to L_T and L_B). The variable "age" is just the age in years of the subject whose data is being analyzed.

Comparing equations (1) and (6) brings us to our final assumption, that is

$$L_V = k \cdot L_P . \qquad (7)$$

In this last equation, k is just a (as yet unknown) constant. In other words, the output of our program, L_P, based on the photometer's luminance image, is taken to be directly proportional to the veiling luminance based on the Vos/CIE disability glare formula.

If equation (7) is substituted into equation (5) we get,

$$\frac{L_T - L_B}{L_B + k L_P} = c \qquad (8)$$

and rearranging this gives,

---

[24] More details about the photometer are given in the *discomfort glare* section. Also the actual CCD is 1024 x 1024 but "border" pixels two thick on each side don't participate in the light detection.

$$L_T = ck \cdot L_P + (c+1) L_B. \tag{9}$$

This last equation is the one on which our disability glare analysis is based.

Since L_B is constant (and known) throughout all the trials, a linear fit of L_T against L_P will yield the intercept value $(c+1)L_B$. From this c can be computed. With c and the slope of the fit line, namely ck, then in hand, the value of the proportionality constant in equation (7) can then be deduced. The numerical value of k then allows a computation of veiling glare from photometric data based on equations (6) and (7), the former requiring a computer program.

Furthermore, a linear fit to equation (9) will give a pretty good check on the assumptions mentioned thus far. If the L_T, L_P data do **not** fall on a straight line[25] then one of the assumptions is probably not true.

Before doing that fit though, the data had to be processed to deal with the scattering issue mentioned earlier. In the course of our investigation we did a rough, preliminary fit to the data and had a worse result than anticipated. A look at Figure 2 shows why.

The bright pixels far away from the glare source represent the scattering of the light from that source (the LED) by the optics of the photometer. In retrospect, this is not surprising; *there is no reason to expect the photometer's optics to be immune to the same scattering phenomenon as the eye's optics experience*. It does however pose a tough problem. Since the "veiling luminance" from glare is the whole point of the exercise, how does one compute it when the photometer data is "corrupted" by that very same phenomenon?

---

[25] The phrase "fall on a straight line" naturally means in the statistical sense with a least squares fit. In other words, what is the reduced χ^2 value for the fit? That computation is done later in this section.
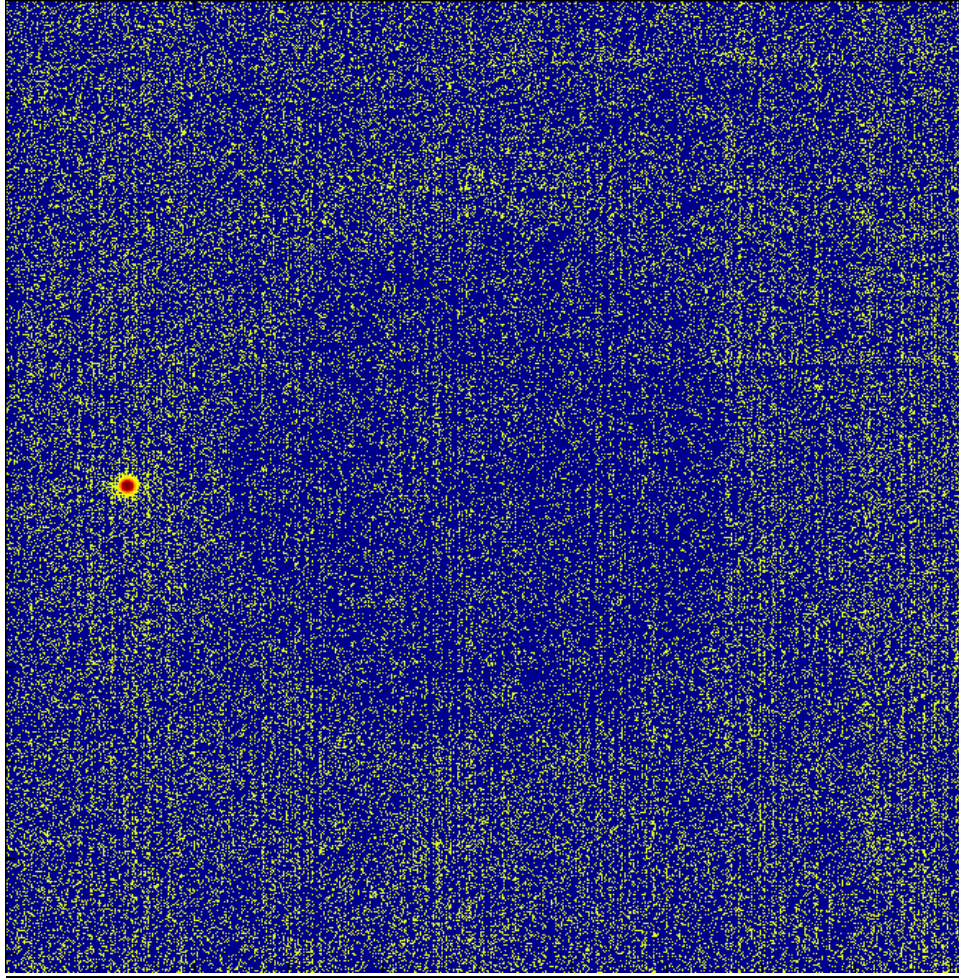
Figure 2: An example (false color luminance image) of the scatter occurring in the photometer's optics.

A glance at equation (6) shows this problem quite clearly. A high value of L_{ij} that "shouldn't be there" (i.e. in the absence of scattering) at a small angle θ_{ij} (away from the glare source but close to the line of sight) can grossly skew the value of L_P from what is truly intended.

Equation (6) is "linear" in the sense that it performs a sum over all pixels individually.[26] Thus many pixels containing the scattered light can *really* skew the value of L_P even when they are not necessarily all at small angles. On the other hand, the form of equation (6) is theoretically correct and, if there was no scatter in the photometer, multiple glare sources would not be a problem since one could just sum over all pixels individually without having to worry about identifying glare sources.

But in the world of real photometers with scatter, we had to take a fairly radical approach. We didn't want to change the form of equation (6) seeing as it was based on the hard-earned and carefully deduced equation (1) (by committee no less). Therefore, every luminance image of the

---

[26] This is in distinction to the "nonlinear" formulas used in *discomfort glare* where the contributions of individual pixels cannot be added in one at a time but, rather, must be treated as groups. This is explained in more detail in the section on discomfort glare.

LED was examined separately to change every luminance value outside of that glare source to *zero*. The result is Figure 3.
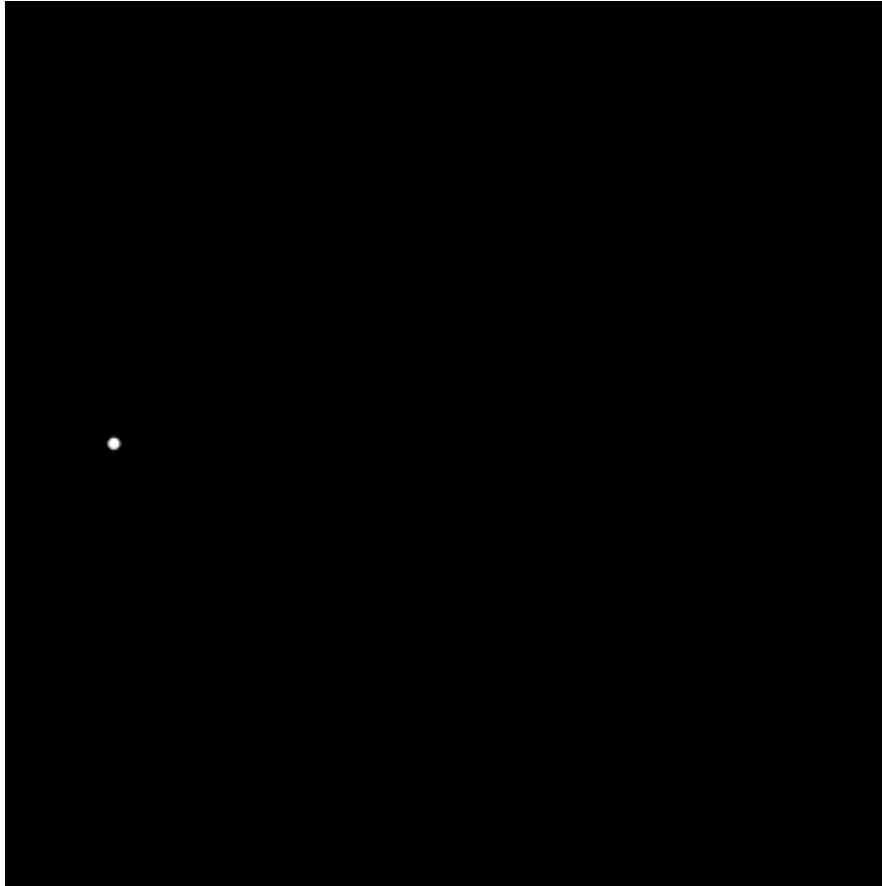

Figure 3: A typical example of what the luminance image of the glare source becomes when scattering is removed. (The LED is at position 1 on high intensity in this figure and the previous one.)

Since each file of glare source luminance for every condition had to be corrected "by hand" as it were, one can see the method is tedious and not robust enough for a practical glare meter in the field. Even an automated correction, say by setting a threshold below which pixels are sent to zero, may not work because a handful of "stray" pixels of high value (above the threshold) near the line of sight (the center) could cause the value of L_P to be wrong. Perhaps the methods of glare source identification used later in the discomfort glare sections of this report would make for a more automated approach, but this means a lot more computational work before equation (6) could be used. In any event, once the luminance data files had the LED glare sources "isolated" in this way, equation (6) gave values of L_P that lead to vastly better fits.

Those fitting routines were done after assigning uncertainties to the data. The error bars on L_P (once the "isolation" process just described was done) are negligible compared to those of L_T. These latter uncertainties were taken to be the luminance equivalent of from one to two button pushes as described earlier.

This error bar estimation was a judgment call. The long sequence of trials was tedious enough without repeating them multiple times to get a sample standard deviation for each subject. It was

clear from the process that the uncertainty with a glare source present was at least one button push in most cases. Three pushes seemed too high an uncertainty. Therefore between one and two button pushes were assigned as the error bar depending on how the individual subject reported his or her ease of finding the threshold. Using the curves in Appendix B, the uncertainties in terms of button pushes were converted to luminance values. Since the "*button push to grayscale to luminance*" conversion is nonlinear, a one-button-push uncertainty at one L_T value is **not** the same as a one-button-push uncertainty at a different value.

The fit itself was done with a program called FFIT. This does a weighted least-squares fit to a line and provides the residual or difference plots, the fit coefficients, their uncertainties and the reduced chi-square value of the fit. We took L_T as the y or ordinate value and L_P as the x or abscissa value. (This assignment holds through the next several graphs up to figure 13 inclusive; the axes in the figures are not labeled.) Only the σ_y values just discussed were used to weight the fit. A typical result is shown below along with its difference plot in Figure 4.

Although the resolution of these screen captured pictures is somewhat poor, the reduced χ^2 value is legible as 0.77. That value[27] along with the difference or residual plot (bottom half of the figure) shows that the calculated least squares line (dotted white line) is a very good linear fit.

Unfortunately, one has to depend on the statistics more than usual because of the nature of the experiment, namely that while the data do indeed fit a line well, the spacing of the data points is **not** linear but logarithmic (or exponential depending on how one wants to look at it). The N = 11 in the upper part of the figure means that there are eleven data points. But even with the picture greatly expanded, all 11 points are not easily seen. This is because the visual system behaves with a roughly logarithmic response. Thus a natural "spacing" of the data is logarithmic while the best fit is a linear one. That is clearly the case here. Hence, unless a lot more points are taken or some are left off and plotted separately, a great many points end up getting "bunched up" near the origin.

---

[27] The reader will recall that a reduced chi-square value near one combined with a residual plot showing no obvious patterns is a good sign that the data really fit a line. A very small χ^2 (say 0.1) usually is indicative of over estimated error bars and a large χ^2 (say ten or more) usually means a poor fit to a line or wildly underestimated error bars or a point plotted in error such as transposing the x and y values.
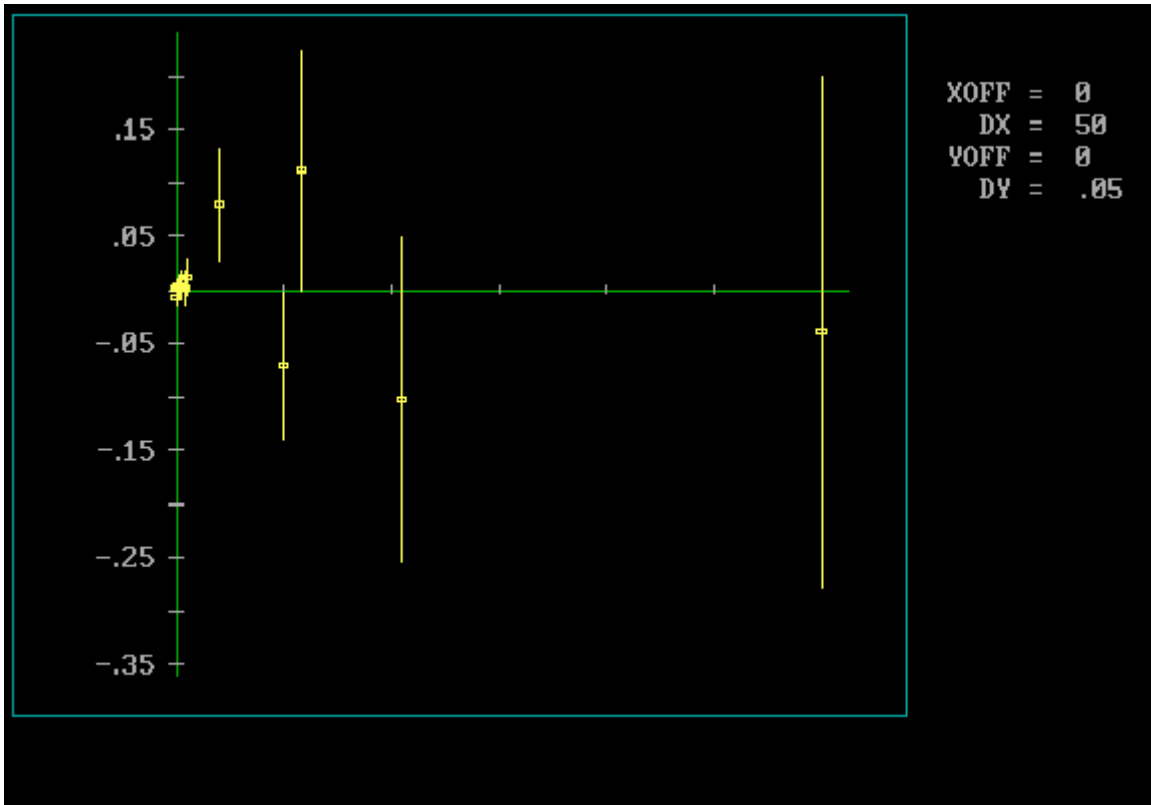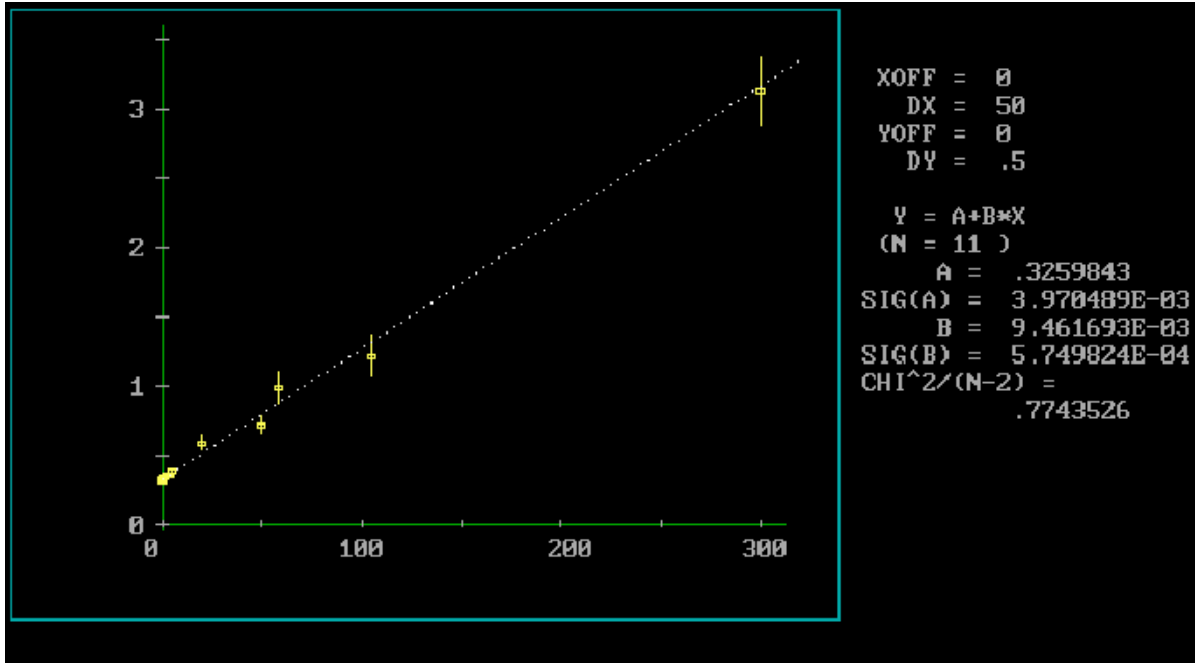
Figure 4: Linear fit to the data and difference plot for one subject. L_P is the x-axis and L_T is the y-axis.

To avoid the "bunching" seen here, one can plot the data on a log-log scale. This same data is shown in that format in Figure 5.
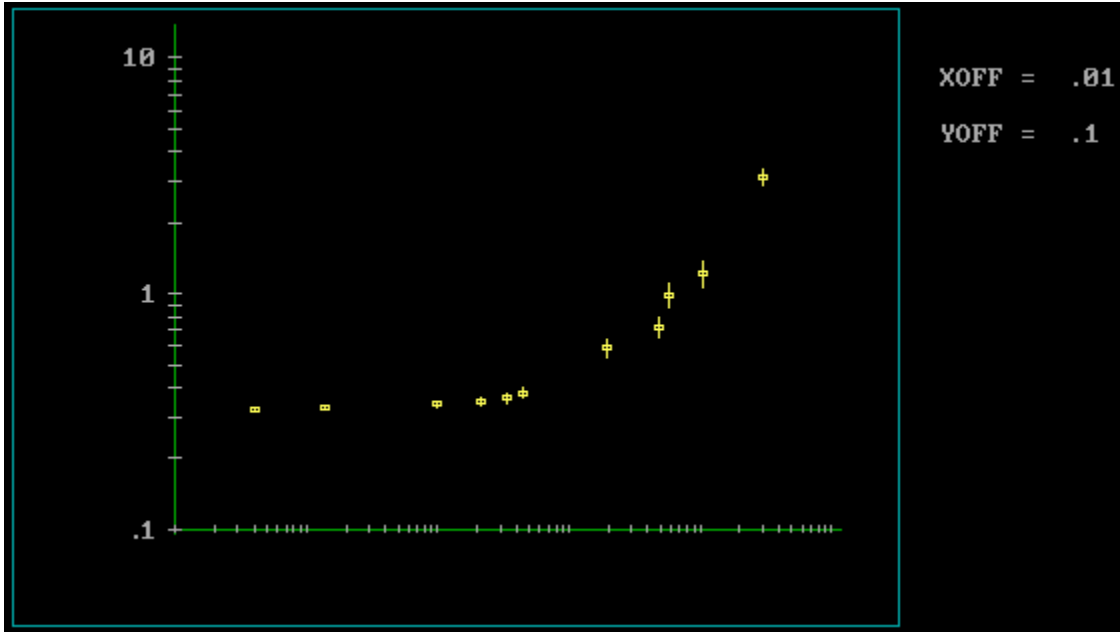
Figure 5: Data from the previous figure plotted on a log-log scale.

Clearly the manner in which the data lays out is much more easily seen in this figure. Unfortunately, it doesn't look like a line on this kind of a plot. To see that it really is a "line", consider the formula for a line:

$$y = m\,x + b$$

and take the logarithm of that:

$$log\ y = log\,(m\,x + b) = log\left(x\left(m + \frac{b}{x} \right) \right)$$

$$= log\ x + log\left(m + \frac{b}{x} \right).$$

If we define $w \equiv log\ x$ and $z \equiv log\ y$ then when x is very large,

$$z \approx w + log\ m = w + const.$$

while if x is very small,

$$z = log\,(m\,x + b) \approx log\ b = a\ constant\ .$$

Hence the log-log scale plot is effectively a w-z plot on a linear scale. The part of the data that represents small values of x will behave as z = a constant or, in other words, it looks like a horizontal line. This is just what is seen on the leftmost portion of the curve.

The rightmost portion of the curve should look like a line with "slope" one $\left(\dfrac{\Delta z}{\Delta w} = 1, \text{ that is} \right)$.

This too is seen in Figure 5.

This digression to convince the reader that a linear relation looks like what is seen on a log-log scale in Figure 5 is because with this type of data one can either see 1) a linear fit to "bunched up" data points, or 2) a curve with each data point distinct, *but one can't see both on the same plot*. Since data from several individuals is overlaid in the next few figures we have chosen the second type of plot.

The entire group of subjects is plotted in Figure 6. The program FFIT *does* allow for color-coding of overlaid data but not for up to 15 individuals. This figure is just meant to illustrate the range of individual variability.
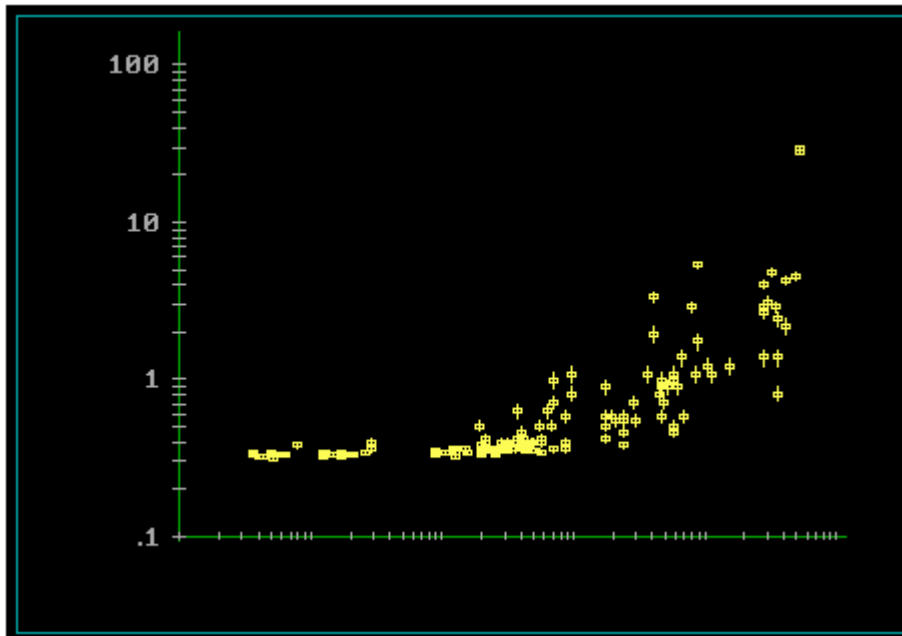
Figure 6: The data for all 15 subjects on a log-log scale.

By plotting subsets of individuals with color-coding, patterns begin to emerge. This is shown in Figure 7.[28] While all the curves tend to crowd together at low values of L_P, separation shows up at higher values. The plots for five individuals are shown; this is the maximum number of distinct plots that can be overlaid using color-coding (yellow, blue, green, brown and pink).

Note that the yellow and blue curves essentially share a point at the top right. They are comparable curves with only a couple of blue points deviating from tracking yellow. Similarly, the green, brown and pink points roughly track with pink having one deviating data point in the middle.

---

[28] Points on different curves at *approximately* the same L_P value do not always align vertically (i.e. L_P values are slightly different) because of the different ages of the subjects; see equation (6).
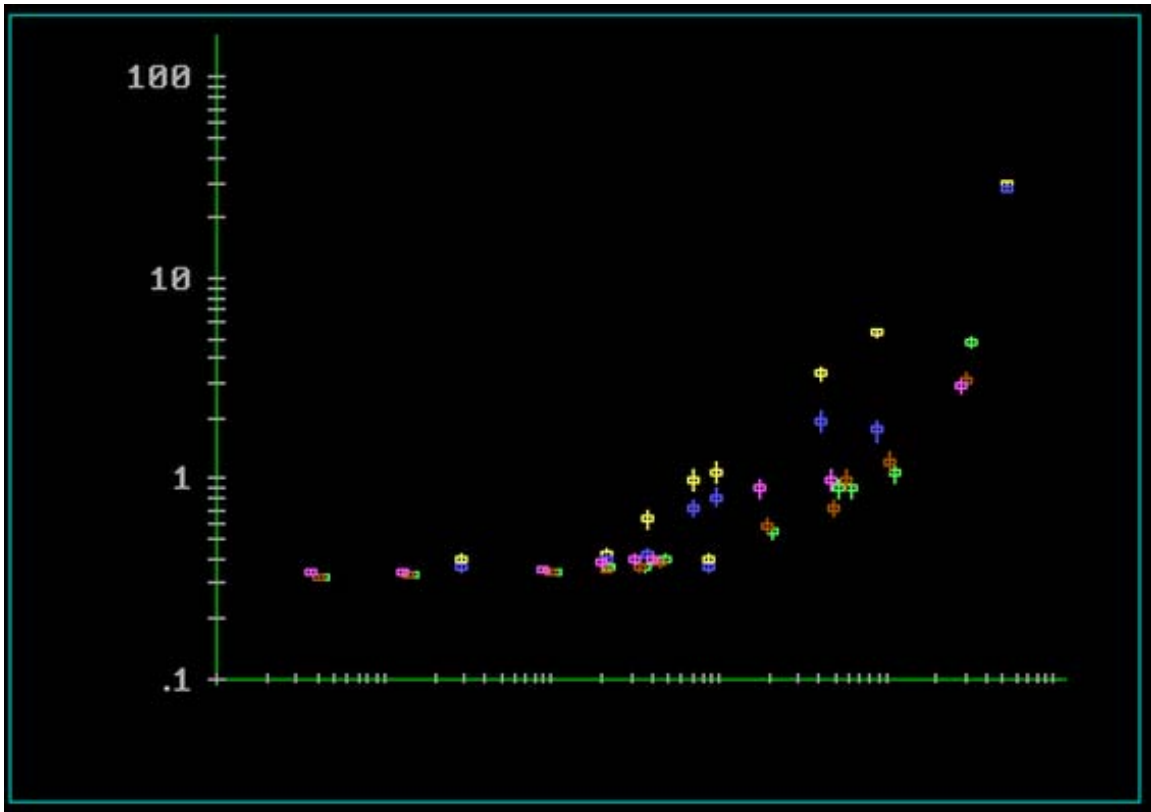
Figure 7: A color-coded plot for 5 individuals.

If we now plot the same pink, brown and green curves, but substitute two new individuals for the yellow and blue representations, we see the plot in Figure 8. Here the yellow and blue data points bound the other curves from below whereas in the previous figure they bounded them from above.

The yellow and blue curves roughly track together and the pink, green and brown data points do likewise, with a couple of exceptions. The separation between the two sets of curves becomes greater with increasing L_P or L_T. This is also true of Figure 7.

While there is no doubt almost a continuum if enough subjects were tested, our data fell into very roughly three sets of curves: two bounding extremes and a cluster of curves in the middle. This is shown in Figure 9.
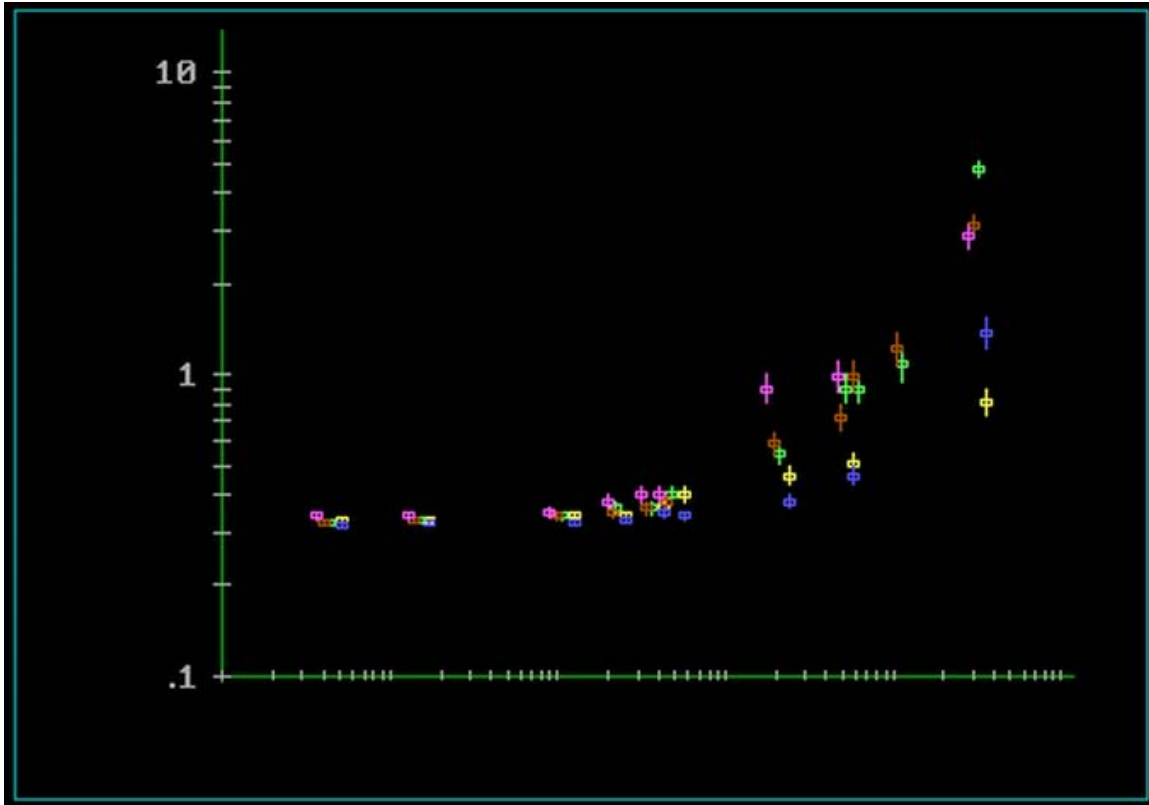
Figure 8: Again the data for 5 subjects is shown. The pink, green and brown curves represent the same 3 individuals as in the previous figure.

Figure 9 shows three curves. Yellow and blue represent the extremes and green is an individual representative of those clustering in the middle. Yellow points here represent a *higher* value of L_T for a given value of L_P relative to green points. Alternatively, the individual represented in yellow will have a higher ck product than the person represented in green. Thus a higher contrast is needed for a given glare setting or a greater veiling glare is experienced or both. The blue points represent someone who needs a *lower* value of L_T for a given value of L_P relative to the person whose data points are green.

In general lower curves mean a greater ability to see objects in the presence of glare than higher curves. The two subjects with the highest two curves were also the two oldest subjects and both reported greater difficulty seeing in the presence of glare than when they were younger. The youngest subjects however, did not have the lowest curves.

Figure 10 is identical to Figure 9 except that it is on a *linear* scale instead of a log-log scale. This clearly illustrates the futility of expecting much visual insight from an inspection of the data on a completely linear scale, except for the fact that the "actual" separation of the curves (lines) on the rightmost section is greater than one might think by looking at the log-log representation of them (at least for the two extremes—yellow and blue). (The actual fit lines are not shown but the reader can easily imagine them.)
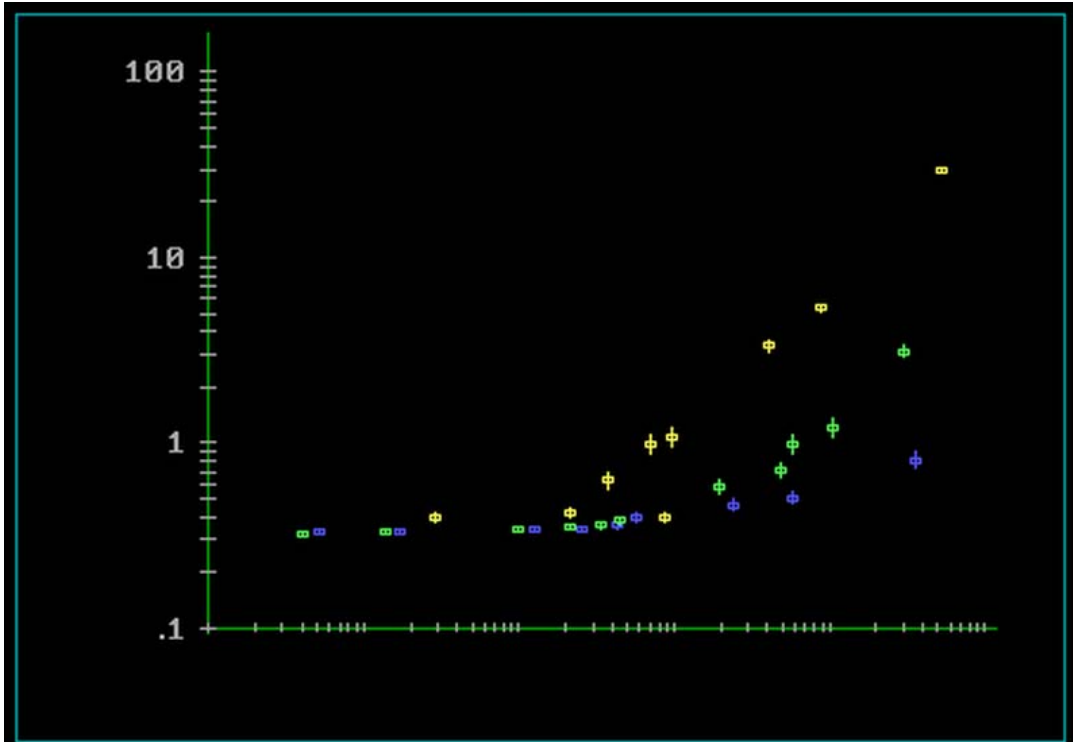
Figure 9: Three representative curves. Yellow represents a high disc luminance for a given value of L_P while the blue data points represent a lower necessary disc luminance. The green falls somewhere in the middle. (There is one anomalous yellow point.)
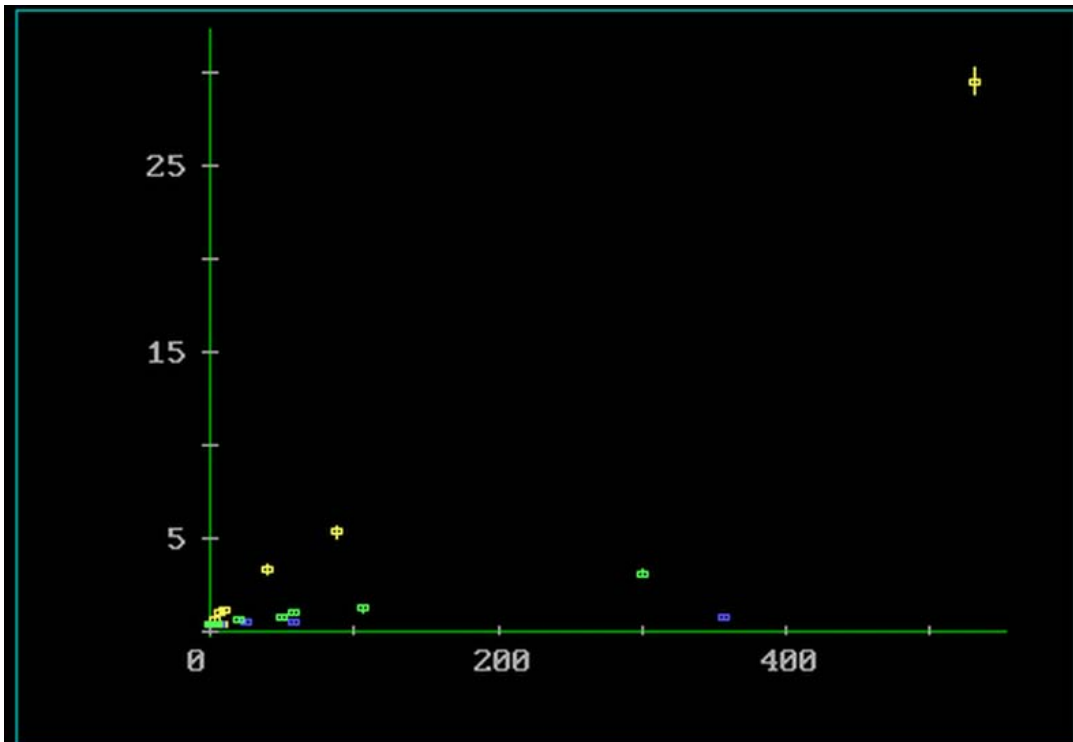
Figure 10: The exact same data with the exact same color-coding as in the previous figure, except the scale is linear-linear rather than log-log. Note the wide gap between the blue and yellow "lines" at the right of the plot (actual lines not shown).

We did two types of fits to the data: an individual fit for each subject and a combined fit to the group of subjects clustering around the average performance; this group represented the largest plurality of our subjects.

All of these results are shown in the Tables 1 and 2. (The second is really just a continuation of the first.) The same subjects who participated in these *disability* glare tests also participated in the *discomfort* glare tests with only a couple of exceptions which are duly noted. The subjects are listed in the same order for both types of glare experiments.

The careful reader will see that three subjects had 11 data points while all the others had 9. These extra measurements were added in as a check on the linearity of equation (9) in the otherwise sparse data regions of the plot. This check was decided on after all the data had otherwise been taken and most observers were no longer available. Hence, only three subjects took data at these points. Details on the precise positions of these additional points are provided in Appendix E.

Each individual fit produced an intercept that FFIT denoted by A and a slope denoted by B along with their corresponding uncertainties (sigmas). As mentioned above the intercept is,

$$A = (c+1)L_B \tag{10}$$

and consequently,

$$c = \frac{A}{L_B} - 1 \ . \tag{11}$$

Since the background luminance (here $L_B = 0.305 \ cd \ m^{-2}$ in all cases) is constant and its uncertainty is very small, the uncertainty for c is given by,

$$\sigma_c = \sqrt{\left(\frac{\sigma_A}{L_B}\right)^2} = \left|\frac{\sigma_A}{L_B}\right| \tag{12}$$

where σ_A is the uncertainty in the intercept (provided by FFIT).

[The calculation of k follows after Tables 1 and 2.]

Subject	Age (yrs)	Lt sigma in steps	# of points fit	Reduced χ^2	Intercept, A	Sigma A	Slope, B	Sigma B
# 1	61	1	11	1.53	0.3309	4.47E-03	4.93E-03	3.86E-04
# 2	28	1	9	0.47	0.3335	4.26E-03	4.24E-03	4.99E-04
# 3	53	1.5	9	1.35	0.3392	6.54E-03	1.61E-03	3.20E-04
# 4 (*)	25	1	9	1.04	0.3179	3.66E-03	1.24E-02	7.22E-04
# 5 (*)	27	1	9	1.96	0.3407	5.29E-03	9.25E-03	7.52E-04
# 6	53	1	9	0.58	0.3190	2.64E-03	2.79E-03	3.22E-04
# 7 (*)	45	1.5	11	1.43	0.3244	6.09E-03	1.10E-02	8.76E-04
# 8	68	2	9	3.62	0.3673	1.59E-02	9.79E-03	1.10E-03
# 9	53	2	9	1.26	0.3424	1.05E-02	4.00E-03	8.43E-04
# 10 (*)	60	1.5	9	1.16	0.3367	7.82E-03	1.05E-02	8.98E-04
# 11 (*)	52	1.5	9	1.30	0.3446	8.53E-03	8.08E-03	9.36E-04
# 12 (*)	29	1.5	9	1.46	0.3465	8.45E-03	1.01E-02	1.17E-03
# 13	71	2	9	10.63[†]	0.2323	2.72E-02	5.03E-02	2.30E-03
# 14	71	2	9	20.44[†]	0.2144	1.88E-02	4.03E-02	1.75E-03
# 15 (*)	39	1	11	0.77	0.3260	3.97E-03	9.46E-03	5.75E-04
# 16	54	This subject did not participate in disability glare.						
Group [people with (*)]	-	1.5	67	1.18	0.3306	2.59E-03	1.01E-02	3.67E-04

Table 1: Results from the disability glare fits—part 1.

[†] If the fifth data point of subject # 13 is excluded and the remaining 8 points are fit, this reduced chi-square becomes a nice value of 1 and the intercept A becomes a realistic 0.366 (it must be above 0.305 to keep the value of c positive as reality demands). Similarly, if the fifth and eighth points are excluded for subject # 14 and the remaining 7 points used, the reduced χ^2 also becomes 1 and A becomes 0.311. This is not to suggest those points aren't valid data, just that the departure from linearity is not as bad as these subjects' reduced chi-square would indicate (see text below).

Subject	Age (yrs)	c	Sigma c	Proportional const. k	Sigma k
# 1	61	0.0849	0.0146	5.81E-02	0.0110
# 2	28	0.0935	0.0140	4.53E-02	0.0086
# 3	53	0.1120	0.0214	1.44E-02	0.0040
# 4 (*)	25	0.0423	0.0120	2.92E-01	0.0847
# 5 (*)	27	0.1170	0.0173	7.90E-02	0.0134
# 6	53	0.0458	0.0087	6.09E-02	0.0135
# 7 (*)	45	0.0637	0.0200	1.73E-01	0.0557
# 8	68	0.2044	0.0523	4.79E-02	0.0134
# 9	53	0.1227	0.0344	3.26E-02	0.0114
# 10 (*)	60	0.1038	0.0256	1.01E-01	0.0264
# 11 (*)	52	0.1299	0.0280	6.22E-02	0.0152
# 12 (*)	29	0.1361	0.0277	7.42E-02	0.0174
# 13	71	-0.2383[†]	0.0891	-2.11E-01[†]	0.0795
# 14	71	-0.2970[†]	0.0615	-1.36E-01[†]	0.0287
# 15 (*)	39	0.0688	0.0130	1.38E-01	0.0273
# 16	54	**This subject did not participate in disability glare.**			
Group [people with (*)]		0.0838	0.0085	1.20E-01	0.0129

Table 2: Results from the disability glare fits—part 2.

[†] See the footnote on the previous page.

The slope of the fit, B, is equal to $c{\cdot}k$; hence using equation (11):

$$k = \frac{B}{c} = \frac{B}{\dfrac{A}{L_B} - 1} = \frac{BL_B}{A - L_B}. \qquad (13)$$

This means an uncertainty of,

$$\sigma_k = \sqrt{\left(\frac{BL_B}{\left(A - L_B\right)^2}\sigma_A\right)^2 + \left(\frac{L_B}{A - L_B}\sigma_B\right)^2} \qquad (14)$$

in the proportionality constant, where σ_A and σ_B are produced by the fit.

With the table of results filled out in this way for individuals, a couple of observations are worth noticing. The first is that, with the exceptions marked in red in the table, the fits are remarkably linear. The second is the fairly wide spread in values of k.

Two of the fifteen subjects tested did not have reduced chi-square values that justified a linear fit. These values are marked in red in the tables. Any linear fit parameters that come out of a regression on such data are not valid and that is obviously the case here as c and k for these subjects ended up with unphysical negative values (also noted in red).

But this doesn't mean that nothing can be gathered from these subjects' data. Consider the plot for subject # 13 as seen in Figure 11.
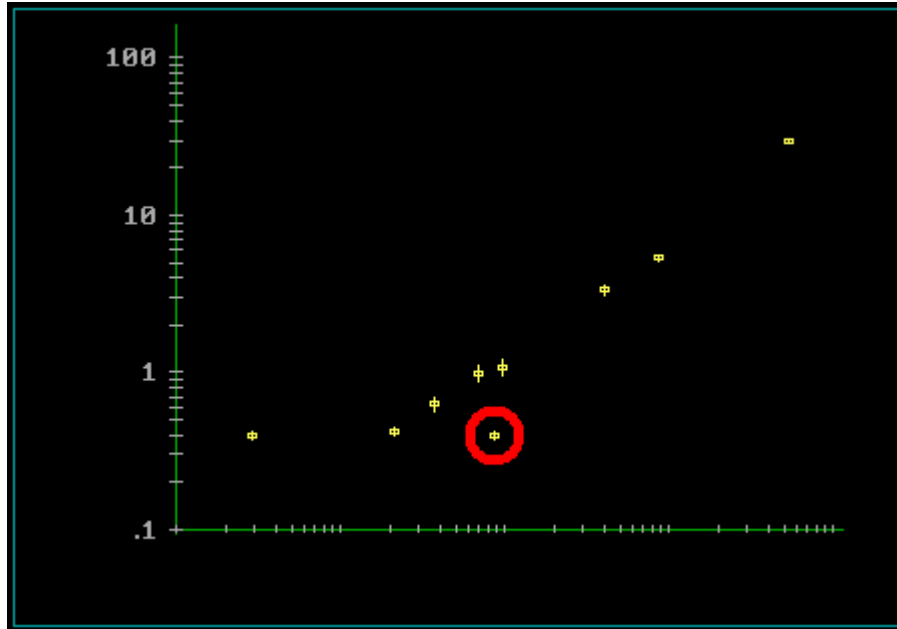
Figure 11: Data points for subject #13. Only one point, circled in red, keeps the data from fitting a line well.

Here again the log-log scale is used so that the data points are clearly visible. It is clear that the fifth point from the left is the problematic one when trying a linear fit. Indeed, if this point is dropped, the linear fit becomes quite reasonable and the fit parameters also make sense.

This is not to suggest that the data point isn't valid; it is just to suggest that a couple of seemingly anomalous points for a couple of subjects shouldn't lead one away from the conclusion that a linear fit to the data is excellent.

Indeed, the other 13 out of 15 total subjects show *remarkable linearity* in the fits in light of the reduced chi-squares and the difference (residual) plots (not shown here). This gives us high confidence in the basic correctness of equation (9), and, since that is based on equation (1) (from Vos and the CIE), strong confirmation that that equation is valid under these conditions as well. *Equation (9) along with the program generating L_P from photometer data thus becomes the primary tool for assessing disability glare.*

In terms of experimental measurements, it should also be noted that had we used fewer subjects, say five in total, and had subjects # 13 and # 14 been two of them, the results of our disability glare studies would have been very murky. This points up the importance of using as large a population of subjects as is practical given the resource constraints, something that is sometimes forgotten in psychophysical studies.

Subjects # 13 and # 14 were also the two oldest of our subjects and one of them mentioned upcoming cataract surgery. Something like that may have contributed to violating the assumptions that go into equation (9). Nevertheless, the "anomalous" points of these subjects, those causing a deviation from linearity, *were all below the line that would have been a good fit in their absence*.

In other words, their ability to distinguish objects under glare was better for those anomalous points than for the bulk of their trials. Hence, any standard of glare mitigation based on a linear

fit to their data (with the anomalous points removed) would err on the *conservative* side of safety.

Just which fit to invoke as a standard is a difficult choice as can be seen by the wide range of values of k, the proportionality constant in equation (7). For example, the values of k for subjects # 3 and # 15 differ by a factor of about ten.

For this reason, rather than trying to pick out an individual fit, we grouped the responses for seven subjects whose data points "clustered". This group, just under a majority of responses, seemed most representative. The members of the group are denoted with a "(*)" mark in the tables. The group fit parameters are the last row in the tables.

The least squares fit for this group, considered as a whole, is shown in the next set of figures. Figure 12 is the linear fit and its difference plot. Figure 13 is the group data in yellow in a log-log scale plot with the fit itself shown in blue. (The error bars on those blue points are entirely artifacts from the fitting program (FFIT) and have no meaning.)
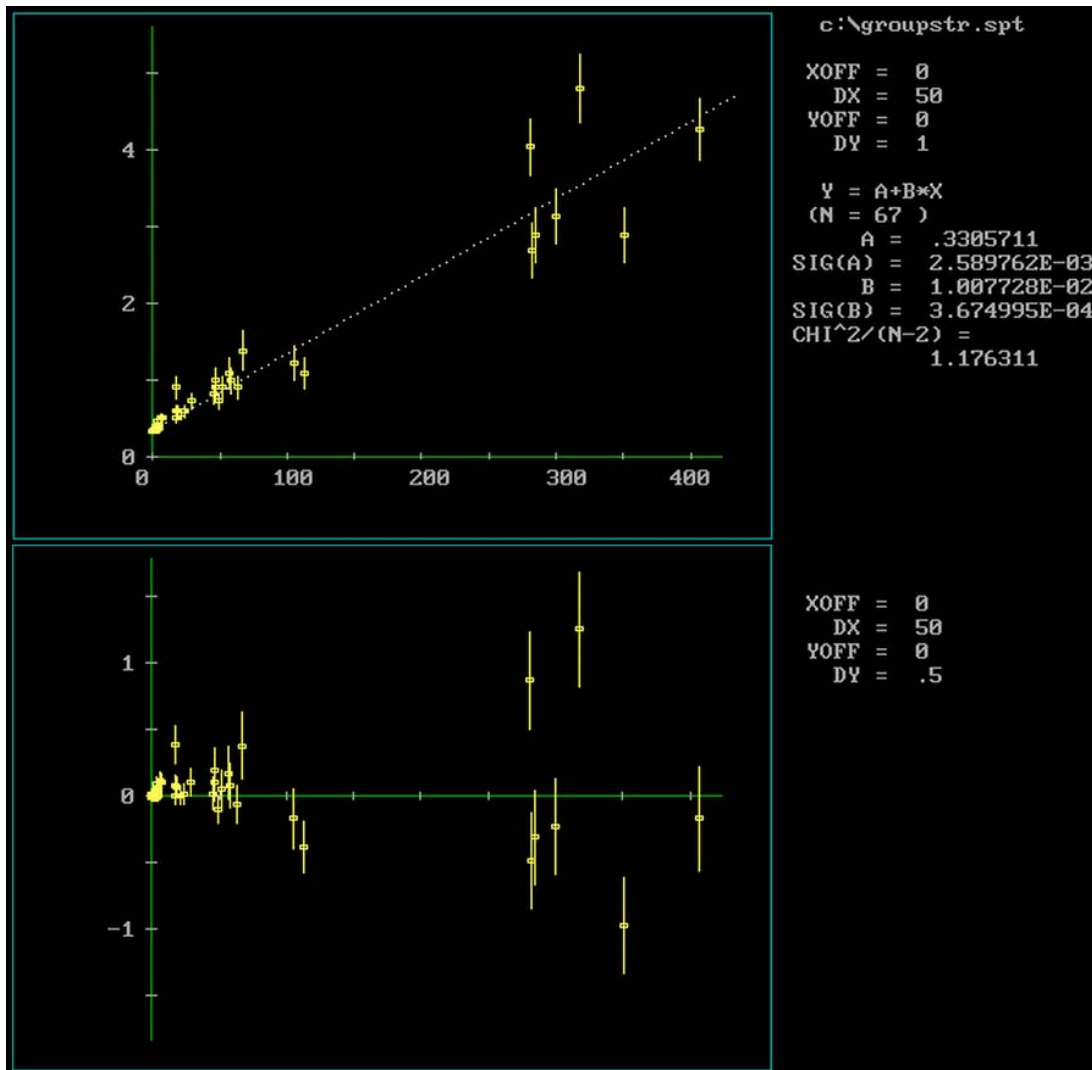
Figure 12: The fit to the grouped data and its difference plot.
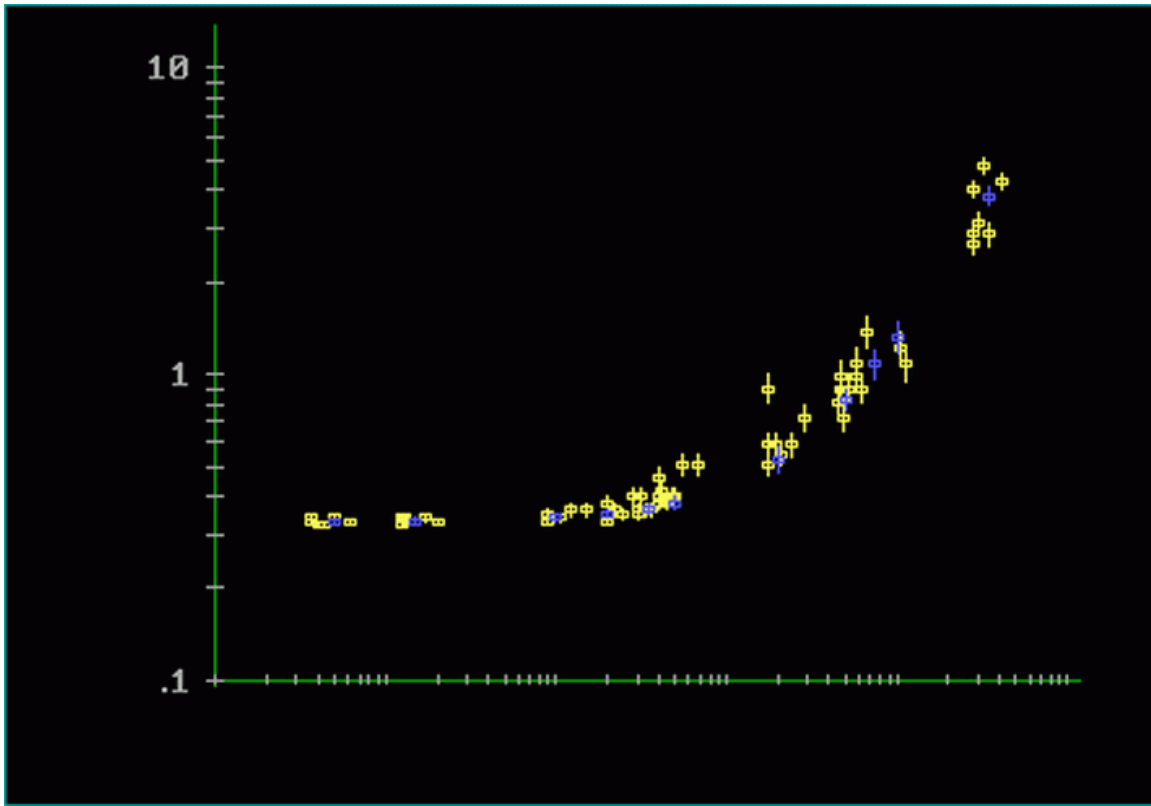
Figure 13: The grouped data (yellow points) plotted on a log-log scale for clarity. The blue points represent the fit and are not actual data.

VDL makes no claim that this would be the average fit for the general driving population, as there is no guarantee that we had a sufficiently random sample from that population. But neither would we be surprised if such a fit came close in its parameters to the above group fit.

Our data also was done with only one background luminance level, but given that we are operating within the Weber's law region, both in this experiment and in nighttime driving, as explained earlier in this section, it is likely that equation (9) would still be equally valid for all conditions of interest.

Unlike, *discomfort glare* a simple numerical score cannot be assigned to a glare situation involving *disability glare*. The threshold luminance necessary to distinguish a target, in the presence of glare, from a background would vary with the target. A different level of glare mitigation would be needed to allow a driver to see a pedestrian in dark clothing than in light-colored clothing for example. Since there are tradeoffs in glare mitigation such as cost and since complete removal of glare in all situations is impractical, the levels of threshold luminance necessary to distinguish objects in the presence of glare would have to be set by traffic authorities, with possibly different levels set for different situations.

Also, traffic engineers and transportation officials would have to decide whether to design against a worst-case scenario or an average case scenario. In other words, should something like Figure 11 be the operative curve or should Figure 12 be the curve against which standards are set?

Once those decisions are made however, implementation is fairly straightforward.[29] This is illustrated in Figure 14. Suppose that the fit line for the group above had been chosen as the "decision line" and that an object of 2 cd/m^2 had to be seen against a background of 0.305 cd/ m^2. A photometer centered on where the object would be (i.e. directly ahead of the driver) records the glare source in the field of view. The luminance image data is processed by our program to yield an L_P of 300. This result shows that the object falling at (300, 2) (red dot in Figure 14) will **not be seen** by the typical driver *because it falls below the "decision line"*. If glare mitigation is then estimated to decrease L_P by half and that indeed turns out to be the case (green dot) then the **object will be seen** by the driver *because it is now above the decision line*.
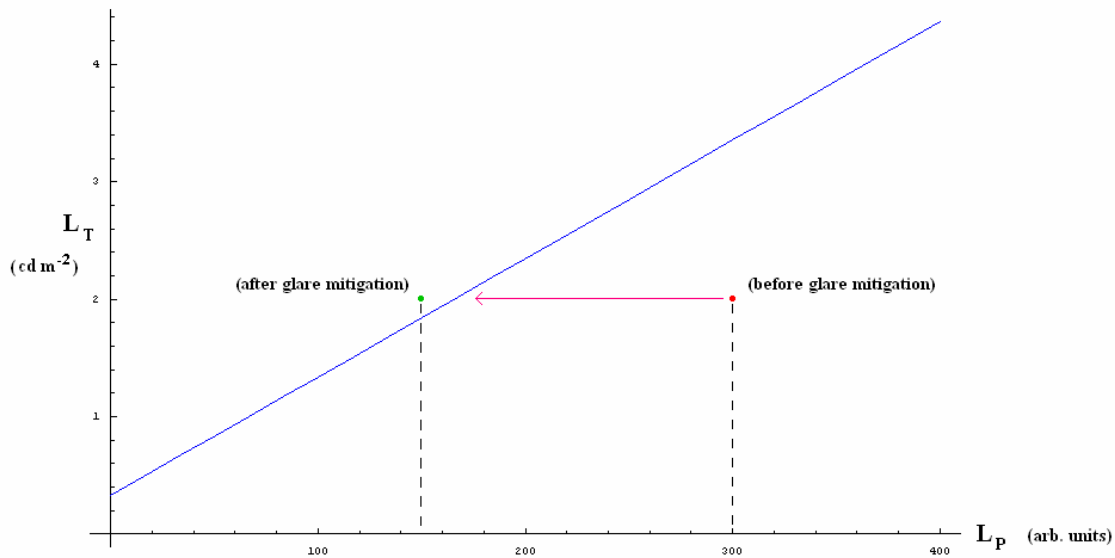
Figure 14: Illustration of how to know when and by how much disability glare must be mitigated.

The reader can see that a single "score" cannot just characterize a disability glare situation because one needs to know the luminance of objects needing to be seen. But once a "decision line" is agreed upon[30] by transportation authorities and the objects needing to be seen are identified, then a photometer along with our program (which is just an implementation of equation (6)[31]) can be used to decide if glare mitigation is required. The photometer can provide the L_T of the objects that need to be seen, the background luminance, and the input to the program to produce the value of L_P under a glare source. In practice, this will take more than one image.

---

[29] This assumes of course that challenges such as the scattering and dynamic range issues mentioned earlier have been met.

[30] Essentially this is a decision on the values of c and k to use based on how they fall out in the driving population. L_B can vary in different situations.

[31] This equation needs an age as an input. This is something else that traffic engineers, say, would need to decide.

4. Discomfort Glare Experimental Methods

We conducted a series of experiments with human observers to rate discomfort for various scenes displayed on a computer monitor with varying conditions of glare. Then we employed the Glare Meter Tool to acquire and analyze the images to estimate the magnitude of discomfort glare objectively. The results could then be compared to assess the accuracy of the Glare Meter Tool in estimating the magnitude of discomfort glare present.

On a computer monitor we alternated presentations of three different nighttime driving scenes. We introduced glare with a high-intensity white LED intended to simulate the headlights of an opposing vehicle. We presented observers with the various scenes, and varying intensities and eccentricities of the glare source, in each case asking them to rate the severity of the discomfort on the De Boer scale.

The three nighttime scenes were actual photographs taken from the driver's point of view with a digital camera and displayed on a computer monitor. The scenes were chosen to represent three different conditions of ambient illumination, two urban with ambient lighting, and one rural with no roadway lighting. In the two urban scenes, the driver's low-beam headlights were illuminated, and in the rural scene, the high-beam headlights were on. The scenes are shown in Figure 1.

Figure 1a. The first of two urban scenes presented to the observer.

Figure 1b. The second of two urban scenes presented to the observer.

Figure 1c. The rural scene presented to the observer.

The observer was asked to fixate straight ahead in his or her lane while the glare source was positioned at one of three different positions horizontally removed toward the left with respect to the direction of gaze. The glare source could also be varied among three different levels of intensity. The luminance of the glare source at each intensity level and the eccentricity of the glare source are fully described in appendices B and C. For each scene, each position of the glare source, and each intensity of the glare source, the observer was asked to rate the discomfort on the **De Boer Rating Scale for Evaluation of Discomfort Glare**, shown below. Thus for each observer, 27 separate De Boer ratings were obtained.

<div align="center">

9 Unnoticeable

8

7 Satisfactory

6

5 Just Acceptable

4

3 Disturbing

2

1 Unbearable

</div>

A photograph of the experimental setup is shown in Figure 2.

Figure 2. Experimental setup for the discomfort glare experiment. In the actual experiments the room was darkened and the glare source, which can be seen near the left edge of the display, was activated.

Figure 3 shows the experiment in progress, with the three scenes respectively, and the glare source illuminated in each case.

Figure 3a. Observer is viewing the first of the three scenes, with the glare source in the intermediate position at low intensity.

Figure 3b. Observer is viewing the second of the three scenes with the glare source in the position closest to the direction of gaze and set to medium intensity.

Figure 3c. Observer is viewing the rural scene where there is no roadway lighting. The glare source is at high intensity and in the position closest to the direction of gaze, simulating hi-beam headlights of an opposing vehicle.

5. Discomfort Glare Analysis and Results

As mentioned previously, *disability glare* is the more relevant of the two main categories of glare when road safety is the primary consideration. If only one type of glare meter could be had, then a measure of disability glare would take precedence over that of discomfort glare.

Nonetheless, a glare meter tool for *discomfort glare* is useful for three reasons: 1) while disability and discomfort glare are distinct in concept they obviously are correlated; a situation of high discomfort glare is likely (but not certain) to have high disability glare as well; 2) discomfort glare scores (typically the De Boer scale) have been used historically in many instances, including street lighting and headlight glare[32]; 3) discomfort glare can be assigned a single score unlike the more complicated case of disability glare. A discomfort glare measure can serve as an adjunct to a disability glare "score", especially since both types of glare can be quantified from the same photometric image.

As detailed in the previous section, for each of the three scenes the LED simulating the opposing headlight glare was in one of three positions and had one of three intensity settings. This gives rise to $3 \times 3 \times 3 = 27$ scenarios that subjects had to rate on the De Boer scale.

Ideally this would equate to twenty-seven photometric "images" that could then be immediately processed by computer program to yield twenty-seven numeric scores that could then be compared to the ratings by the subjects. In practice, the path to a glare meter tool didn't turn out to be nearly this simple, for a number of reasons.

First and foremost, the dynamic range of the photometer is limiting; this requires some explanation. While the VDL staff finds the *Radiant Imaging PM-1613F-1 photometer* to be a superior product with a greater dynamic range than many comparably priced photometers, its 16-bit dynamic range ($2^{16} = 65,536$ possible values) still proved to be less than is needed for a "one-shot" (simultaneous) measurement of both a high-intensity glare source and the associated background scene (e.g. a nighttime highway environment).

In advance of ordering the imaging photometer, we had made preliminary measurements using a handheld spot photometer to evaluate nighttime scenes which included glare sources. These measurements indicated we might succeed in being able to make a single exposure that would encompass all elements of the scene with an instrument with 16-bit dynamic range. However, there proved to be difficulties owing to limitations of the technology, specifically CCD signal digitization issues at the low end of luminance, and difficulties in avoiding CCD blooming and optical scattering at the high end. The preliminary estimates with the *spot* photometer, whose sensor takes in only one measurement at a time, did not take into account that a *video* (or *imaging*) photometer must take in a range of values *simultaneously* over the face of its sensor (a CCD). In other words, the problem comes about because different parts of the imaged field can have very different values of luminance.

---

[32] De Boer, J. B. and Schreuder, D. A. (1967). **Transportation Illuminating Engineering Society** (London), **32**, 117.

If the photometer's CCD is to remain unsaturated[33], as it should, then the maximum luminance value to be recorded should not exceed the limit of the dynamic range. For example, on its highest setting the LED has a luminance value as high as $3 \times 10^6 \, cd \, m^{-2}$ within its field. Thus the step size in this case would be that peak value divided by 2^{16} or a minimum of $3 \times 10^6 / 6.5 \times 10^4 \approx 46 \, \text{cd m}^{-2}$. But 50 candelas per square meter is a typical number that might be seen in a reasonably well-lit room at night.[34] A darkened roadway, median strips, foliage at the side of the road, etc. are all going to be at luminance values much less than this. Consequently, *most of the scene*, except for illumination sources, *would all get assigned to one numerical value*, <u>destroying any differential luminance in the scene that is below the step size</u>. This is an extreme example of what is known in electrical engineering parlance as *quantization noise*.

Conversely, setting the maximum of the photometer's range to any luminance value in a typical nighttime roadway scene *without* the glare source, such that the darker elements in the scene were clearly imaged, would cause the immediate saturation of the photometer once the glare source is introduced. Thus, any attempt to *simultaneously* capture the photometric image of both the glare source and the corresponding scene was doomed to suffer too great an information loss about the scene or the glare source. While this limitation did not impede analysis of the laboratory experiments, it does have the result that in any field situation, multiple exposures would be required to produce the requisite image. This would have the effect of reducing the practicality of the glare meter since only stationary scenes could be analyzed until such time as imaging photometers with higher dynamic range become available.

Thus, in the lab experiments, two separate photometric images are required for each trial, and these must be combined. Now this superficially seems like less work since only 12 components are needed to produce the full 27 composite photometric "images" -- 9 of the LED glare source (3 intensities at 3 positions) and 3 of the background scene. While it is true that only 12 images are needed to generate the conditions corresponding to the 27 trials for each subject, the combining operation is more difficult than simply generating a single image. Furthermore when using tristimulus values (which include luminance) as well as luminance alone in the analysis, the number of conditions balloons to 81 (each of the 27 scenarios mentioned for each of the 3 tristimulus variables—usually denoted X, Y (equivalent to luminance) and Z).

Several complications arise when combining luminance (or tristimulus) "images". Each "image" is exported by the *Radiant Imaging* software as an array or matrix that is 1020 x 1020 where each entry is a numerical value written in ASCII text and separated by a space from the next entry. In other words, the "image" is a 1020 x 1020 space delimited ASCII table. Since the luminance (and for that matter other tristimulus values) is so much greater for the glare source, even on the lowest intensity setting, than it is for the rest of the scene, in theory the two matrices

---

[33] For the reader unfamiliar with this, s*aturation* is when the magnitude of a stimulus or quantity being measured exceeds the maximum possible reading on the recording or measurement device. In the case of old analog dial gauges this is known as "pegging the meter" because the pointer arm of the dial moves beyond the printed scale and is only halted by the 'stops' or pegs that prevent mechanical damage to the pointer. In the present case, saturation will typically happen only in the neighborhood of those pixels of the CCD imaging the brightest source. Nonetheless, it is quite undesirable for obvious reasons.

[34] For comparison, light-colored walls with bright, diffuse reflections that are near the light source in the room might be on the order of 100 cd m^{-2} and, exclusive of the light fixtures and sources themselves, nothing in the room is likely to exceed 150 cd m^{-2}.

representing the "images" could just be directly added. After all, a glare source of 20,000 cd/m^2 added to a dark scene portion of say 8 cd/m^2 gives 20,008 cd/m^2, which is a small error.

This idealized procedure fails to account for 1) glare scattering in the photometer (owing to both saturation of the CCD as discussed above, and to scattering within the lens of the instrument), 2) noise cancellation procedures, and 3) alignment.

As mentioned previously, the photometer optics can scatter the glare source light giving rise to large luminance (tristimulus) values at places in the CCD "image" where the glare source is not present. Adding 20,000 to (say) 8 where the value should really be 20,000 makes a relatively small error, but adding 20,000 to 8 where the value should be 8 is an error of gigantic proportions. Thus the glare source "image" had to be circumscribed. This was done by reviewing each glare source image as *seen* with the *Radiant Imaging* software and noting which CCD pixels "really" constitute the glare source. Any values at pixels within the glare source boundary were retained and any pixels falling outside the glare source boundary *were set to zero*. This situation is equivalent to the instrument itself actually suffering from "disability glare". Clearly this procedure is a big burden for any practical glare tool.

In order to attain the highest resolution possible in the photometric image, the photometer and its controlling software use *noise cancellation procedures*. A given scene is imaged and then it is retaken with the *shutter closed*. This latter "dark image" is then subtracted from the former, matrix entry by matrix entry, or pixel by pixel if one prefers to think of it that way. The theory is that the dark image will contain only instrument noise and that subtracting it from the image of the desired scene will then leave only "signal". This is essentially correct but it comes with a complication.

Since noise, by definition, has statistical fluctuation over time, the noise value at one pixel may be greater than at another pixel at a given moment, even if the time averaged noise value of both pixels should be the same. Alternatively, a given pixel can have different noise levels at different times, even if it is receiving the same signal in both instances. Thus consider a scene with low light levels (e.g. a dim highway away from the glare source). It may happen that the signal value (the "true" light level at that pixel) is very small and so, say, is the noise level at that pixel at that moment. Then suppose that the noise at that same pixel during the "dark image" capture fluctuates to a comparatively large amount. At that particular pixel, the final, recorded entry after noise 'cancellation' becomes "small signal value" + "small noise value" – "large noise value" which can be negative. Now negative luminance, indeed negative tristimulus, value *is physically impossible*.

Negative entries in the photometer data are thus a sign that the light intensities, at least in some portion of the imaged field, are very low and comparable to the noise levels. Now, the "dark image" noise cancellation procedure can be dispensed with, but then the light levels in the dim portion of the imaged field are *all* recorded too high. Finer grained resolution can only be had at the expense of saturation in the brighter portions of the field. Thus the only practical recourse, and the one that VDL staff took, was to set all negative entries to zero by fiat. This procedure can be automated and is much less of a burden than the scattering problem mentioned above. It is nonetheless an additional, necessary step that surfaces in a practical implementation of a glare tool, one that might not occur to someone only considering a glare tool more abstractly.

The problem of alignment would not normally be present. Even though the luminance image of the glare source (LED) and of the scene (video monitor) need to be taken at different times by the photometer, the photometer would be held in place by a tripod at the appropriate place and the lab glare source just turned off for the image of the scene. Nevertheless, care must be taken to insure no movement of the apparatus when multiple exposures are involved, or complicated post-exposure spatial shifting algorithms would have to be implemented.

The reader can therefore see that before any "glare score algorithm" can be implemented or even tested, separate images must be taken of the glare source and roadway scene, photometer data must be exported for processing, negative values must be "zeroed out", alignment issues (if any) must be dealt with, and the separate images properly combined to yield 27 luminance data files or 81 tristimulus data files. This is a lot of preliminary processing before the heart of the "glare meter" can be invoked!

That central conception, the glare score algorithm, depends critically on answering the following question. How does one connect what is essentially a *subjective* and *psychological* impression, the De Boer glare score, to photometric measurements (luminance and/or tristimulus)? VDL's original proposal addressed a potential method for identifying and delineating the glare source, but it remained to the development phase of this project to perfect the methodology.

Formulae connecting situational geometry and luminosity to De Boer scores have existed for a while, but they have an *ad hoc* quality to them. A lot of the quantitative work on *discomfort glare* does not even mention the De Boer scale. The broader approach has been to define a "Discomfort Glare Index" (denoted "*GI*", and hereafter generally referred to simply as "Glare Index") in the form[35]

$$GI = \sum_{sources} \frac{L_S^a \, \Omega^b}{L_B^c \, p(\theta)} \tag{1}$$

where

L_S = *glare source luminance*

L_B = *background luminance*

Ω = *solid angle of the glare source (steradians)*

p = *position factor*

θ = *angle from glare source to observer's line-of-sight (degrees).*

The "background" here is <u>not</u> the general background other than the glare source, but rather it is the area of the scene immediately surrounding the direction of gaze. How this is specifically determined in the present case is explained below.

The angle θ is measured between the observer's line-of-sight ("dead ahead") and a line from the observer to the centroid of the glare source. The centroid (luminance-weighted center of the

---

[35] From **Reflections on Glare**, *Johannes J Vos* in **Lighting Res. Technol.** 35, 2 (2003) pp. 163-176.

glare source) is used because the glare source in the general case is extended and non-uniform rather than a point source. The angle in the present case is assumed to always be non-zero; in other words, the glare source is **never** directly in line with the observer's gaze.

The position factor represents the geometry of the situation and should be monotonically increasing with increasing θ. Since p is in the denominator this means that the glare index *decreases* with *increasing* angle, in accord with one's expectations.

The sum in equation (1) is over all glare sources. Since the variables involved in the summand are raised to powers (that don't usually equate to one), the sum is "nonlinear" over the sources. Thus, unlike with disability glare, the discomfort glare index of a single, extended glare source does **not** equal the glare index of that same source when it is considered as a collection of its conjoined constituent parts, each part being a "source". Clearly this formula must break down at some point since a union of multiple, barely separated sources would scarcely be distinguished from a single large contiguous source covering the same region and yet the two cases could give very different glare indices. Therefore the unstated assumption for validity of this formula is that there are a few widely spaced glare sources in the field of view.

This *nonlinearity* in the case of *discomfort* glare is in sharp contrast to the *linear* behavior of *disability* glare. In the former case, source boundaries must be identified, background areas must be identified, centroids must be computed, and thus *groupings of pixels* must be treated as a cohesive unit. In the latter case, on the other hand, computations can be done *pixel-by-pixel* and then summed over all pixels, as was seen in the earlier section on disability glare analysis. Therefore not only is disability glare more relevant to road safety issues, but given the same photometric data, computations are simpler than for discomfort glare (at least in theory).

There are two final, important, general observations to be made about equation (1): First, there are other potential "contenders" for a glare index formula. Second, other than implicitly using the photopic response curve, $V(\lambda)$, in the (unstated) definition of luminance, the formula has no dependence on color or wavelength.

Many possible formulas quantifying discomfort glare exist[36]. In fact, there are too many of them. In 1979, Einhorn[37] said,

> "There are appreciable fundamental discrepancies
> between existing systems, probably caused by the difficult
> interpretation of observations which in the nature of our
> subject show large statistical variations. …One cannot
> expect a very close agreement with any particular system in
> all practical cases. Fortunately, high precision is not
> necessary."

---

[36] **Discomfort Glare Indices: A Comparative Study**, *M. Rubiño, et. al.* in **Applied Optics** vol. 33, no. 34 (Dec. 1, 1994) pp. 8001-8008.

[37] **Discomfort Glare: A Formula to Bridge Differences**, *H.D. Einhorn* in **Lighting Res. Technol.** 11,2 (1979) pp. 90-94.

At one time or another there have been the VCP, BGI, CGI, GCM, CBE, and Schmidt-Clausen and Bindels' equation[38]. There are probably others of which we are unaware.

In any event, there does not seem to be only one standard expression with universal agreement. To the extent that the answer to the question has "settled" over time, the *form* of the equation seems to be fairly common and widely utilized. But even here, the exponents a, b, c are not agreed upon. Vos remarks that the American 1978 IES Handbook has $a/b \approx 5$ while Einhorn gets $a/b \approx 2$. Vos also says that the CIE gives a/c values of 1.3/1.0 and 1.6/1.0 while the IES handbook has 1.0/0.44. How VDL resolved these discrepancies is explained below.

The other difficulty, as already stated, is the formula lacking a dependence on color, other than that implicit in the photopic curve defining luminance. This *is* a problem because while *disability glare* <u>doesn't depend on color</u> (modulo the photopic curve), *discomfort glare does show a dependence on color*[39]. To quote from the aforementioned reference (Van Derlofske, et. al.),

> *"Thus conventional photometry based on luminous intensity using the photopic efficiency function appears to be appropriate for characterizing disability glare from headlamps.*
>
> *The same is not true for discomfort glare. Two sources having the same standard $V(\lambda)$ photometric properties will not necessarily produce the same amount of discomfort."*

This is reflected anecdotally in the many objections one hears concerning the subjective glare resulting from the increasingly common xenon-plasma high-intensity discharge (HID) headlights on some imported automobiles. The authors noted however, that the spectrum of the glare source had much less effect on discomfort than did the source's luminance.

Given that this is relatively recent (2004) work and that, as just mentioned, discomfort glare score formulae involving luminance measurements have not produced a definitive standard (after decades of research), it should come as no surprise that there doesn't seem to be any formula in the literature that is akin to equation (1) but that uses all three tristimulus values in place of luminance alone.

The VDL staff viewed the development of the glare meter as an "engineering" mandate rather than a "psychophysics" mandate; in other words, we developed the glare meter tool using the *currently available knowledge* about glare, but did not seek (nor are we presently equipped) to conduct the very extensive, fundamental, psychophysical experiments needed to characterize discomfort glare quantitatively in terms of color effects. The sole exception is, of course, our use

---

[38] See the previous two footnotes, and **A Review of Disability and Discomfort Glare Research and Future Direction**, *R. Gibbons and C. Edwards* presented at the 18th Biennial Transportation Research Board Visibility Symposium, April 18, 2007. A pdf copy of this article can be downloaded (at least as of 12/16/08) at http://tti.tamu.edu/infofor/conferences/vs/program/papers/gibbons_edwards.pdf.

[39] **Headlamp Parameters and Glare**, *John Van Derlofske, et. al.*, presented at Society of Automotive Engineers World Congress & Exhibition, March 2004. This reference is available at SAE Publications as **Document Number:** 2004-01-1280. The website, with abstract, is at http://www.sae.org/technical/papers/2004-01-1280.

of tristimulus values as outlined in a later section and even there, the purpose was to identify the glare source and not for explicit computation of the glare score with tristimulus values.

We approached the final iterations of equation (1) with the same viewpoint. If literally decades of research around the world had not settled on a universal standard for the discomfort glare score formula, then we could hardly settle the question definitively with our modest resources. Furthermore, as both Vos and Einhorn point out, the nature of the subject does not admit great precision. Thus within the guidelines already alluded to (e.g. a > b in equation (1)), we felt some freedom to see what exponents and position factor worked best in computing *GI*.

At this point we took two parallel paths in computing a glare score with the aim of ultimately deploying the methodology which demonstrated the better results. Both used a form of equation (1), but differed in both details of the equation, and, more prominently, in how the image was processed prior to applying the equation. In the first method, the position factor was dealt with empirically and taken to be a power law in angle θ following the mathematical form of the other variables. These individual variables were given a multilinear regression to determine the exponents, and the glare source identification was rather unsophisticated but straightforward.

In the second method, the position factor took the form specified in the *EnergyPlus Engineering Reference* (see Appendix J). The individual variables were not fit but rather the exponents were taken from Vos, an overall scale factor was fit from the observers' data, and the glare source identification was achieved by means of the complex methodology outlined in the original proposal for the project and fully described under the heading "Method 2", below.

Method 1

Before examining the algorithm used to compute the Glare Index (*GI)* in equation (3) below, it is important to answer that critical question posed earlier: How does one connect *GI* (luminosity measurements) to the De Boer scale? Although relatively straightforward to answer, that connection hadn't seemed to be forthcoming until Vos answered in 2003[40].

> *"One may wonder why such a completely different type of formula should govern a very much related type of visual discomfort, and the only explanation I can give is that the two formulae stem from different and hardly overlapping interest groups, each with its own history."*

Vos is referring to interior or architectural lighting groups, on the one hand, and those concerned with roadway lighting, on the other. He proceeds by noting the numerical values typical in the two scales. Referring to the De Boer scale as a "Glare Control Mark" (denoted *GM*, and hereafter generally referred to simply as Glare Mark) he finds the following correspondence.

---

[40] **Reflections on Glare**, *Johannes J Vos* in **Lighting Res. Technol.** 35,2 (2003) pp. 163-176.

$$GM = 1 \quad \Leftrightarrow \quad GI = 600$$
$$\textit{(bad)} \qquad\qquad \textit{(just intolerable)}$$

$$GM = 9 \quad \Leftrightarrow \quad GI = 8$$
$$\textit{(excellent)} \qquad \textit{(just perceptible)}$$

This means that whatever exponents or position factors are chosen in equation (1), one would typically get a *GI* score of several hundred in a very bad glare situation and a *GI* score of just a few in a good situation. Here he is also saying that *a low GM (De Boer) score corresponds to a high GI and vice-versa*.

He then observes that as one scale increases arithmetically the other decreases geometrically. In other words, one is the exponential of the other with a minus sign to flip the direction of increase. He suggests looking at something like,

$$GI \overset{?}{\sim} 10^{-GM}, \tag{2}$$

but this is not quite right because changing from 10^{-1} to 10^{-9} is eight orders of magnitude while the corresponding change in *GI* should be about two orders of magnitude (600 to 8). However, to match a change of eight orders to two simply requires dividing by four in the exponent. Thus,

$$GI \sim 10^{-GM/4}. \tag{3}$$

This last equation is only meant to model the functional behavior. To make a true equality out of this expression can still require an overall scale factor. Vos notes that this constant can be put into the position factor (if desired).

In our first method we did something almost the same. For reasons already discussed we felt some latitude in taking the angular dependence (position factor) as a power law. Furthermore, some discomfort glare formula, although not altogether of the form of equation (1) (e.g. Schmidt-Clausen and Bindels' equation), have θ dependence as a power law, and, as we've seen, *disability glare* can have a power law dependence in angle.

We thus took position factor as a simple power law in θ, but put the scale factor on the right-hand side of equation (3). Therefore we have combining equation (1) and equation (3),

$$GI = \sum_{sources} \frac{L_S^a \, \Omega^b}{L_B^c \, \theta^d} = K \, 10^{-GM/4}. \tag{4}$$

The scale factor "K" should be on the order of 1,230 because $600 = K\, 10^{-\frac{1}{4}} \Rightarrow K = 1067$ and $8 = K\, 10^{-\frac{9}{4}} \Rightarrow K = 1423$ using the scale correspondence outlined above.

With only one source (the LED) and letting "log" stand for the *common* logarithm, we have, by taking logs of equation (4):

$$GM = 4\log K - 4a\log L_S - 4b\log \Omega + 4c\log L_B + 4d\log \theta. \qquad (5)$$

If K is 1,230 (the geometric mean of 1067 and 1423) and if we set,

$$
\begin{aligned}
x_1 &\equiv \log L_S, & \alpha &\equiv -4a \\
x_2 &\equiv \log \Omega, & \beta &\equiv -4b \\
x_3 &\equiv \log L_B, & \gamma &\equiv 4c \\
x_4 &\equiv \log \theta, & \delta &\equiv 4d
\end{aligned}
\qquad (6)
$$

then equation (5) gives,

$$GM = 12.4 + \alpha\, x_1 + \beta\, x_2 + \gamma\, x_3 + \delta\, x_4 \qquad (7)$$

which is just a *linear* expression in the *logarithm* of the original variables that yields the De Boer score (*GM*). *This last equation then is the answer to the critical question posed earlier.*

There are of course two problems arising out of this. The coefficients are undetermined and the question arises, just how well does this expression *really* agree with the De Boer ratings (which are subjective)? The answer to both problems is to fit equation (7) against the De Boer ratings of the subjects and (the logs of) the quantities L_S, Ω, etc., the latter being determined by our first glare score algorithm (Method 1).

This algorithm consists of 5 parts, each of which will be discussed in turn:

       a. Identifying a potential glare source [maximum luminance]
       b. Finding the boundary or perimeter of this glare source [lower bound and contour-finding]
       c. Computing a centroid location from this source
       d. Computing the solid angle of this source
       e. Identifying a background area.

Glare source identification and delineation are the primary ways in which this algorithm is different from that of the second method. In Method 1, the (preprocessed[41]) "image" matrices

---

[41] See the discussion on page 41.

containing the luminance values for each pixel of the photometer's CCD are read in and searched for the highest value (entry). The computer program *assumes* that this comes from the glare source.

This maximum luminance then has a factor by which it is multiplied, depending on its value. This is shown in Table 1.

If max luminance is greater than:	But less than:	Multiply by:
10^5	--------	0.005
5×10^4	10^5	0.01
2×10^4	5×10^4	0.02
10^4	2×10^4	0.05
--------	10^4	--------

Table 1. Glare source cutoff determination values (all luminance in candelas per square meter).

The idea here is that any *headlight* glare source is unlikely to be much above a couple million cd/m^2 comparable to our LED's highest setting (even if close to an observer on high beams) and is unlikely to be perceived as glare if it is below ten thousand cd/m^2. (The program stops if there is no luminance above this latter number.) The multiplication factor then yields a *lower bound* of several hundred candelas per square meter. This process provides some "headroom" between this lower bound and, say, the maximum luminance of a storefront sign or streetlight, which may be perceived as "bright" but is unlikely to be considered a source of glare.

There is also an implicit assumption here concerning the distribution of luminance within a glare source. In principle, a glare source *could* be uniform in spatial distribution with a sharp cutoff at its boundaries and then it could be "perfectly" imaged (diffraction limited) by the photometer. In practice, this doesn't seem to be the case. In any event, the contour-finding method (discussed next) can interpolate between pixel values and seems to have no problem with finding a contour based on this *lower bound* method.

The computer program used to implement this process is written in MATLAB™ and shown in Appendix H. MATLAB is a high-level programming language that is geared to numeric processing and mathematics in general[42]. Fortunately, MATLAB comes with a built-in command (coded algorithm) called "contour" that can find level contours in among a matrix of values.

The luminance matrix ("image") can be thought of like a topographical map, with each luminance value being a height. The row and column designation for each matrix entry (i.e. an (x, y) position) can be thought of as longitude and latitude. For every longitude and latitude (matrix entry) there is a height (luminance). On a topographical map one finds contours denoting curves of constant height. The same thing can be done with the luminance matrix; a set of pixel positions (matrix entries) can be found that form a closed curve of constant luminance. Of course, the topographical map represents (in principle) a continuum of heights and positions and the corresponding variables in the matrix are discrete. Fortunately, grubby details like

---

[42] The interested reader can visit the associated website: http://www.mathworks.com/ for further information.

interpolation and approximation of the continuous by the discrete are taken care of by the inner workings of MATLAB. This is probably made easier by the large (1020 x 1020) size of the luminance matrix.

The "contour" command can be made to find contours corresponding to only one luminance value; in the present case that number is the *lower bound*. The idea is illustrated in Figure 4.

This figure represents the luminance "image" of the glare source *and the associated monitor scene* in false color.
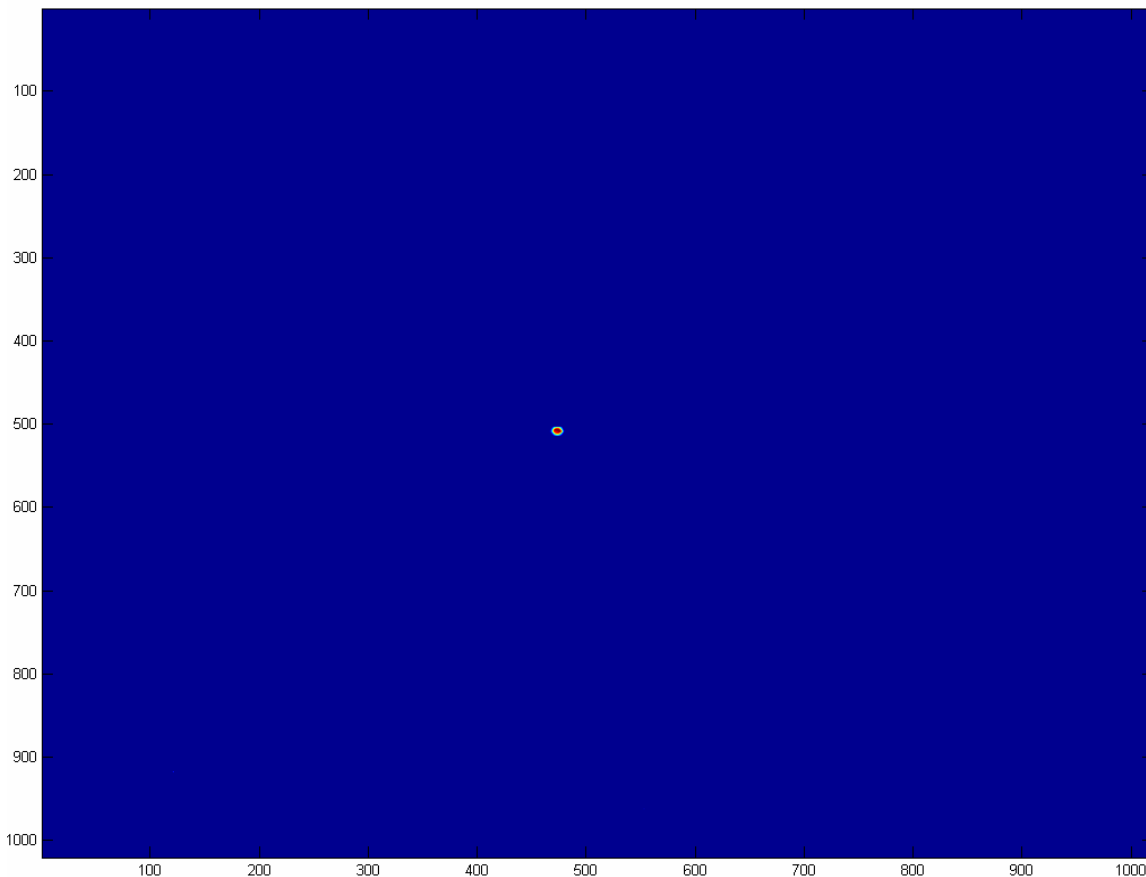
Figure 4. The luminance composite matrix of the glare source *and the monitor scene* shown in false color (scene 1, LED position 3, LED intensity—high). Only variation in the LED luminance can be seen.

The reason that the monitor scene is not visible in this figure is for very similar reasons to the argument given earlier regarding saturation of the photometer and the need for combining LED and monitor scene luminance images. The video display on a computer (from which this figure comes) typically has 256 representable gray levels for a grayscale image or 256 levels each for red, green and blue in color pictures. The reader will recall that the step size is set by dividing the highest number represented by the number of levels. Well, the highest number represented is the approximately three million candelas per square meter on the LED for its highest setting. This means that the step size is so large that any luminance variations below that step size are lost to viewing; one number on the video raster represents them all. Thus <u>only variations within</u>

the LED are seen (if viewing this document electronically the reader can enlarge the figure to see the variations). The remainder of the field is a constant color.

The monitor scene information is still in the luminance matrix of course; it is just the matrix's video representation that loses it. An image that can show both the LED and the monitor scene can be had with a trick. This is seen in Figure 5.
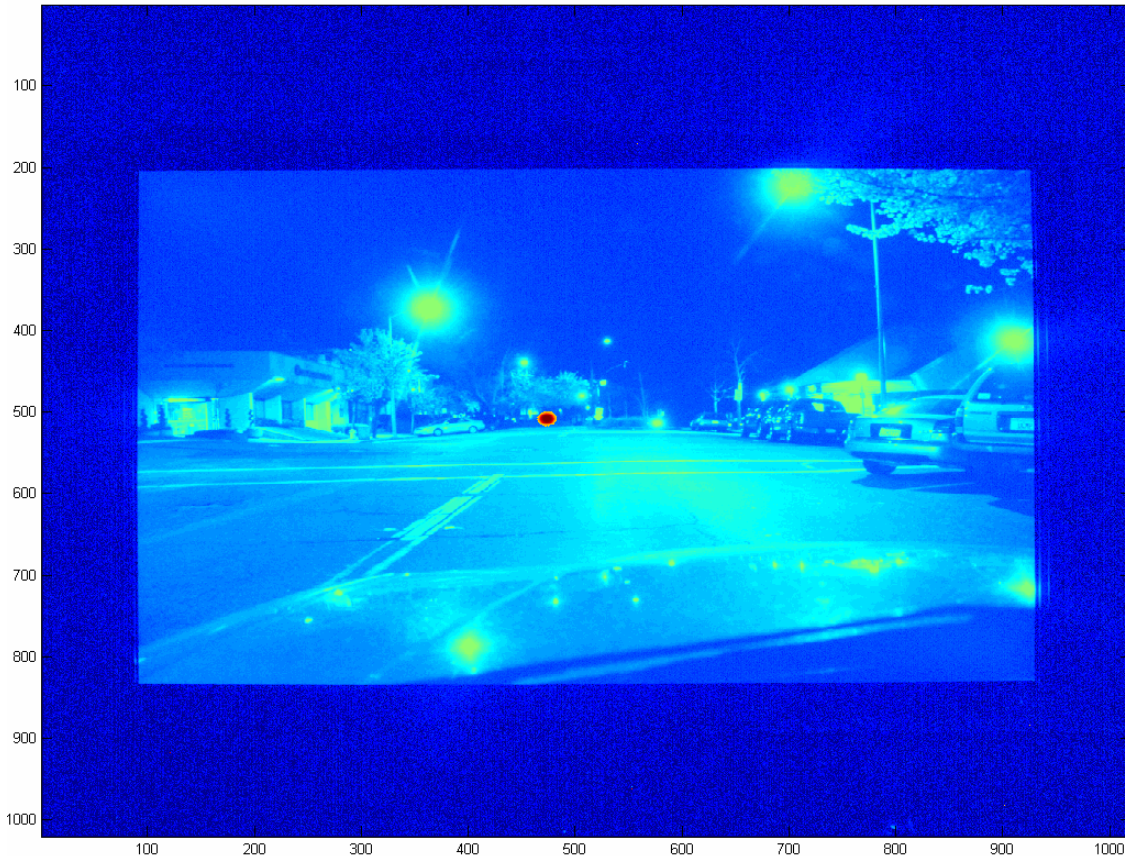
Figure 5. The false color image of the luminance composite matrix with the matrix entries replaced by their logarithms (scene 1, LED position 3, LED intensity—high). The monitor scene is now visible as is the LED (the reddish blob towards the center).

The composite (LED plus monitor scene) luminance image can be transformed by replacing every luminance value with its logarithm, except if that entry is set to zero. In that case a zero value is replaced by 0.01 before taking the log, lest a computational error occur. This transformation makes the step size in video representation smaller in comparison to the variation in luminance (now really log luminance). Thus we can see both the scene and the glare source.

Running the "contour" command in MATLAB on the (original) luminance matrix and only displaying a single contour (namely the *lower bound* discussed above) results in Figure 6.
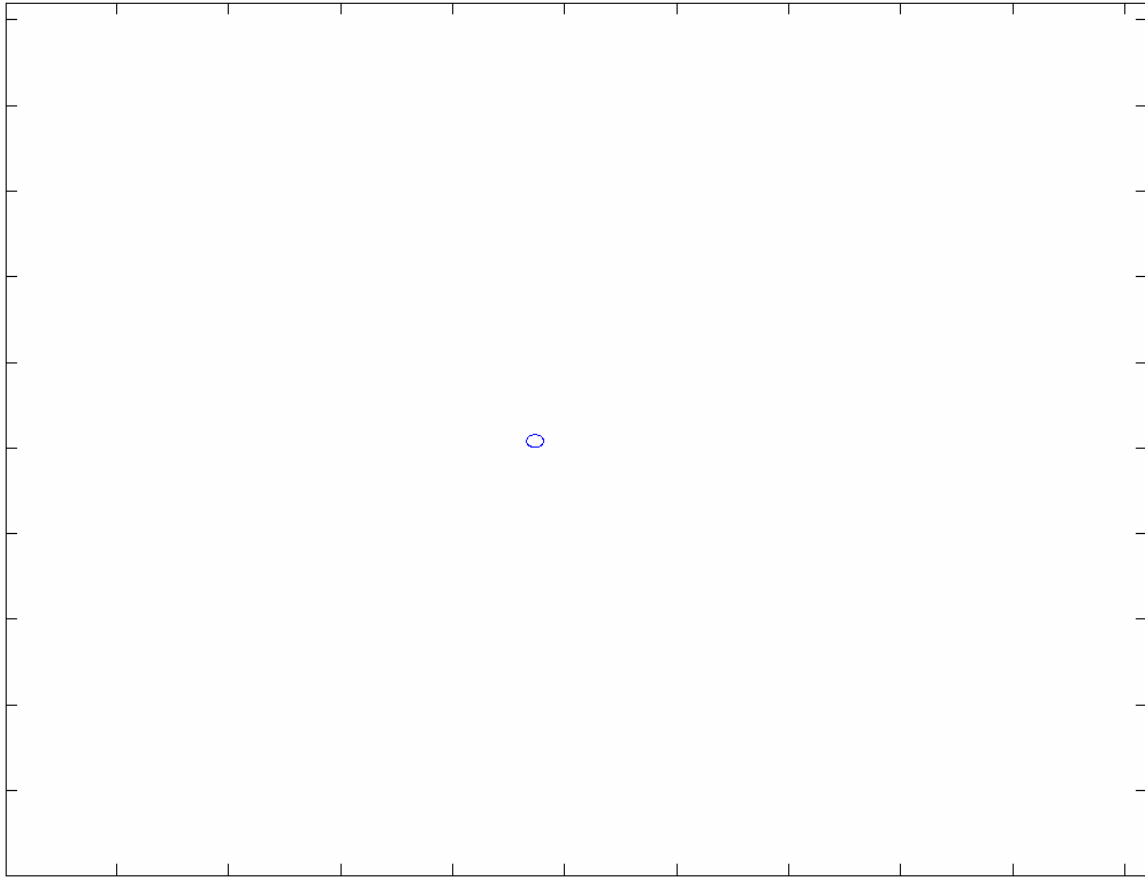
Figure 6. The *lower bound* contour of the LED (glare source) in the previous two figures. This ellipse is taken as the boundary or perimeter of the glare source.

This figure shows the essential challenge in computing *GI* (and hence *GM*)—how does the computer program "find" the glare source? By examining these last three figures, all originating from the same luminance matrix, the reader will see that the "contour" command seems to do a pretty good job.

The "contour" command never failed to find the contour associated with the *lower bound* of the LED (glare source) but a different problem arose. As mentioned earlier, scattering of light from the glare source *within the photometer optics* was a problem. We dealt with it by circumscribing the glare source before combining with the monitor scene, but in at least one of the trials a couple of pixels with very high luminance and widely separated from the glare source remained for some reason. Now one would think that a single (say) "stray" pixel with an abnormally high luminance is not a problem since there are 1020 x 1020 or 1,040,400 pixels overall. But the "contour" command in MATLAB doesn't differentiate. Thus a single very high luminance pixel in an otherwise dim background gets a contour curve of 8 pixels, namely its eight nearest neighbors on a grid.

Rather than redo the composite process (combining LED and monitor scene), the program was amended to simply choose the largest contour[43]. The reason for mentioning this seemingly insignificant detail is that "real world" glare is likely to have multiple sources (e.g. two distinct headlights or several sets of headlights) and simply choosing the longest curve won't suffice. Maybe even choosing the four longest curves won't suffice. One would have to have a cutoff in curve size, etc. One can see that isolating each glare source and removing light scatter from the instrument record rapidly becomes impractical. Thus this method of glare source identification, while straightforward and computationally quick, would need significant modification to become robust outside the laboratory.

With the boundary of the glare source identified the software searches the list of contour curve points to find those with the highest and lowest row (y) and column (x) values. The four points represented by the combinations of these coordinates form the corners of a rectangle. This rectangle is a *bounding box* for the glare source border. This is seen in Figure 7.

This figure comes from the same trial as the previous ones (scene 1, LED position 3, LED intensity—high). Only the glare source boundary (seen in blue) and the *bounding box* (seen in magenta) are shown.

The bounding box allows efficient integration in rectangular coordinates. A double, nested loop is set up. The outer loop in x or column number runs over the rectangle's width while the inner loop in y or row number runs over the rectangle's height. Within the loops a determination is made on whether the matrix entry is less than the *lower bound* value. If it is less than this value on the boundary of the glare source, then it is ignored[44]. If is greater than or equal to the value on the boundary, then the matrix entry and its position are included in various sums representing the luminance, the centroid, the solid angle, and the number of glare source points.

---

[43] In fact, this process itself is a non-trivial task but it is simpler than redoing the composite "image". In brief, the program sorts through the contour matrix generated by the "contour" command in MATLAB and extracts those points (matrix entries) corresponding to the longest contour curve. For the devil in the details, the interested reader can see the MATLAB Function Reference "contourc" in the MATLAB Help Browser, specifically under the section "Remarks".

[44] The inherent assumption here is that a given glare source is what the mathematician's call "simply connected". In other words, the glare source cannot be an annulus for example. That is very unlikely for any (single) headlight.
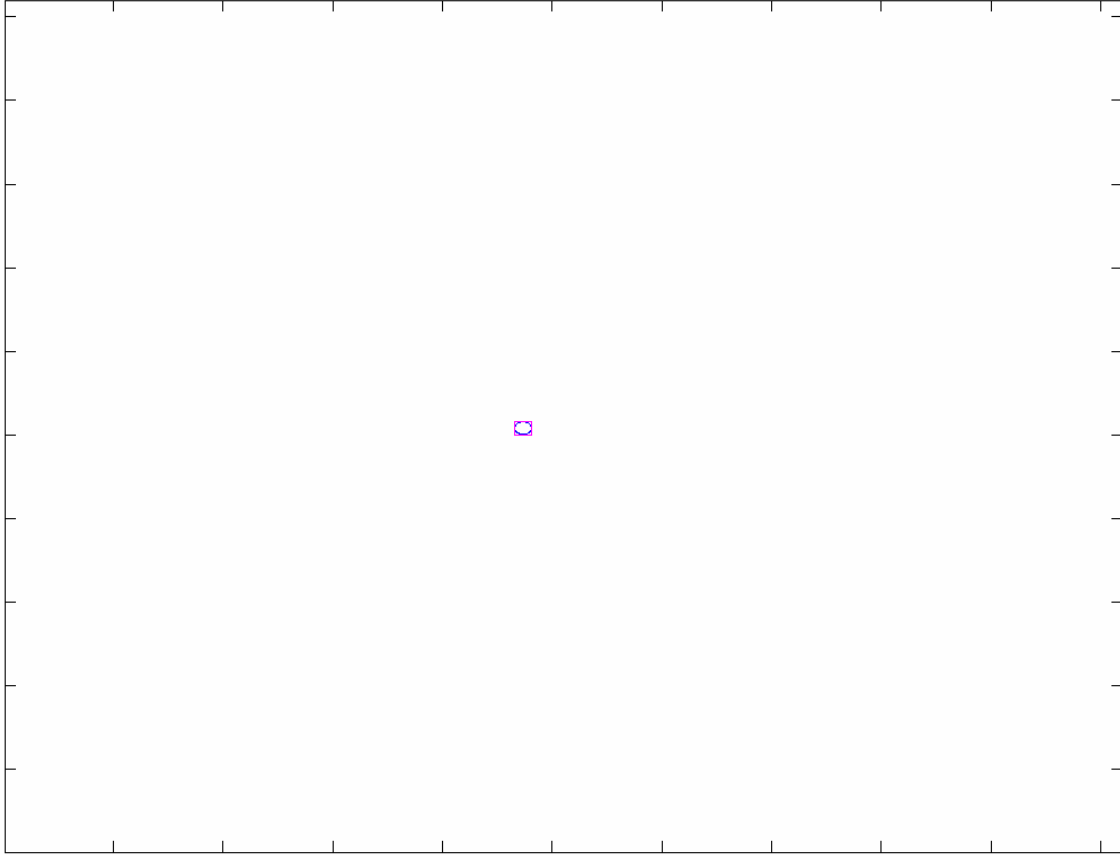
Figure 7. The glare source perimeter (blue) and its *bounding box* (magenta). The close fit assures computational efficiency.

It should be clear how the average luminance is computed. The luminance values from all valid points (that is, those inside the glare source region) are added and then that sum is divided by the number of valid points. The result is the average luminance of the glare source, which is the value used for L_S.

The computation of the centroid is only a little trickier. This computation is necessary because, in the general case, the glare source will be extended. In other words, the glare is not just a point, and thus one must define where the glare source "is". The centroid, a position weighted by luminance, is found in a manner similar to that for a center-of-mass calculation with "luminance" replacing "mass". The relevant equation is,

$$centroid_{row} = \frac{\sum\limits_{i=1}^{1020}\sum\limits_{j=1}^{1020} i\, L_{ij}}{\sum\limits_{i=1}^{1020}\sum\limits_{j=1}^{1020} L_{ij}}, \quad centroid_{col} = \frac{\sum\limits_{i=1}^{1020}\sum\limits_{j=1}^{1020} j\, L_{ij}}{\sum\limits_{i=1}^{1020}\sum\limits_{j=1}^{1020} L_{ij}} \tag{8}$$

where i is the row number of the pixel and j is the column number and L_{ij} is the luminance at that pixel at the ith row and j^{th} column.

Armed with the centroid coordinates, the angular deviation of the glare source from the observer's line-of-sight can be calculated. In order to do this however, there must be some sort of "baseline" that relates coordinates in pixels in the "image" from the photometer's CCD to angular deviation from the center of the CCD.

Since this relation can be particular to a given photometer and, indeed, particular to a given lens on the instrument, such a "baseline" must be made for each individual lens on a specific photometer. This was painstakingly done for our photometer and lens used in these trials. The procedure is detailed in Appendix D entitled *"Angle-Pixel Scaling and Measurement for the Radiant Imaging Photometer"*.

The bottom line from that investigation is the relation

$$t = 6.72437 \times 10^{-4}\, p \tag{9}$$

where t is the tangent of the angle separating the given pixel from the center of the CCD (crosshairs, observer's line-of-sight) and p is the corresponding distance in pixels between them. Here measurement in "pixels" refers to the *length* of a side of the (square) pixel in the CCD[45].

The luminance matrix or CCD "image" is a square grid 1020 x 1020. The row numbering for this matrix starts in the upper left corner pixel (matrix entry) and that is row number one. As one proceeds *down*, the row numbers increase. Note that this 'y coordinate' a) does not start with zero, and b) increases in the opposite direction to standard Cartesian coordinates. As one proceeds to the *right*, column numbers increase. The column number is the same as the conventional 'x coordinate' except that it begins with 1 not 0. The integer pixel coordinates are taken to be at the center of the pixel.

While this positional scheme is standard for matrices or computer graphics, it is a little different from the standard mathematical, Cartesian coordinates and thus care must be used when applying standard formulas. In any event, both the row and column number of the center of the CCD is 510.5. (This is because the center is at the meeting of four pixel corners when the row and column lengths are even numbers.)

Therefore, the "pixel deviation" of the centroid from the center of the CCD is,

$$p = \sqrt{\left(centroid_{row} - 510.5\right)^2 + \left(centroid_{column} - 510.5\right)^2}. \tag{10}$$

Putting this in equation (9) above and taking the arctangent then gives the angle θ.

The computation of solid angle (Ω) is complicated enough that its details are relegated to Appendix F. It should be clear to the reader though that a plane made up of equal area pixels and

---

[45] Sometimes in this document "pixel" may stand for an area and at other times (like the present case) it stands for a length, but the usage should be clear from context.

normal to an observer's line-of-sight will not have those pixels all subtending an equal solid angle with respect to that observer. This is in distinction to equal areas on a sphere subtending equal solid angles when the observer is at the center of the sphere. The complications thus arise from the projection of such a sphere onto a plane.

Finally, the background luminance, L_B, is needed to complete the computations. Here too, a ruthless empiricism prevailed. What constitutes "background" in the general case is somewhat ambiguous, beyond meaning the area without the glare source that is "dead ahead" of the observer.

Since the monitor scenes were all taken from the same vehicle and position inside that vehicle, the area used for background luminance could be the same in each case. Therefore a judgment was made as to which section constituted background, based solely on human observation of the scene.

One can see that this judgment is very hard to automate in an algorithm designed to handle the general case. Unless conditions of measurement (i.e. observation vehicle, photometer position and alignment in the vehicle, etc.) were very, very standardized, human intervention at some level of the calculation would be required. While certainly not fatal to an automated (discomfort) glare measurement tool, it is another difficulty to be surmounted.

Fortunately for VDL, the three scenes were essentially "standardized" in this respect and human intervention only had to check three cases. We took for the background luminance area that shown in Figure 8; it is outlined with a purple rectangle.

Figure 8a. This picture (previously seen in Figure 5) shows the area taken for background comprising matrix entries from row 550 to 650 (inclusive) and column 475 to 650 (inclusive). This area is shown bordered by a purple rectangle.

Figure 8b. The same rectangle is shown in the original scene. The rectangles look somewhat different because of the different aspect ratios in the two pictures, but they represent the same set of pixels (matrix entries) in the CCD.

The rectangular area taken for background luminance calculations runs from row 550 to row 650 (inclusive) and column 475 to 650 (inclusive); this can be seen in the upper picture in Figure 8 using the scale around the left and bottom edges. This same set of matrix entries was used in all three scenes for background luminance. That luminance was just the average luminance over the area bordered by the purple rectangle.

With a computer program that could now provide all the values of all the relevant variables in equation (7) for every set of conditions, we proceeded to construct Table 2 from the photometric data. Here the trial conditions are abbreviated in a straightforward way; for example, *"M_Pos2_S1"* means *medium LED intensity*, *LED in position 2* and *scene number one*. "Number of valid points" means the number of pixels or matrix entries that constitute the glare source. The other table headings are self-explanatory, except one should note that while solid angle was computed in steradians, the angle θ was computed in degrees and not radians. The use of degrees was merely to facilitate comparison to geometric measurement in the laboratory.

Conditions:	Number of valid points	Glare luminance in candelas per square meter	Solid angle (steradians)	Background luminance in cd. per square meter	Angle offset (degrees)
H_Pos1_S1	167	1.103E+06	6.873E-05	19.25	14.28
H_Pos1_S2	167	1.103E+06	6.873E-05	5.72	14.28
H_Pos1_S3	167	1.102E+06	6.873E-05	3.72	14.28
H_Pos2_S1	168	1.076E+06	7.384E-05	19.25	7.86
H_Pos2_S2	168	1.076E+06	7.384E-05	5.72	7.86
H_Pos2_S3	168	1.076E+06	7.384E-05	3.72	7.86
H_Pos3_S1	166	1.167E+06	7.499E-05	19.25	1.42
H_Pos3_S2	166	1.167E+06	7.499E-05	5.72	1.42
H_Pos3_S3	166	1.167E+06	7.499E-05	3.72	1.42
M_Pos1_S1	120	2.736E+05	4.930E-05	19.25	14.41
M_Pos1_S2	120	2.736E+05	4.930E-05	5.72	14.41
M_Pos1_S3	120	2.736E+05	4.930E-05	3.72	14.41
M_Pos2_S1	123	2.546E+05	5.404E-05	19.25	7.93
M_Pos2_S2	124	2.526E+05	5.448E-05	5.72	7.93
M_Pos2_S3	123	2.546E+05	5.404E-05	3.72	7.93
M_Pos3_S1	127	2.515E+05	5.737E-05	19.25	1.42
M_Pos3_S2	127	2.515E+05	5.737E-05	5.72	1.42
M_Pos3_S3	127	2.515E+05	5.737E-05	3.72	1.42
L_Pos1_S1	96	1.403E+04	3.944E-05	19.25	14.41
L_Pos1_S2	93	1.443E+04	3.820E-05	5.72	14.41
L_Pos1_S3	93	1.443E+04	3.820E-05	3.72	14.41
L_Pos2_S1	93	1.375E+04	4.086E-05	19.25	7.93
L_Pos2_S2	93	1.377E+04	4.086E-05	5.72	7.93
L_Pos2_S3	93	1.375E+04	4.086E-05	3.72	7.93
L_Pos3_S1	91	1.489E+04	4.111E-05	19.25	1.42
L_Pos3_S2	91	1.489E+04	4.111E-05	5.72	1.42
L_Pos3_S3	91	1.489E+04	4.111E-05	3.72	1.42

Table 2. Computational results based on photometric measurements for the 27 trial conditions.

The information in this table can now be used along with the subject data for the 27 corresponding trial conditions to do a multilinear regression on equation (5), the expression relating the De Boer score (*GM*) to the logarithms of the photometric variables.

The complete observer data is given in Appendix K, but for fitting purposes only the averages over subjects are needed. This is given in Table 3. The left column has the trial conditions in the same order as Table 2. The right column is the subject average De Boer score.

The entries in Table 2 were put into an *Excel* file after taking their common (base 10) logarithms (except for "conditions" and "no. of valid points" of course). The entries in Table 3 were put into the same *Excel* spreadsheet and then a multilinear fit was done using the built in regression routine in *Excel*.

Conditions	Average De Boer score (GM)
H_Pos1_S1	2.9
H_Pos1_S2	3.1
H_Pos1_S3	3.1
H_Pos2_S1	2.8
H_Pos2_S2	3.0
H_Pos2_S3	2.3
H_Pos3_S1	2.0
H_Pos3_S2	1.8
H_Pos3_S3	1.5
M_Pos1_S1	4.6
M_Pos1_S2	5.2
M_Pos1_S3	4.9
M_Pos2_S1	4.8
M_Pos2_S2	5.2
M_Pos2_S3	4.5
M_Pos3_S1	3.8
M_Pos3_S2	3.8
M_Pos3_S3	3.6
L_Pos1_S1	7.5
L_Pos1_S2	8.0
L_Pos1_S3	7.6
L_Pos2_S1	7.7
L_Pos2_S2	8.0
L_Pos2_S3	7.4
L_Pos3_S1	6.9
L_Pos3_S2	7.0
L_Pos3_S3	6.8

Table 3. The (averaged) subject scores for each trial.

One item of note in doing the fit is that the 'y' or dependent variable that was fit was really *GM* – 12.4 with a forced intercept of zero rather than *GM* as the 'y' variable with an intercept determined by the fit. This was done in order to preserve the form of equation (7).

A partial summary of results of the regression is seen in Table 4.

Variable Name	Coefficients	Standard Error	t Stat	P-value	Lower 95%	Upper 95%
Intercept	0.000	#N/A	#N/A	#N/A	#N/A	#N/A
com. log of glare luminance	-2.440	0.062	-39.124	1.51E-22	-2.569	-2.311
com. log of solid angle	-1.008	0.086	-11.662	3.90E-11	-1.186	-0.829
com. log of background lum.	0.057	0.187	0.305	7.63E-01	-0.331	0.445
com. log of angle in deg.	1.058	0.134	7.898	5.34E-08	0.781	1.335

Table 4. Results from the fit to equation (7).

Referring back to equation (7) we now have,

$$
\begin{aligned}
\alpha &= -2.440 \implies a = 0.61 \\
\beta &= -1.008 \implies b = 0.25 \\
\gamma &= 0.057 \implies c = 0.014 \\
\delta &= 1.058 \implies d = 0.26 \; .
\end{aligned}
\tag{11}
$$

Of course some of these coefficients are more tightly bound than others. Clearly the coefficient of (log of) *background luminance shows that that quantity has almost no effect on the fit*. Its standard error is bigger than the coefficient itself. Looking at the 95% confidence intervals is revealing too. While the coefficient of (log of) glare luminance is bounded by –2.6 and –2.3, that for the (log of) background luminance runs from –0.33 to +0.44. The *sign* of the coefficient isn't even clear.

Indeed the background luminance exponent is the only one that seems to be atypical. Vos[46] himself suggests a = 0.8 which is actually quite close to 0.6 given the large uncertainties and variations in this subject. The ratio of our a/b is 2.44, which is comparable to the expected ratios Vos discusses. His suggested b is 0.5, which again, compares favorably to our 0.25 given the wide range of numbers found by many investigators. Only the background luminance exponent seemed unusual. (Vos takes it as 0.25.)

The exponent of background luminance is even consistent with zero, meaning no contribution to a glare score at all. This can probably be explained by the experimental situation. While solid angle didn't vary by much, glare luminance varied by a factor of about 100 between extremes, and angle offset (θ) by a factor of 10. But background luminance only changed by a factor of 5. Upon taking logarithms for the fit, the change isn't very big.

Furthermore, the rule of thumb when doing a multilinear regression is to take data points that are 10 to 20 times the number of coefficients that need fitting. In the present case, we had 27 observations and at least 40 would be needed to feel more confident that the background luminance had little effect. Also, only three actual background numbers were used. Since our mandate was to investigate headlight glare *at night*, the background luminance would not be expected to vary much. Without a wider range of background luminance, its exponent or the coefficient of its logarithm cannot be pinned down with any specificity. In fact, for these limited circumstances, the background luminance could safely be ignored, although we do not follow that path here.

Overall, the fit is quite good as seen in Figure 9. Here the (subject average) De Boer scores (or *GM*) for each of the twenty-seven trial conditions is plotted in blue while the predicted scores, using the above regression coefficients, are shown in pink. The order of the observations is the same as in Tables 2 and 3. Thus observation number one is high intensity for the LED, position 1, and scene 1. Observation 27 is low LED intensity, position 3 with scene 3. The three big

---

[46] **Reflections on Glare**, *Johannes J Vos* in **Lighting Res. Technol.** 35, 2 (2003) pp. 163-176.

"steps" in the figure (going left to right) therefore correspond to high, medium and low intensity of the LED[47].

Within each big "step" one can see downward progression (lower score, more discomfort) as observation number increases. This is because the LED is moving more toward the center of the scene (smaller θ). In the pink (predicted) curve this is seen as three small steps inside the big step. Each small step in pink, representing fixed intensity, fixed position but changing scene, is essentially flat. This reflects the fit having little dependence on background luminance, which is the only *obvious* factor changing between scenes. The observed curve in blue seems to show the same general trends as the pink curve, *except* for scene two. With the exception of observation # 8, the second scene has a higher or equal De Boer score (less discomfort) relative to the other two scenes when the other variables are constant. There seems to be some effect from scene two, albeit minor, which is not captured by this fit. Since scene two had a background luminance value between that of the other scenes, background luminance would not seem to explain it, however the overall distribution of background luminance, concentrated on the left side of the scene owing to the positions of the overhead luminaires, may have played a role.
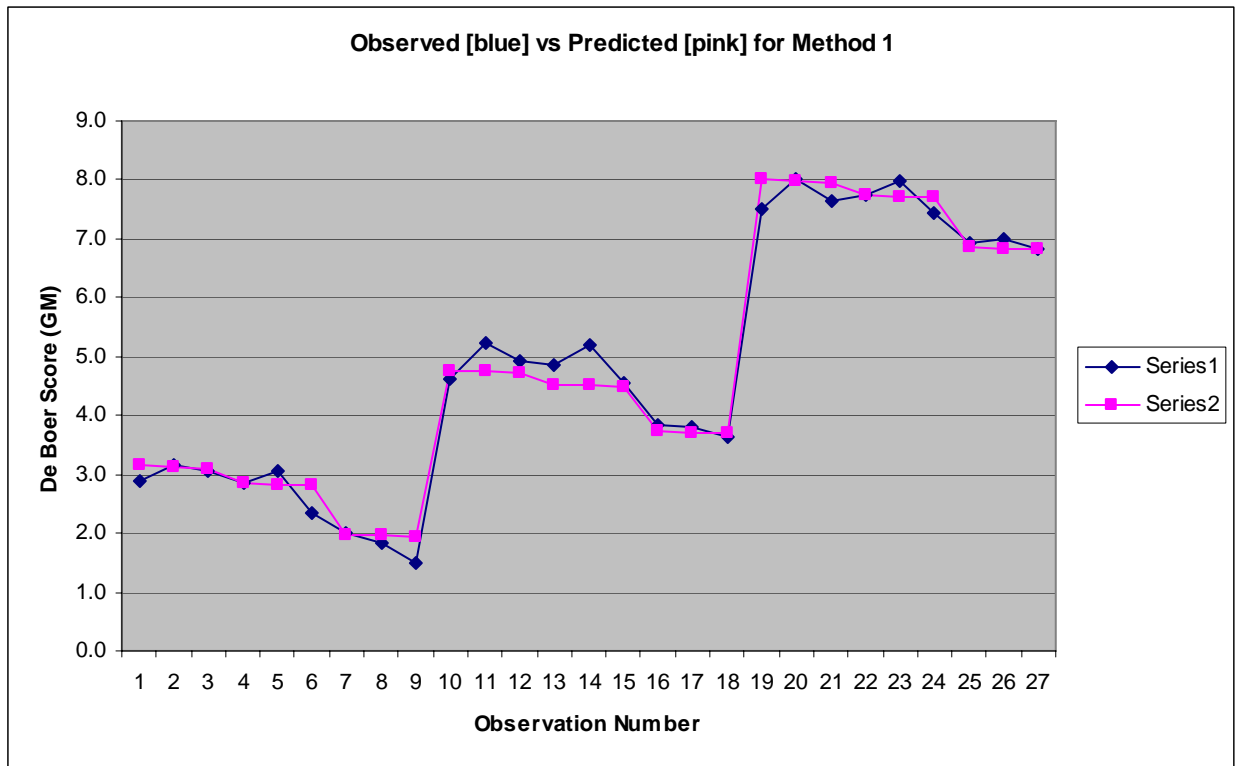
Figure 9: A comparison of the observed De Boer (*GM*) scores (shown in blue) and those predicted by the regression (shown in pink).

Not shown in the figure but worth mentioning is the subject variation in De Boer score. The standard deviations for the subject averages for each trial condition can be found in Appendix K. They differ for each trial condition but generally speaking are of order one. Thus the "error

---

[47] The reader will recall that high De Boer score is low discomfort and vice-versa.

bars" on each pink dot in the figure, were they shown, would be about one De Boer score unit on either side of the dot. Hence, the fit in Figure 9 is quite good.

For reference, the data used in the plot is shown in Table 5.

Actual Score	Predicted Score
2.9	3.1
3.1	3.1
3.1	3.1
2.8	2.9
3.0	2.8
2.3	2.8
2.0	2.0
1.8	2.0
1.5	1.9
4.6	4.8
5.2	4.7
4.9	4.7
4.8	4.5
5.2	4.5
4.5	4.5
3.8	3.7
3.8	3.7
3.6	3.7
7.5	8.0
8.0	8.0
7.6	8.0
7.7	7.7
8.0	7.7
7.4	7.7
6.9	6.9
7.0	6.8
6.8	6.8

Table 5. Subject average De Boer scores and predictions using method 1 for the 27 trial conditions.

VDL's first method for analyzing discomfort glare in the lab thus yields the formula,

$$GI = \sum_{sources} \frac{L_S^{0.61}\,\Omega^{0.25}}{L_B^{0.014}\,\theta^{0.26}} = 1260 \cdot 10^{-GM/4} \qquad (12)$$

and if there is only one source or one source strongly dominates the glare this can be written more directly as,

$$GM = 12.4 - 2.44\,log\,L_S - log\,\Omega + 0.057\,log\,L_B + 1.06\,log\,\theta \qquad (13)$$

Both of these allow computation of *GM*, that is the De Boer score, *from measured photometric quantities*. This then is the (discomfort) glare meter.

Method 2

In this method, we used image analysis to identify high contrast areas in the scene and determine where there are sources of glare, and to then determine levels of conspicuity in an attempt to estimate levels of discomfort glare.

A full-color imaging photometer was interfaced with a notebook PC with specialized software developed within our laboratory. In essence, it would take an image as would be seen by a human eye and then compute a glare rating on the image. This proposed Glare Meter Tool (Method 2) for discomfort glare leveraged a previous Caltrans task order (MOU 328), where the Visual Detection Laboratory developed a model to identify the conspicuous elements in a visual scene based on the human visual system's sensitivity to spatially varying patterns of light/dark, red/green, and blue/yellow[48]. The basic operation of the model is illustrated in Figure 10. The illustrations in this figure are for illustrative purposes and do not represent the nighttime traffic scenes to which this methodology would be applied. The model takes as its input a digital color image (Figure 10a) which provides luminance and color (red, green, blue and yellow) data for each pixel within that image. The image is first divided into its luminance, and color opponents: red-green and blue-yellow sub-images. Each sub-image is then filtered spatially, and subdivided into 30x30 pixel squares. The contrast of each square is then computed according to:

$$\text{contrast of square i} = \frac{\text{brightness of square i}}{\text{brightness of overall sub-image}}.$$

The contrast arrays of the three sub-images are then recombined by simple averaging. The most conspicuous element of the scene is the square having the greatest numerical value of contrast. This is depicted graphically in Figure 10b where white squares correspond to the most conspicuous elements and black squares to the least conspicuous elements.

a. Original Scene   **b. Conspicuity Grid**
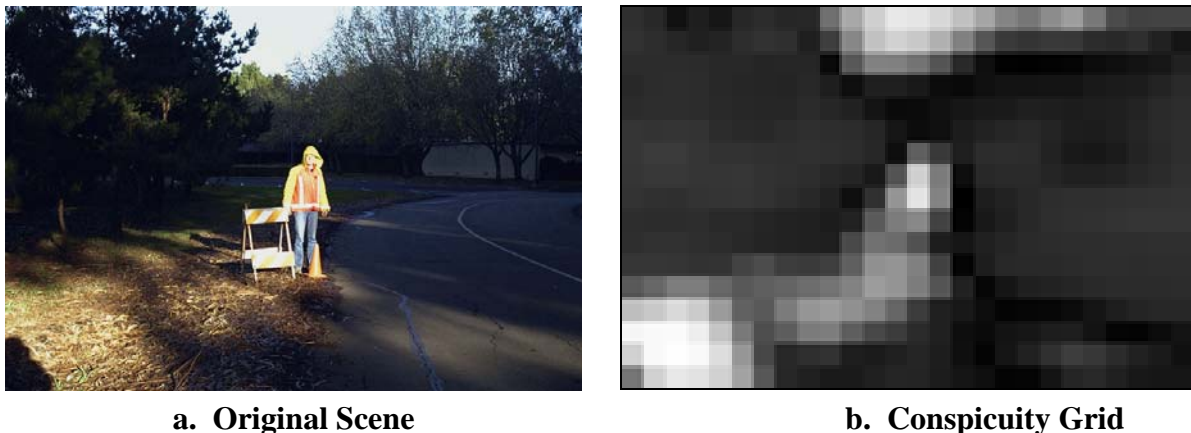
Figure 10. Operation of the Glare Meter model

---

[48] J.E. Barton and J.A. Misener, Roadway and Work Crew Conspicuity, UCB-ITS-PRR-2000-23, December, 2000.
  http://www.path.berkeley.edu/PATH/Publications/PDF/PRR/2000/PRR-2000-23.pdf

Consider now the case in which a small bright source of glare is introduced into the scene's background, as in Figure 11[49]. It will become one of the most (if not *the* most) conspicuous elements and will distract the observer away from the nearer object of interest (which in this case is the construction worker). The goal of the Glare Meter Tool is to develop an algorithm that distinguishes sources of glare from other conspicuous elements in a scene and also provides a relative measure of these sources' "distractiveness".

Figure 11. Notional glare source in staged roadside model

The Glare Meter Tool development (Method 2) proceeded in the following manner:

1.   In order to obtain absolute photometric data for a particular scene, we acquired an image with the Radiant Imaging full-color video photometer to provide color and photometric data for every pixel in the scanned scene.

2.   Using this data and the previously developed conspicuity algorithm, the conspicuous elements in the scene were identified and a conspicuity grid developed (see Figure 12a).

3.   A photometric luminance grid was then developed using a modified version of the conspicuity algorithm which analyzes only the photometric luminance of each pixel in the scene (see Figure 12b).

4.   The two grids were then combined in a logical AND operation (see Figure 12c). The result identified those elements that are both conspicuous and bright. These elements make up the candidate pool for sources of glare.

---

[49] Although the photometer scan of a source of glare will accurately capture the degree of its conspicuousness, this does not carry over when rendering an image on a paper medium or monitor screen, such as above.

a. Conspicuity Grid

b. Photometric Luminance Grid
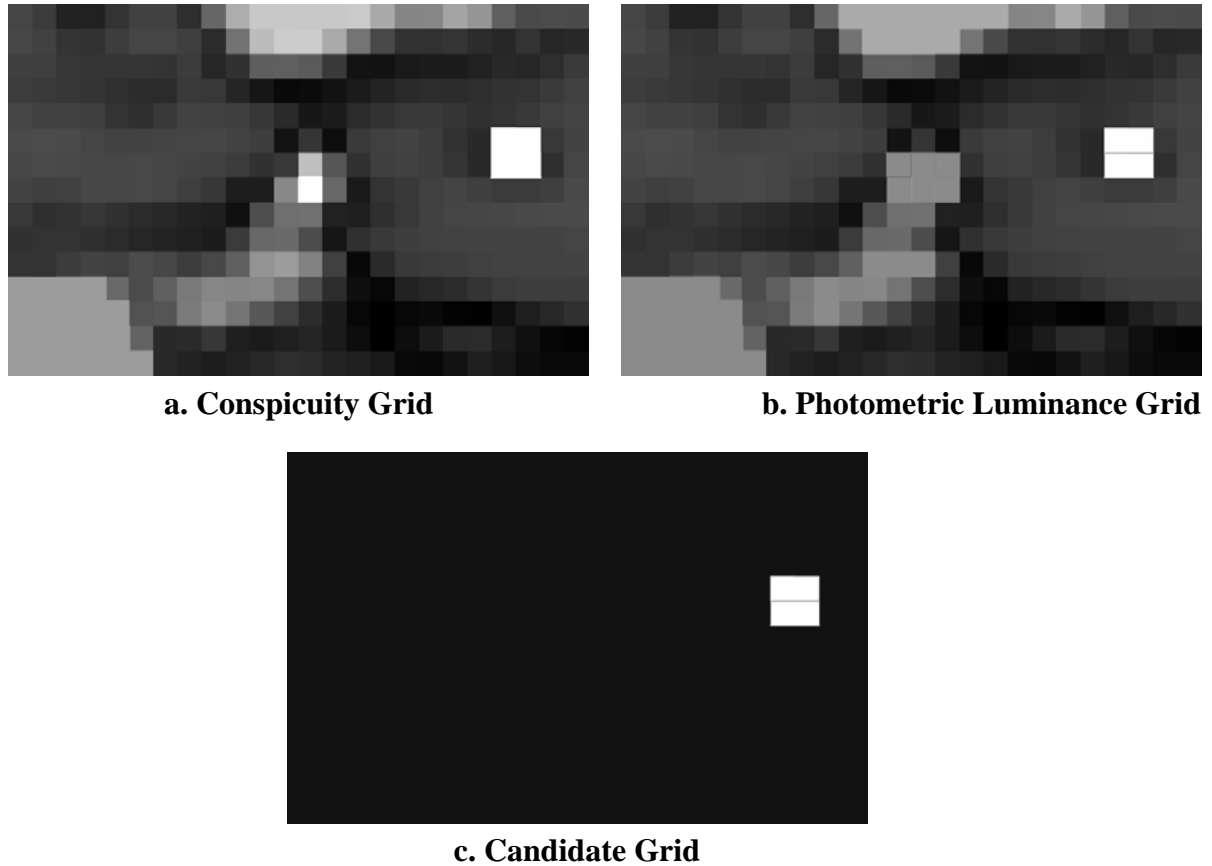
c. Candidate Grid

Figure 12. Our Glare Meter Tool development sequence was based on prior Caltrans-funded work.

5.   Any square in the candidate grid whose photometric luminance exceeded a certain absolute value was classified as a source of glare. This required specifying the size of the squares to be constructed in making up the grids, as well as the luminance level.

6.   In addition we specified the position of the source of glare relative to the object of interest (direction of gaze) so that the eccentricity of the source could be taken into account. This was done in a manner consistent with the position factor of Petherbridge and Longmore described in the *EnergyPlus Engineering Reference*, excerpted in Appendix J.

7.   With the sources of glare and their luminance and position identified as in the previous steps, we then followed a methodology similar to that of Method 1 (with some difference to be described later) to predict the rating on the De Boer discomfort glare scale thus ranking the severity of the glare source.

We applied this methodology to the 81 tristimulus data files taken in groups of 3 (X, Y, and Z tristimulus data for a given trial), each group representing the 27 combinations of nighttime scene and position/intensity of glare source employed in the laboratory experiments. As an example, we employed the MATLAB program shown in Appendix I to analyze the scene and superimposed glare source shown in Figure 13.
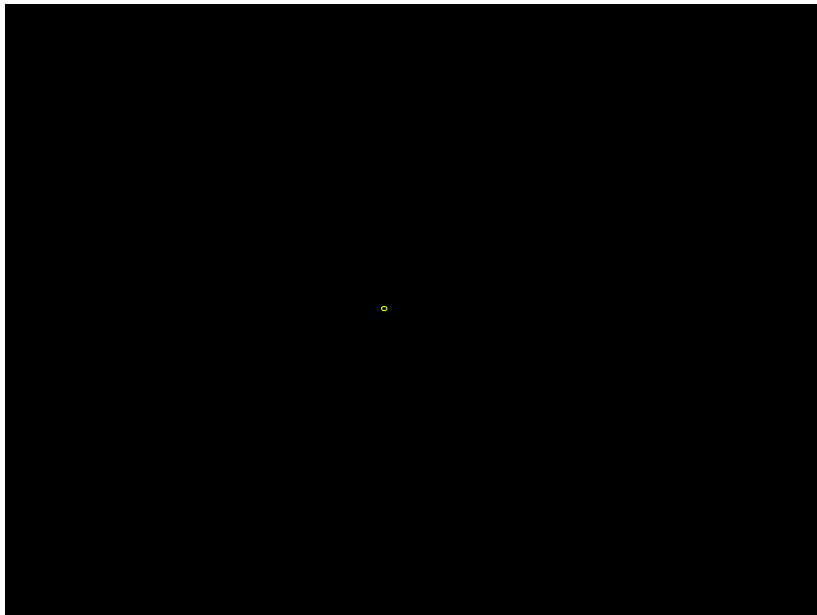
Figure 13a. Original Scene[50]
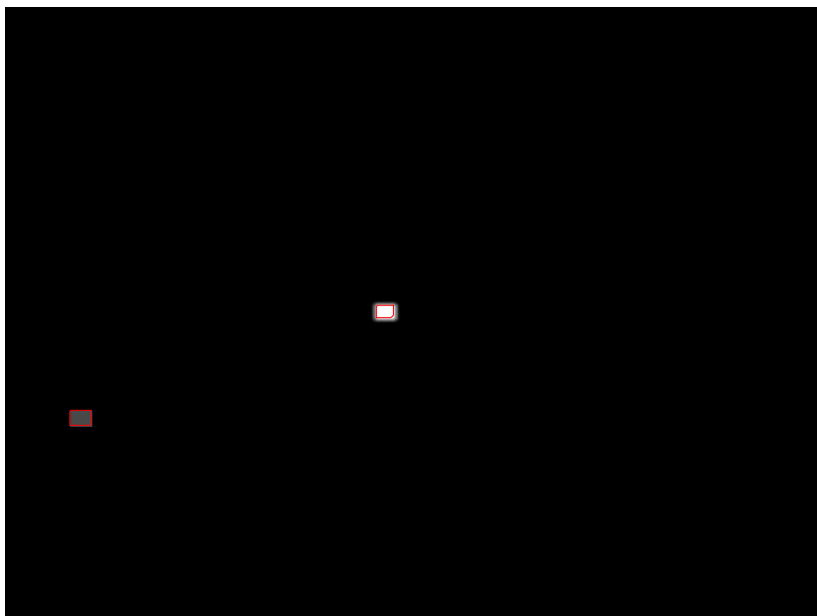
Figure 13b. Filtered RGB Scene

---

[50] These figures suffer the same scaling issue when being displayed as was mentioned earlier. Refer to figures 4 and 5 above in method 1. In addition there is the "blocking" into 30 x 30 pixel squares for some of them (see Figure 10b and Figure 12). Thus these scenes will only show the glare source or potential glare sources and not the rest of the image one might expect.

Figure 13c. Filtered Luminance Scene
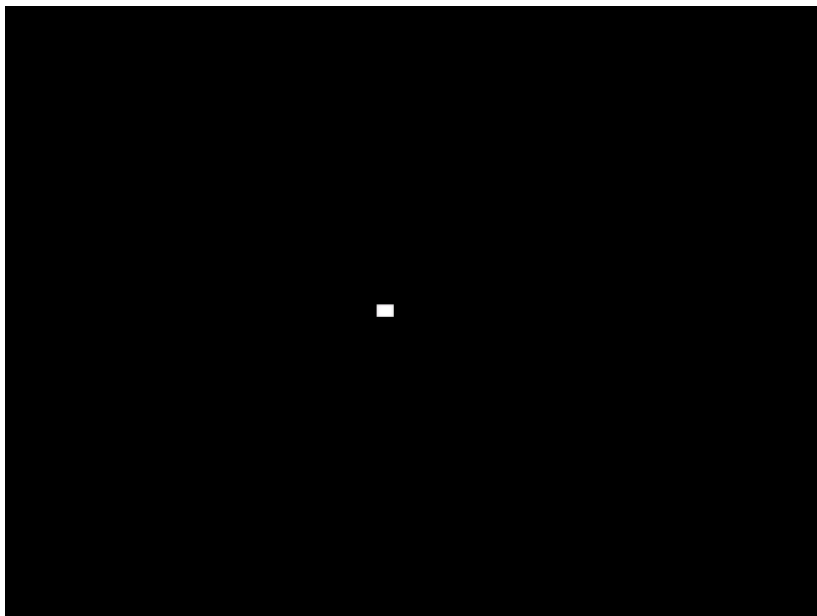
Figure 13d. Glare Candidates

After identifying the glare source (Figure 13d), we applied a "glare index" formula due to Baer[51] similar to that used for the first method (hence the subscripted "2" on the index to distinguish it), with some differences as noted below.

$$GI_2 = 2 \sum_{sources} \frac{L_S^{1.6} \, \Omega^{0.8} p}{L_A} = C \, 10^{-GM/s} \qquad (14)$$

Here the position factor, p, appears in the numerator instead of the denominator and is obtained by interpolating within the table on p.147 of Appendix J, and the average luminance (denoted L_A) was for the entire scene rather than just a limited area surrounding the direction of gaze. The constant C here takes the place of the constant K in equation (4) and rather than assuming a scale factor of 4 in the exponent on the far right hand side of equation (14), the parameter s appears as an unknown that will be determined by a fit to the data.

Again the Glare Index was converted to a De Boer rating (or Glare Mark) by similar means to that in employed in Method 1. Taking the common log of equation (14) gives,

$$GM = s \log C - s \log GI_2 = s \log C - s \log \left(2 \sum_{sources} \frac{L_S^{1.6} \, \Omega^{0.8} p}{L_A} \right). \qquad (15)$$

Here, unlike in Method 1, the individual factors (glare luminance, solid angle, etc.) were **not** individually fit. Rather the Glare Index was taken as a whole (middle equality above) and the scale factor s and the constant C emerged from the regression. In Method 1, K (comparable to C) was fixed before the fit and the scale factor in the exponent of 10 (here s) was fixed at 4. In the current fit, the scale factor s turned out to be 2.67 or approximately 3 (see the regression coefficients in Table 6), and the constant C can be found from the intercept in Table 6:

$$s \log C = 18.58 \Rightarrow C = 10^{18.58/s} = 10^{18.58/2.67} = 9.095 \times 10^6.$$

This value of C is almost four orders of magnitude greater than that of K, but that is not really surprising since the exponents of the luminance and solid angle are bigger. What is reassuring is that the value of s rounds to 3 which (in this naturally inexact estimation) is close enough to 4 to show the same type of exponential scaling between *GM* and *GI* as in Method 1.

The statistics in Table 6 (95% confidence bounds) show, again allowing for the inexact nature of the subject, reasonably tight bounds on the fit coefficients.

---

[51] **Beleuchtungstechnik; Grundlagen (Fundamentals of illuminating engineering)** *Baer, R.* **VEB Verlag Technik**, Berlin, 1990.

With C and s now determined from the regression, equations (14) and (15) can now be implemented to get the predicted De Boer scores. The resulting glare scores, both predicted and actual, are shown in Table 7 along with the GI_2 values for the various trial conditions.

	Coefficients	Standard Error	P-value	Lower 95.0%	Upper 95.0%
Intercept	18.58	1.105	3.87E-15	16.31	20.86
Log glare score	-2.67	0.212	2.63E-12	-3.11	-2.23

Table 6. Fit coefficients and statistical Analysis of Glare Scores from Discomfort Glare Analysis Method 2

conditions:	computed glare score	log base ten of glare score	predicted De Boer score	actual subject Avg. De Boer score
H_Pos1_S1	3.82995E+05	5.5832	3.7	2.9
H_Pos1_S2	3.84979E+05	5.5854	3.7	3.1
H_Pos1_S3	3.88816E+05	5.5897	3.7	3.1
H_Pos2_S1	7.95536E+05	5.9007	2.8	2.8
H_Pos2_S2	7.99961E+05	5.9031	2.8	3.0
H_Pos2_S3	8.08031E+05	5.9074	2.8	2.3
H_Pos3_S1	1.49905E+06	6.1758	2.1	2.0
H_Pos3_S2	1.50669E+06	6.1780	2.1	1.8
H_Pos3_S3	1.52093E+06	6.1821	2.1	1.5
M_Pos1_S1	1.29774E+05	5.1132	4.9	4.6
M_Pos1_S2	1.33352E+05	5.1250	4.9	5.2
M_Pos1_S3	1.40739E+05	5.1484	4.8	4.9
M_Pos2_S1	2.65859E+05	5.4247	4.1	4.8
M_Pos2_S2	2.73934E+05	5.4376	4.1	5.2
M_Pos2_S3	2.86082E+05	5.4565	4.0	4.5
M_Pos3_S1	4.97160E+05	5.6965	3.4	3.8
M_Pos3_S2	5.11731E+05	5.7090	3.3	3.8
M_Pos3_S3	3.56716e+004	4.5523	6.4	3.6
L_Pos1_S1	6.58610E+03	3.8186	8.4	7.5
L_Pos1_S2	7.97163E+03	3.9015	8.2	8.0
L_Pos1_S3	1.66905E+04	4.2225	7.3	7.6
L_Pos2_S1	1.28058E+04	4.1074	7.6	7.7
L_Pos2_S2	1.64485E+04	4.2161	7.3	8.0
L_Pos2_S3	3.45575E+04	4.5385	6.5	7.4
L_Pos3_S1	2.42326E+04	4.3844	6.9	6.9
L_Pos3_S2	3.10146E+04	4.4916	6.6	7.0
L_Pos3_S3	6.37475E+04	4.8045	5.8	6.8

Table 7. Glare Scores from Discomfort Glare Analysis Method 2

Figure 14 shows a graph comparing the observed De Boer ratings with those predicted by Method 2 (last two columns of the above Table 7).
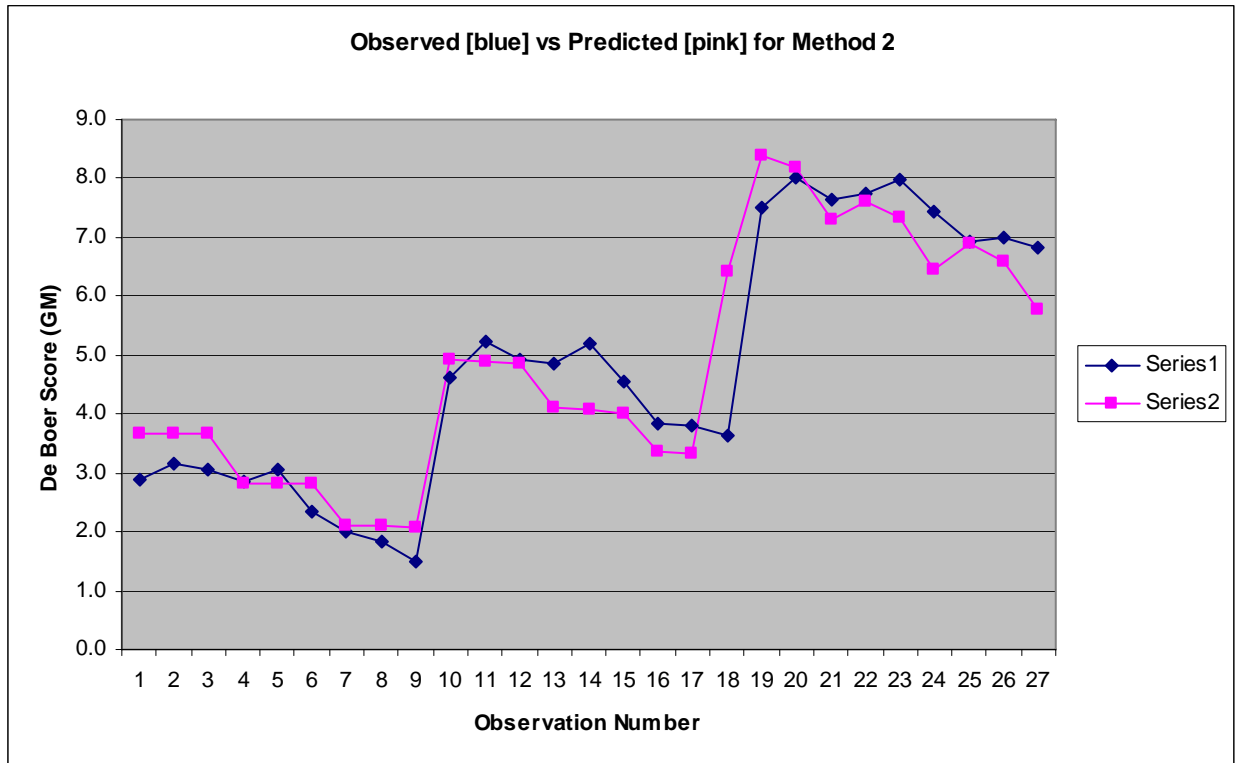
Figure 14. A comparison of the observed De Boer (*GM*) scores (shown in blue) and those predicted by the regression (shown in pink) for Method 2.

These results can be compared to those obtained by Method 1, as shown in Figure 9 in the previous section. While both Method 1 and Method 2 can be seen to produce remarkably accurate predictions for the actual De Boer ratings given by observers, it is evident that Method 1 is slightly better. The root mean square (rms) difference between predicted and actual De Boer scores is 0.27 for Method 1 and 0.77 for Method 2. We believe that this is because of the greater degrees of freedom that come with fitting the luminance and geometric factors individually. We standardized on Method 1 for purposes of analyzing the results of the field experiments, reported in the next section.

V. Field Experiments

Experimental Methods

Field experiments were conducted in order to determine if the Glare Meter Tool, having been validated in the laboratory, could successfully be used in the field to predict De Boer scale ratings of discomfort glare. For this purpose, we set up experiments on the test track at the UC Berkeley Richmond Field Station. A stationary vehicle was positioned in one lane with the headlights set to low-beam. In the other lane, another stationary vehicle was positioned and its headlights employed as a source of discomfort glare. De Boer ratings were made by observers seated in the primary vehicle, viewing through its windshield. This was done for a variety of conditions (to be described in detail later) including presence or absence of mainline lighting (provided by a standard luminaire installed at the test track), the presence or absence of a glare screen (barrier temporarily moved onto the centerline of the roadway to partially obscure direct view of the opposing headlights, condition of the windshield (clean or dirty), and beam of the opposing headlights (high or low).

At the same time, for each combination of conditions, images of the scene were acquired by the video photometer, placed inside the primary vehicle and viewing through the windshield, thus duplicating the driver/observer's view of the roadway. Images were subsequently analyzed by the software developed for the Glare Meter Tool and results compared to the subjective assessments by the observers.

Photographs of the field experiment sessions are shown in Figure 1.
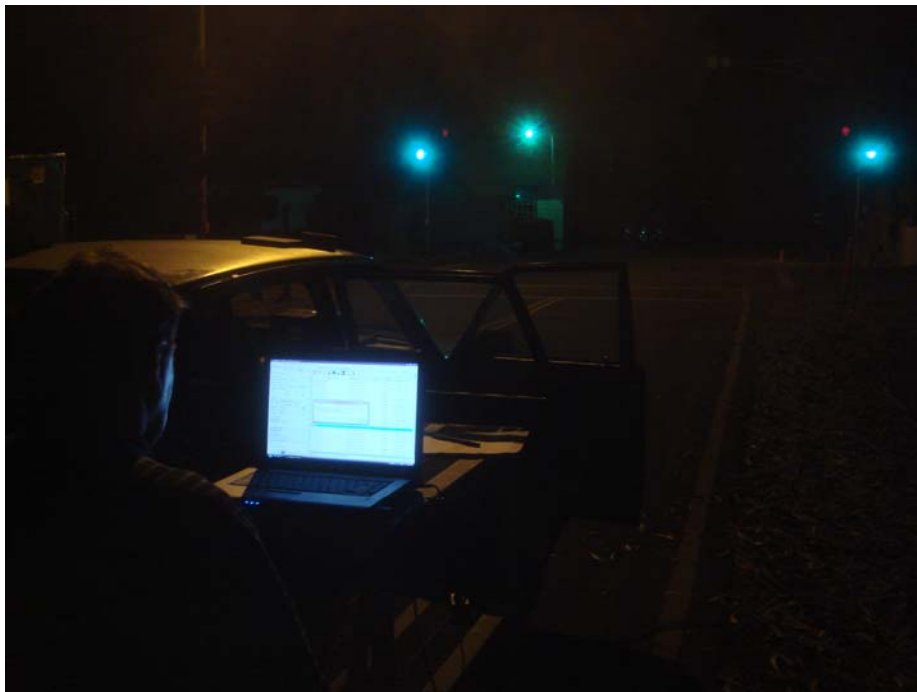
Figure 1a. Field experiment showing primary vehicle on test roadway with Glare Meter Tool in view. Video photometer is inside the vehicle and the associated computer is set up externally.

Figure 1b. Video photometer component of Glare Meter Tool shown inside vehicle pointing forward through windshield in equivalent of driver's view.

Figure 1c. Observer in vehicle looking ahead on roadway, prepared to rate discomfort glare from headlights of opposing vehicle (not in view). Video photometer is seen in the foreground.

Figure 1d. Primary vehicle in foreground and headlights of opposing vehicle in the background, causing discomfort glare.

Figure 1e. Glare from headlights of opposing vehicle as seen through windshield of primary vehicle.

In all, we evaluated discomfort glare in six different scenarios, the variables being:
Mainline lighting (overhead luminaire) <u>on</u> vs. mainline lighting <u>off</u>.
Glare from <u>high-beam</u> headlights of opposing vehicle vs. glare from <u>low-beam</u> headlights.
Viewing through <u>clean</u> windshield vs. <u>dirty</u> windshield.
<u>Unobstructed</u> view of glare source vs. <u>partially obstructed</u> view from interposition of a <u>glare screen</u>.

We had originally intended to experiment on a curved portion of the roadway as well as straight but practical considerations concerning geometry of the test track available to us forced us to abort this particular scenario. However, the range of luminances and eccentricities of the glare sources in the other scenarios covered a range sufficiently large to provide ample opportunity for evaluation of the Glare Meter Tool in field conditions.

The precise combinations of conditions we employed in our observations are summarized in Table 1.

scenario	glare source	mainline lighting	glare screen	windshield
#1	lo-beam	on	no	clean
#2	hi-beam	on	no	clean
#3	hi-beam	on	yes	clean
#4	lo-beam	off	no	clean
#5	hi-beam	off	no	clean
#6	hi-beam	off	no	dirty

Table 1: Field test conditions.

For each set of conditions, two observers rated the discomfort glare on the De Boer scale. At the same time, we used the video photometer component of the Glare Meter Tool to acquire images of all the scenes from a position inside the vehicle, looking through the windshield just as the observers had. We then performed an analysis, outlined below, using the methodology outlined in Method 1 of the discomfort glare section of this report, but with the additional factor that we now had two sources of glare (the two headlights) rather than just one (the LED).

Analysis and Results

The images were processed to identify the glare sources and specify their average luminance, solid angles, and eccentricities relative to the direction of gaze. The background luminance was also extracted. These values are shown for each scenario in Table 2.

scenario	glare source (headlight)	glare luminance	background luminance	solid angle	eccentricity (degrees)
#1	left	1.53E+04	1.41E+00	1.88E-05	4.98
#1	right	1.83E+04	1.41E+00	2.21E-05	3.18
#2	left	1.30E+05	1.41E+00	3.87E-05	3.38
#2	right	1.38E+05	1.41E+00	4.52E-05	1.66
#3	right*	3.55E+04	1.41E+00	3.34E-05	1.42
#4	left	1.53E+04	6.61E-01	1.88E-05	4.98
#4	right	1.83E+04	6.61E-01	2.21E-05	3.18
#5	left	1.30E+05	6.61E-01	3.87E-05	3.38
#5	right	1.38E+05	6.61E-01	4.52E-05	1.66
#6	left	9.58E+04	1.29E+00	1.38E-04	3.27
#6	right	1.02E+05	1.29E+00	8.49E-05	1.41

* glare screen blocked off left headlight and partially obstructed right headlamp, so there is only one glare source

Table 2. Values of variables for calculation by equation (12).

The first equality in equation (12) from the previous section was then used to calculate the Glare Index (*GI*) for each glare source separately (each of the pair of headlights). Then the two Glare Indices were summed.

$$GI = \sum_{sources} \frac{L_S^{0.61}\, \Omega^{0.25}}{L_B^{0.014}\, \theta^{0.26}} = 1260 \cdot 10^{-GM/4}$$

Finally, the conversion from Glare Index to Glare Mark (De Boer scale) was accomplished using the inverted form of the second equality in equation (12):

$$GM = -4\log_{10}\left(\frac{GI}{1260}\right).$$

Table 3 reproduces the information in Table 1, with the experimental results added.   In the next to last column are the subjective ratings of discomfort glare on the De Boer scale by the two observers. In the last column is the De Boer rating as calculated objectively by the Glare Meter Tool.

Scenario	glare source	mainline lighting	glare screen	windshield	De Boer ratings, two observers	De Boer rating predicted by Glare Meter Tool
#1	lo-beam	on	no	clean	5, 6	6.2
#2	hi-beam	on	no	clean	3, 3	3.4
#3	hi-beam	on	yes	clean	4 ½, 5	5.9
#4	lo-beam	off	no	clean	5, 6	6.2
#5	hi-beam	off	no	clean	2 ½, 3	3.4
#6	hi-beam	off	no	dirty	2, 2	3.3

Table 3: Field test conditions with glare ratings.

As can be seen, there is a generally close agreement between the subjective ratings and those predicted by the Glare Meter Tool, although there was a consistent tendency for the algorithm to slightly overestimate the De Boer rating (and hence slightly underestimate the severity of the glare)[52]. This could be explained by the optical scattering and diffusing effects of the windshield, which were a factor in all the scenarios (the windshield being on a 23-year-old car and thus somewhat worn), and especially in scenario #6[53] where the windshield was given an added layer of dust and dirt. While the image analysis software, at its present stage of development, can successfully identify and delineate all major sources of glare, it is not able to take into account all the micro-sources of glare that are added when a worn or dirty windshield is interposed in the optical path. Software that has this capability would have required an investment of time, effort, and expertise that were clearly beyond the scope of the present study. Nonetheless, we think the results obtained in the field experiments were sufficiently accurate as to validate the underlying concepts and implementation of our prototype instrument.

---

[52] We should also point out that there is a standard deviation of about one De Boer scale unit on the *observers' rating* (see Appendix K for the detailed numbers).

[53] There is another potential explanation for scenario #6 involving "undetected saturation". This phenomenon was deemed too abstruse for the main section of this report, but it is discussed briefly in Appendix L. Unfortunately, there is no way of knowing if this phenomenon was involved in this particular instance without redoing the test under *exactly* the same conditions.

VI: **Conclusions and Recommendations**

We have taken major steps toward development of a working Glare Meter Tool which can assess the severity of disability glare and discomfort glare in a roadway environment. The original contract for this project only specified development of a means to assess *discomfort* glare but we enlarged the scope of the project to include *disability* glare because of its importance in evaluating the total impact of glare on traffic safety. Additionally, while only a single methodology was originally proposed for analyzing an image to identify sources of illumination for purposes of evaluating discomfort glare, we developed a second method which in fact proved to produce more accurate results.

Disability glare causes contrast reduction resulting from optical scattering within the eye. Consequently, ability to perform certain visual tasks, such as detecting hazards in the roadway, may be compromised. The disability glare component of the Glare Meter Tool takes an image of a driving scene, acquired by use of a Radiant Imaging 16-bit full-color video photometer, and analyzes it pixel by pixel, using software developed in our laboratory, summing the contribution from each pixel to the total disability glare on the basis of its luminance and position relative to the direction of gaze. The equation of Vos is used which includes a position factor (the more eccentric the glare source, the less its effect) and an age factor (the older the observer, the greater the degree of contrast reduction resulting from a particular glare source). We have essentially developed a highly accurate instrument using advanced technology that replaces the historical Fry-Pritchard glare lens, a rudimentary device that was intended to assess disability glare by introducing the position factor through optical means. The net output of our device is an "equivalent veiling luminance" which can be used to calculate the contrast reduction for any particular visual task. Using this equivalent veiling luminance, traffic engineers can make decisions as to how much disability glare should be allowed in any particular scenario. With the Glare Meter Tool, they have a means of assessing how disability glare is mitigated with the implementation of certain countermeasures such as mainline lighting and glare screens.

Discomfort glare represents a distraction or annoyance to an observer without necessarily reducing his or her ability to perform visual tasks, and is thus a subjective response, without a clear underlying mechanism. The discomfort glare component of the Glare Meter Tool uses the same image as for the disability glare analysis, but subjects it to completely different processing. Because discomfort glare from multiple sources is not strictly additive on a pixel-by-pixel basis like it is in the case of disability glare, it is first necessary to use software developed in our laboratory to identify the sources of glare in terms of their position, their extent, and their luminance. Then we use additional software to implement the equations of Vos and Baer to produce a Glare Index score. Finally our computer program implements an equation of Vos to convert the Discomfort Glare Index score to a Glare Control Mark score (number on the standard De Boer Rating Scale for Evaluation of Discomfort Glare). As with the disability glare component of the Glare Meter Tool, traffic engineers now have a means at their disposal to assess the effectiveness of various means of glare reduction, without requiring the use of human observers.

One potential improvement that could be implemented in a future iteration of the software involves the possible color dependence of discomfort glare. As noted earlier in the report, and in the literature review in Appendix A, some researchers[54,55] have noted a spectral power distribution dependence of discomfort glare, where higher color temperatures (as, for example, with HID lamps) result in greater discomfort, other factors being equal. While this effect is small, a spectral component could be introduced into the Discomfort Glare Index equation with the potential result that a more accurate De Boer score could be predicted.

The Glare Meter Tool, which has been shown to produce remarkably accurate results for both disability glare and discomfort glare, has been very successful from a *proof-of-principle* perspective and as a laboratory device. There are nonetheless some practical difficulties that limit its use in the field at the current level of development.

The primary hardware limitation is that the dynamic range of the video photometer prevents simultaneous capture of the glare source and detail of a nighttime scene in a single image without problems of excessive quantization noise or saturation of the CCD sensor. Multiple exposures are thus required to capture the full dynamic range of a scene. Consequently, use of this prototype instrument is limited to situations in which both the viewpoint (driver) and the sources of illumination (ambient or glare) are stationary.

Optical scattering within the lens of the photometer itself is another form of "noise" that must be addressed. Although this difficulty can be circumvented using software techniques, the approach is time-consuming. Also, the software techniques for image analysis are quite complex, processor-intensive, and requiring of a certain degree of expertise. As a result, considerably more development work would be required to produce an instrument that could be easily deployed in the field for a fully automated assessment of glare.

Recommendations for furthering the work discussed in this report fall into two categories: (1) further development of the Glare Meter Tool itself; (2) glare mitigation experiments with and without observers, performed either without the Glare Meter Tool (but informed by the knowledge acquired from our testing), or using just the hardware component of the Glare Meter Tool and a "by hand" implementation of the methodology developed in the present project.

---

[54] **Subjective and Objective Aspects of Headlamp Glare: Effects of Size and Spectral Power Distribution**, Flannagan MJ. in **The University of Michigan Transportation Research Institute, November, 1999**; Ann Arbor, Michigan: 1-13.
[55] **Blue Content of LED Headlamps and Discomfort Glare**, Sivak M, Schoettle B, Minoda T, Flannagan MJ. in **The University of Michigan Transportation Research Institute, February, 2005**; Ann Arbor, Michigan: 1-15.

Prospects for improving the Glare Meter Tool consist of (a) waiting for better hardware to become available; (b) software improvement, and (c) more extensive disability glare testing.

Better hardware for the Glare Meter Tool would seem to depend on simply waiting for the state of the art to progress. Dynamic range considerably greater than the 16 bit range of the present instrument is needed to avoid some of the problems discussed above, and reduced exposure times (for the same quality data) and higher data throughput are needed to allow dynamic measurements (i.e. on moving traffic) in addition to stationary ones. Additionally, if color information is ultimately incorporated into the software that analyzes a scene for discomfort glare, then it would be advantageous to have an instrument that captures chromaticity in a single exposure rather than multiple exposures with a rotating filter wheel as is done in the present instrument.

Software development is a different story. Here the problems are difficult but not insurmountable. The primary difficulty is getting rid, *via software,* of the scattering due to the optics in the photometer. It is scattering within the eyes of the observers which is the reason for the existence of disability glare in the first place. Unfortunately, all glass lenses incorporated into imaging photometers, even lenses that use advanced multicoating techniques, suffer from the same scattering effects when imaging bright sources.

The way to reduce the scattering via software is by using pattern matching or image processing. Headlights are, roughly speaking, disks or contiguous "blobs". The scatter on the other hand shows up as tiny "speckles" or bright points that are widely distributed. While humans can easily recognize the difference, it is harder to program a computer to make a distinction. Thus a programmer with expertise in pattern matching might be able to build on what we have done by getting the computer to identify the headlights[56] and then subtract out the "noise" (scatter)[57]. The "dirty windshield" scenario might be an exception to the above discussion since the scattering is now external to the photometer and thus is not an "artifact" but a true cause of glare. Despite the different approaches to disability and discomfort glare in terms of image analysis, a software method of scatter removal would be useful in the measurement of both types of glare, provided it is implemented at the initial stage of image processing (i.e., before the pixel-by-pixel analysis used in the disability glare analysis, or the pattern matching techniques used in the discomfort glare analysis).

---

[56] This could perhaps be multiple pairs of lights at varying distances and angles in the general case.
[57] Of course if hardware advances to the point that only one exposure is needed one must be careful that the background doesn't get subtracted out with the noise.

In addition to improving the software, the Glare Meter Tool should ultimately be validated for *disability* glare over a greater range of conditions than we employed in our laboratory testing. The incorporation of disability glare into the Glare Meter Tool was beyond the scope of the project as originally proposed. Due to limited resources, we included only one background luminance in the disability test. This made the analysis much easier, but any future work should include several values for background luminance, even if the background is not likely to vary widely for a nighttime scenario.[58]

We did not perform any *disability* glare field tests (only *discomfort* glare), also due to limitations of time and resources. However, any future development work should include these tests. These would not be as straightforward as for discomfort glare. Any future requirements for such tests should be developed *after* discussions with traffic engineers *who are acquainted with disability glare* (see page 32 of this report). Since most foreign objects on the road are not self-luminous, unlike the computer-generated disk in our lab tests, the objects (or pedestrians) must be detected by contrast with the surrounding roadway. The design of a disability glare field test might fix the luminance of the object ("L_T") to be tested, and then adjust the intensity of the glare source ("L_P") to determine the point at which the object can no longer be detected. The reader should note that *without these two pieces of information regarding disability glare* (performance under varying background conditions, and disability field test results) *it is hard to say in any quantitative way what would happen with given glare countermeasures*.

In addition to further development of the Glare Meter Tool, glare mitigation experiments could be done, both with and without observers, using the ideas in this report. Various countermeasures such as increased ambient lighting, increasing the width of the median, or introduction of glare screens, could then be tested to determine if the effects of disability glare or discomfort glare are reduced. Without a more robust version of the Glare Meter Tool such experiments would, of necessity, be inefficient, but perhaps the urgency of glare mitigation outweighs waiting around for further development of an automated tool.

If observers are employed, the estimation of *discomfort* glare could be achieved as in classical discomfort glare experiments, without the Glare Meter Tool, taking care that proper sampling techniques are employed. One would assemble a group of observers who meet the criteria of being currently licensed drivers with no (major) visual impairments and then have them estimate the strength of the discomfort glare using the De Boer rating scale. A reasonable cross-section of people, in age especially, should be used. Based on our experience in the present study, we would recommend that at least 15 observers be used in order that the effect of "outliers" be minimized (by the inclusion of enough observers so that most observations fall within normal ranges). There is a temptation in psychophysical research to use as few people as subjects as necessary; it should be resisted. Anyone planning such tests can refer to Appendix K to get an idea of the variance in De Boer ratings among observers.

---

[58] Street lighting as a mitigation strategy for glare would, of course, result in a much bigger change to L_B.

Using observers for *disability* glare tests of glare mitigation strategies would require great care in planning to produce meaningful results. There are two reasons for this. First, although we have mentioned the veiling luminance as the most readily understood *physical* measure of disability glare, this is a slight over-simplification. The product of the threshold contrast *and* the proportionality constant for the veiling luminance is actually the most operationally relevant criterion.[59] This number must be obtained by linear regression on the data of several observers, not just a simple averaging process as can be done in the case of De Boer scores.

Secondly, *disability* glare measurement in roadway scenarios requires a careful choice of target to be detected, in contrast to *discomfort* glare where no target choice is involved. This is why traffic engineers should be involved in designing disability glare tests—to determine what targets are of the most interest (e.g. pedestrians, objects that have fallen onto the roadway, etc.) and to determine what backgrounds (e.g. different roadway surfaces) are important to consider.

Without using observers, tests could be done with the hardware component (imaging photometer) of the Glare Meter Tool but without the software, using just the photometer data and the methods outlined here. This would mean that all the calculations are done "by hand" as it were, and this could be quite tedious. An extensive, systematic testing program without observers should therefore probably await further development of the Glare Meter Tool, but a handful of tests would be manageable.

For example, in the case of *disability* glare and a test regarding a wider median as a glare mitigation method[60] something akin to Figure 14 (page 32) would apply. Equation (6) for L_P (page 13) could be approximately calculated (for a fixed age) by measurements directly off of the photometer image. This would be done for pre- and post- mitigation efforts (that is, for lesser or greater eccentricity of the glare source relative to the direction of gaze). If traffic engineers have established a given "ck" value[61] (slope of the line in Figure 14) and a desired threshold luminance that needs to be achieved in a given background luminance, then the calculation of L_P should indicate whether or not the attempted mitigation would be successful.

---

[59] This is "ck" from equation (9) on page 15. See also figure 14 on page 32 where ck represents the slope of the line.
[60] Testing another mitigation method such as increased street lighting would mean taking into account a varying background luminance. Since our tests were at a constant background value, figure 14 would not directly apply in that case.
[61] This is another reason that disability field tests are desirable beyond the development of the Glare Meter Tool. Although we had a sizable portion of our subjects align near a particular value of ck in our lab tests, we make no claims that this is the definitive value to use. Furthermore, traffic engineers are not likely to know the likely values of L_T needed without further measurements. A desired situational need like "*a light-colored raincoat on a pedestrian 200 feet away on the side of the road on a moonless night*" would have to be turned into actual luminance values.

Similarly, *discomfort* measurements without observers can be made with the photometer, absent the software, by doing "hand" calculations on the photometer image. Techniques described in Appendices D and F would allow for estimation of the angle of the glare source (eccentricity) and the solid angle the source subtends.

In summary, we have developed a Glare Meter Tool and tested it in a series of laboratory and field experiments. We have found it to be highly accurate, both for predicting the equivalent veiling luminance due to disability glare (verified by a psychophysical threshold contrast task) and the De Boer rating of discomfort glare (verified by comparing the prediction of the instrument with the subjective ratings by human observers). The Glare Meter Tool at its current stage of development is useful as a laboratory device but impractical for most field work. We have described how the Glare Meter Tool can be improved with future iterations of hardware and software. We have also made recommendations concerning potentially useful experiments with glare countermeasure strategies that can be performed at the present time, using methods of analysis we have developed in this project.

VII Acknowledgments

VIII – Appendices

A. Literature Review

B. Notes on the Luminance Values of the Concentric Disks in the Disability (Contrast) Test

C. Measured Current in the Disability Glare Test LED for the Three Settings and Other Data

D. Angle-Pixel Scaling and Measurement for the Radiant Imaging Photometer

E. Notes on the Calculations for Positions α and β

F. Calculations for the Solid Angle Subtended by CCD Pixels in an Imaging Photometer

G. Disability Glare Raw Data Tables

H. Matlab program for Discomfort Glare Analysis Method 1

I. Matlab program for Discomfort Glare Analysis Method 2

J. Position Factor for Discomfort Glare Analysis Method 2

K. Discomfort Glare Raw Data Tables.

L. Glare Meter Tool – Condensed Instructions for Use.

Appendix A: Literature Review

We have searched a variety of sources in libraries, on the internet, and elsewhere, in order to learn the history of research concerning glare and driving, with particular attention given to finding sources that describe means of glare reduction. The sources we consulted for the literature review, including those which looked promising but proved irrelevant to the present purpose, can be found in the reference list at the end. We have chosen to present the history chronologically. We have concentrated largely on trying to locate material specifically relevant to the current study, thus restricting this survey to papers which concern transportation in general and headlight glare in particular. We cover both disability glare, which results in reduced contrast sensitivity and may negatively affect task performance, and discomfort glare, which may not affect task performance but presents an annoyance and distraction to the driver. We have photocopied each source and converted them to PDF format, with a compilation available on DVD as an additional resource.

While this survey is intended to present previous research on nighttime glare on roadways, there is a vast literature on the subjects of disability glare and discomfort glare in general. Certain of these references, while not specifically related to transportation, proved very useful to this project and will be cited in footnotes in the sections following the literature review.

"Headlighting With Minimum Glare" (1948) - Val J. Roper: Illuminating Engineer, General Electric Company's Lamp Department

Roper states that glare cannot be reduced with the then current means without compromising visibility. Roadway visibility is obviously a crucial necessity to driving, especially at night time. Sealed beam headlamps satisfy all the requirements needed for a driver to see the road in front of him clearly. There is sufficient amount of light above and below the horizontal, making it safe to drive at all reasonable speeds when no other cars are approaching. However, the sealed beam headlamps are extremely glaring. The solution is to find a middle ground between the two extremes. An ideal driving setting for any particular driver is to use his upper driving beam while the approaching cars are using lower beams or even parking lights, but this scenario obviously puts the other driver at a disadvantage. The compromise reached has been implemented into our cars today with the lower beam for regular traffic and the upper or high beam for instances when there are no approaching cars. In the United States, the compromise leans toward visibility, while in Europe, the compromise sides more with glare reduction. In order to provide safe seeing distance, the United States sacrificed comfort by coping with the higher level of glare from approaching vehicles. Europe, however, only has glaring at the level of the United States' parking lights, but the visibility distance has been greatly reduced.

A prominent automotive company, the Polaroid Corporation, and the General Electric Company have all cooperated to develop polarized headlighting, which provides adequate visibility while reducing glare. They ran experiments where the driver tried to spot the observer while opposing headlights are visible. The methodology was compromised, however, by assuming an attention factor of 0.5, and the observers and drivers were not naïve as to the test methods; therefore, the driver was attentively searching for a pedestrian in dark clothing on the road. The attention factor was only applied to one of the experiments. Thus the experiment was flawed because drivers who expect something to show up will react differently than drivers who are unaware of

the situation. After careful consideration, the automotive company decided not to implement polarized headlighting for many reasons; however, the reasons are not stated in the paper. Roper believes the reasons included cost, the hazard of confusion, complaints during a long transition period with mixed headlighting technologies, and the nuisance of viewing the road through an analyzer. In the meantime, the author offers that the way to minimize glare annoyance and maximize safety with present lighting systems is to keep headlamps properly aimed and to emulate the example of the safe driver who observes the law regardless of the circumstances and actions of other drivers, this based on a Connecticut survey categorizing types of drivers on the roads at night.

"Interim Measures for the Prevention of Dazzle on Roads" (1948) - Road Research Board:
Road Research Laboratory's Department of Scientific and Industrial Research

As in other studies, the authors acknowledge that there is no definite solution to having the maximum illumination to light the road, while at the same time eliminating glare from approaching vehicles. A compromise has been the policy for years, but the question arises of which to compromise more, visibility or glare reduction. Instead of trying to implement a whole new approach that may take years to approve and put into effect, the study focused on finding a solution using presently available means. The Road Research Laboratory specifically aimed to answer the following question with this study: What can be done with the lamps and vehicles already in use?

The authors began by presenting the current regulation at that time in relation to headlamps. "No lamp showing a light to the front shall be used on any vehicle unless such a lamp is so constructed, fitted and maintained that the beam of light emitted therefrom" satisfies one of these four conditions:

1. Is permanently deflected downwards to such an extent that it is at all times incapable of dazzling any person standing on the same horizontal plane as the vehicle at a greater distance than 25 feet from the lamp whose eye level is not less than 3 feet inches above that plane
2. Can be deflected downwards or both downwards and to the left at the will of the driver in such a manner as to render it incapable of dazzling any such person in the circumstances aforesaid
3. Can be distinguished by the operation of a device which at the same time causes a beam of light to be emitted from the lamp which complies with sub-paragraph (1) of this paragraph
4. Can be distinguished by the operation of a device which at the same time either deflects the beam of light from another lamp downwards or both downwards and to the left in such manner as to render it incapable of dazzling any such person in the circumstances aforesaid, or brings into or leaves in operation a lamp or lamps (other than the obligatory front lamps) which complies or comply with sub-paragraph (1) of this paragraph.

This regulation shall not apply to any lamp fitted with an electric bulb, if the power of the bulb does not exceed 7 watts and the lamp is fitted with frosted glass or other material which has the effect of diffusing the light."

Even with these regulations implemented, dazzle has not been eliminated. The researchers believe it was due to the vagueness of the word "dazzle." Regulations were difficult to enforce because the intensity of the passing beam was left undefined. In order to better understand the situation, a survey was done on drivers' behaviors, whether or not they dipped their lights when other vehicles approached, what lamps they used, and whether those lamps were dazzling. There is no way to precisely measure the levels of dazzle; therefore, this survey attempted to set up a standard. The conclusions were as follows:

1. Vehicles causing dazzle on main roads
    a. 1 of 4 on unlighted roads
    b. 1 of 10 on lighted roads
2. 100 cases of dazzle on unlighted main roads
    a. 38 were caused by dipped headlamps of passing beams
    b. 37 by passlamps of passing beams
    c. 25 by undipped headlamps of driving beams
3. On unlighted main roads
    a. Of every 100 dipped headlamps: 17 were dazzling
    b. Of every 100 passlamps: 40 were dazzling
4. Proportion of drivers without dipped lamps on main roads
    a. 1 in 20 on unlighted roads
    b. 1 in 50 on lighted roads
5. Continuous passing beam usage on main roads
    a. 80 of 100 on unlighted roads
    b. 90 of 100 on lighted roads.

Based on the results of the survey, the researchers recommended improvements of passing beams from both dipped headlamps and passlamps. The adjustment might have proved to be effective if drivers ensured that their lamps were properly adjusted. The improvement could be as large as eliminating three-quarters of all instances of dazzle. In addition to guidelines, driver education would be necessary to obtain the greatest effect of these changes.

"A summary of papers and discussions on Lighting Problems in Road Traffic" (1962) - Bertil Bjorkman: compiled together for The Official Swedish Council on Road Safety Research

To further refine the definitions of glare, Bjorkman describes the specific types of glare that affect drivers directly. The first type is known as physiological glare *(now called "disability glare")* blinding or actual blinding, which is the literal aspect of vision loss. When a driver looks directly into the headlights of approaching cars, the driver's eyes temporarily cannot transmit visual images. The strong opposing headlights prevent the driver from seeing his side of the road. As a result, the driver becomes a hazard to himself as well as to other drivers on the road. This has resulted in the rule about "dipping the lights."

The second type of glare is referred to as psychological blinding or light-irritation *(now called "discomfort glare")*. This particular type focuses on the driver's discomfort level regardless of the level of blinding. Once again, the driver's vision is compromised, causing the driver to be dangerous on the road. On the basis of experiments, experts concur that a driver's vision does not necessarily have to be compromised. With education and visual training, an experienced

driver can improve his visual powers under these unavoidable instances. The authors speculate that an added component to the drivers' training and licensing could emphasize glare blinding education while decreasing the level of psychological blinding.

"Accident Analysis Before and After Installation of Expanded Metal Glare Screen" (1969) - James V. Musick: Chief Traffic Engineer of Columbus, Ohio Department of Public Safety Division of Traffic Engineering and Parking

In Columbus, Ohio, the Department of Public Safety conducted an investigation on the statistics of urban interstate freeway accidents before and after installation of an expanded metal glare screen. The glare screen was placed in the median of a horizontal curve. For the analysis, accident rates were compared by taking into account travel direction, time of day, and type of accidents.

The before period consisted of months ranging from July 1, 1964 to April 1, 1966, and the after period the months ranging from May 1, 1966 to February 1, 1968. The month of April in 1966 was eliminated from the results because the screen took three weeks to install. The steel beam guardrail was installed on Interstate 71 because it is the busiest highway in the city. The reason for the specified location is due to the fact that on the horizontal curve, the southbound vehicles headlights shine directly into the eyes of the northbound drivers. The screen installed was a two-foot high expanded metal glare fence over a stretch of 3,000 feet of freeway. The purpose is to block out all glare from the opposing headlights up to an angle of at least 20 degrees in relation to the centerline of the roadway. 20 degrees will cover all objectionable glare, which is the main focus. The unflattened expanded metal mesh was placed low to account for vehicles with lower headlights, but it was placed high enough to ensure that truck headlights were efficiently blocked as well.

The four aspects this research focused on were accident rates, traffic volumes, time of day, and cost of installation and maintenance. The following questions were considered:

1. Was there a significant change in accident rates when considered by direction of travel and time of day?
2. Did the glare screen reduce the glare sufficiently for the full length of the curve on which it was installed?
3. At what angle on the curve was the glare eliminated during nighttime conditions and can vehicles be seen through the fence during the daytime?
4. What is the cost to install and maintain this type of fence over a period of several years?
5. Did the fence produce any objectionable problems such as snow drifting?

With those questions in mind, the investigators analyzed their data. For accident rates, statistical significance was based upon a Chi square test at the 95% confidence level. Although accident reports were tabulated, the accuracy of the exact accident location may be compromised due to the lack of available technology during that time.

There was a reduction in northbound accidents, which was expected because the screen was installed to prevent southbound headlight glare from northbound drivers' eyes. The reduction was a significant 61.5% for nighttime accidents. On the opposite site of the freeway, the

southbound night accidents increased significantly with no known cause. However, daytime accidents on the southbound side decreased by 68.4%, which was statistically significant. The researchers are uncertain if the fence is effective during daytime hours; therefore, there is no conclusive analysis for the decrease. Although nighttime accidents decreased by 11.8% and daytime accidents decreased by 31.4% as a whole, neither change was statistically significant.

A permanent counting station measured traffic volumes, which steadily increased except for 1966 when they dropped slightly. As for the angles, at 10 and 20 degrees, the vehicles are completely concealed from one side to the other. Starting at 30 degrees, the vehicles become faintly visible. The cost of the fence installation was $5,615.63, which averaged to $1.87 per lineal foot (3,000 lineal feet total). Maintenance for the fence was estimated to be less than $500 per year. In addition, throughout the three years, no drifting of snow occurred. Overall, although there was not statistical significance at the 95% confidence level for the overall data, a reduction was seen in the number of accidents throughout. The authors propose additional study on different types of horizontal curves.

"Effectiveness of Glare Screens" (1973) – John T. Capelli: Assistant Civil Engineer; sponsored by the U.S. Department of Transportation Federal Highway Administration and the Engineering Research and Development Bureau

Capelli reviewed available sources and information related to glare screens. Both he in his review, and we in ours, have found literature to support the effectiveness of glare screens, but no warrants have been established for their extensive usage. Although lateral separation seemed to be effective, the wide range of test conditions and variables results in inconclusive outcomes. Capelli, in his survey, selected numerous different locations, ranging from New York to Michigan and Pennsylvania.

Capelli focused on the types of glare screens that proved to be most effective. Glare screen is the common name to describe an array of glare reduction mechanisms, such as planting, fences, and screens. Planting methods were advantageous in some ways, but there were disadvantages as well. The maintenance of planting required a great deal of ongoing attention. Not only was watering and weeding necessary, but also occasional pruning after the plants were full-grown. Other disadvantages included removal of ruined or wilted plants, inability to survive harsh weather, and stunted growth due to the narrow median. Because of the high maintenance nature of planting, fencing became the favored choice. Fencing consisted of a variety of types, such as wooden baffles, plastic panels, redwood and masonite laths, an earth berm, cedar logs, and expanded metal mesh. The major disadvantage of fencing was the high cost of installation and maintenance. During previous studies, however, the California Division of Highways found expanded steel mesh could be substituted for chain link without reducing the cable-chain link median barrier's effectiveness in retaining a high-speed impacting vehicle. Much like the other studies we have investigated, expanded metal meshes are found to be the most satisfactory among the possible solutions.

"Glare Screen Guidelines" (1979) - National Research Council (U.S.) Transportation Research Board: sponsored by the American Association of State Highway and Transportation Officials, Federal Highway Administration

We found this particular source to be quite insightful. The contents covered include types of glare screens, the relationship between driver and vehicle, design requirements, and future recommendations. To begin, the researchers investigated not only the types of glare screens that prevent glare, but went into depth about the visibility of opposing traffic due to glare screens. Some suggested that opaque glare screens would be best to prevent not only glare, but also gawking of drivers into the other lanes. Others argue that this same prevention would also limit law enforcement views of accidents and necessary aid for the opposing traffic. The three different types of glare screen are shown below with the two extremes on top and bottom and the compromise in the middle. Glare screens aim to offer effective reduction of glare, simplicity of installation, resistance to vandalism and vehicle damage, rapid and safe repair, minimal cleaning and painting requirements, minimal accumulation of litter and snow, wind resistance, reasonable cost including maintenance, good appearance, and emergency access to opposing lanes. The common use of glare screens at the time consisted mainly of expanded metal mesh as well as shrubbery, earth mounds, tall median barriers, metal and polyester mesh, and plastic paddles. Although most have succeeded in decreasing drivers' discomfort from glare, very few have been shown to reduce accidents. In addition, maintenance and repairs were difficult and expensive.
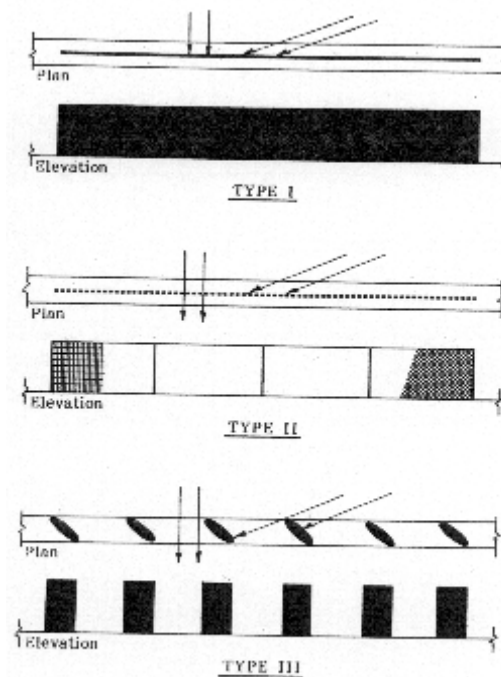
Figure 1. Plans and elevations of glare screen types I, II, and III.

There are many ways to reduce glare, both by highway design and with physical barriers. Highway designs with wide separation could be an easy method of avoiding glare altogether as long as the surrounding provided enough area. With the exception of horizontal curves, a 50 foot wide median between the two opposing traffic could control glare. Separation of grades in hilly terrain could also help reduce glare. Lastly, excess earth left or built in the median was a low maintenance glare reduction method. Since most highways are restricted in space, physical

barriers were a more effective way to reduce glare. Types of physical barriers include guardrails, concrete barriers, plantings, and fences. Glare screens can be mounted onto barriers. The most widely used were the expanded metal mesh, which falls under the type II category shown above. Expanded metal mesh is usually comprised of steel or aluminum with parallel slits in diamond patterns. Another type of metal screen is the double reverse corrugated steel screen, category type I. The screen is slit horizontally and compressed to maximize its strength. Type II also includes knit polyester fabric, which actually diffuses rather than blocks light from opposing traffic. An example of a type III glare screen would be paddles that are placed individually at intervals to block headlamps.

The paper includes discussion of many factors including the following:

Sensitivity to Glare: Sensitivity to glare varies widely among individuals and most importantly with age. Older drivers are more sensitive to glare, particularly after they reach the age of 45 or 50.

Types of Glare: Two types of glare are recognized - that which causes disability and that which causes discomfort. Disability glare causes a decrease in visual task performance; it can be assessed in terms of reduced seeing distance of a target under varying glare conditions. Discomfort glare causes annoyance to the driver without necessarily impairing visual performance. The two types overlap and may result in a driver's losing orientation relative to the roadway or to other traffic.

Optical Devices: Except for polarized headlamp systems, there are no optical devices that will overcome glare for the driver. In particular, colored glasses and tinted windshields, although seemingly helpful in reducing glare, actually reduce seeing ability at night. Polarized headlamp systems have been shown to be effective, but they have never gained the acceptance necessary for general use.

Driver Licensing: Current legal requirements for obtaining a driver's license do not include a test for glare sensitivity and probably will not in the foreseeable future.

Design Cutoff Angle: The accepted cutoff angle of 20 degrees on tangent for the design of type II and type III glare screens. This value was derived from measurements of peripheral vision and the limitations of tunnel vision. In any event, experience has shown that 20 degrees is a practical value.

Dwell Points: Two different studies indicate that drivers do not normally look very far ahead in order to obtain information necessary for vehicle control. Information farther than 90 feet from the driver is of relatively little value for determining velocity. On two-lane roads, drivers' eyes normally dwell on the center of the lane about 500 feet in front of them under daytime conditions and about 230 feet at night. On curves, the dwell point moves toward the edge of the lane in the direction of curvature. The dwell point also shifts toward glare sources.

Intensifying Effects of Glare: Relatively common conditions, such as rainfall, dirty windshields, dirty eyeglasses, and driver fatigue intensify the effects of glare.

Veiling Brightness: Veiling brightness, which is defined as the intensity of disability glare from all sources, can be measured by a Fry-Pritchard glare lens used with a Pritchard Telephotometer. Disability veiling brightness was defined as light on the retina of the eye that does not contribute to the image being viewed.

Targets: Controlled tests of the detection distance under glare conditions are usually conducted with black, diffuse targets that correspond roughly to a pedestrian in dark

clothing. The diffuse targets obviously are much more difficult to see under glare conditions; however, the vehicle reflectors might seem to be more realistic and usable targets for tests on divided highways.

Glare Distance: For a given lateral separation, the effects of disability glare were present even at distances of 3000 feet or more and the rate of change of the effect with distance was small for most of this distance. This may account for the observed brightness of headlights on a highway with a narrow median, in that the glare sources in all lanes seem to be of equal brightness.

Glare Test Vehicles: Most reported tests of target detection distance have been conducted with single vehicles, some with high beams and some with low beams, as glare sources.

Alertness of Drivers: In most of the reported tests, the drivers have been aware they were looking for a specific object. Studies made to compare the detection distance of "alerted" and "nonalerted" drivers show that the alerted ones are able to see targets at much greater distances – up to twice as far.

Height of Driver's Eye: The accepted height of a driver's eye for highway design purposes is 3.75 feet. A recent study shows the driver's eye height for the 15th percentile of sample cars to be 3.49 feet, for cab-over-engine trucks to be 8.41 feet, and for cab-behind-engine trucks to be 7.80 feet. There is also a trend toward greater eye heights in vans and pickup trucks, which represent an increasing share of vehicle sales.

Lateral Dimensions: A study suggested that test vehicles be assumed to drive the center of a 12 feet lane, that the driver's eye be assumed to be at 4.25 feet from the left edge of the lane, and that the headlights and taillights be considered to be at the side of the vehicle 2.75 feet from the edge of the lane. These dimensions allow calculations to be made on the basis of lateral separation; the minimum separation of an undivided highway is 7 feet. The lateral separation of divided roadways can be calculated by adding the width of the median and any intervening lanes to the basic 7 feet.

Headlight Height: An average height for automobile headlights is about 26 inches. The height of truck headlights is more variable; some are mounted very low for seeing in fog. An average of 3.75 feet for the higher lights has been used for one design.

Headlight Aim: The standard established by the American Association of Motor vehicle Administrators for motor vehicle inspection provides that the top of the headlight beam shall be aimed within 4 inches above or below horizontal at a distance of 25 feet. In practice, however, many headlights are misaimed, either through neglect or by the loading of the vehicle.

Taillight Height: There seems to be no standard placement of automobile taillights. A few random measurements show the average mounting height on smaller passenger vehicles to be about 32 inches.

Headlamp Intensity: The National Highway traffic Safety Administration recently increased the permissible intensity of headlamp systems from 75,000 to 150,000 candlepower by a revision to Federal Motor Vehicle Safety Standard No. 108. Data on which this decision was made included an apparent 20 percent increase in seeing distance when no car is approaching and only a 1.5 percent decrease when approaching vehicles use high beams with the 150,000 candlepower lamps, as compared to the present 75,000 candlepower lamps.

Use of High and Low Beams: The rules of the road in most states require that motorists use the low beam when approaching an oncoming vehicle within 500 feet and when approaching another vehicle from the rear within 300 feet. If followed, this would limit

headlight use to low beams on any divided roadway with an appreciable amount of
traffic. Little information was found that related headlight use to traffic volume on
divided highways.

Traffic Volumes: Although there are no published data on the relation of headlight glare to
traffic volume, it seems logical that glare will increase in proportion to volume.
However, the effect of multiple lanes is not known.

Few studies have focused on the relation between median width and glare. The available
references recommend glare screen installations on tangents and very flat curves for medians 20
feet or less in width. The height normally recommended is 50 inches with sag verticals up to 80
inches. Cutoff angle was agreed upon to be 20 degrees for tangents and 20 degrees plus angle of
curvature for horizontal curves. Further studies related to geometric design standards were
recommended.

**"Field Trials of Tests to Determine Susceptibility to Glare and Defects" (1980) - M.L.
Wolbarsht:** sponsored by La Prevention Routiere Internationale

While engineers focused on reducing glare for drivers through various methods, Wolbarsht
proposed to quantitatively measure the susceptibility of drivers to glare as well as evaluate their
peripheral vision by a more comprehensive vision screening test prior to receiving their driver
licenses. The experiment used the Bausch and Lomb Orthorater to measure glare sensitivity;
however, the author states that any equivalent instrument would be sufficient. 1500 observers
were tested but measurements on only 952 of them were used to determine the levels of elevated
glare sensitivity or peripheral vision defects. The results showed a positive correlation between
the sensitivity to glare and age as well as the individual's elevation in glare sensitivity and his
appreciation of his own visual problem. Wolbarsht confirmed that, due to age-related ocular
diseases, individuals of older age would exhibit increased glare effect and veiling glare. Causes
include but are not limited to cataracts, cloudy corneas, turbid vitreous humor, and floaters in the
aqueous humor. In addition, he suspects that neurological disturbances in the visual system may
also cause increased sensitivity to glare. Wolbarsht strongly recommends a test to gauge visual
sensitivity for potential drivers in order to reduce hazardous drivers on the road. Subsequent
retests should also be assessed periodically.

**"On the Reduction of Disability Glare Under Night Driving Conditions" (1980) - W.
Adrian:** sponsored by La Prevention Routiere Internationale

Adrian described in detail the effects of disability glare on the eye and also introduced an
approach to alleviate the cause. Disability glare is due to light scattering and diffusion from
various ocular structures. This scattered light actually superimposes with the image on the
retina, which in turn masks the object from the viewer's eye by reducing contrast. Once again,
age becomes a major concern in drivers because of the increase in scattered light produced in the
aging lens. Nighttime driving is the most difficult for drivers because of the high luminance in
the visual field from headlamps of approaching cars or from non cut-off lanterns in low-quality
lighting installations.

Through multiple formulas and mathematical calculations, Adrian was able to find relationships
between glare angles, scattered light, wavelength of light, and age. Using his data, a new

spectacle design was created for the purpose of reducing stray lights in the eye and counteracting the glare effects. In Adrian's anti-glare lenses, an annular zone is arranged in a way to cover only parts of the field in which glare sources can occur. This annular zone shows a density gradient with high values close to the center and decreasing with the inverse square of the angle, which represents the positional aspect of the disability glare equation used. The purpose of the spectacles is to cover the glare source areas while keeping the periphery clear to allow unimpaired vision in that part of the visual field. Adrian concludes these types of lenses reduce the scattered light, and thus glare.

"Assessment of anti-dazzle screen on M6" (1980)- A. E. Walker: Researcher for TRRL; sponsored by Transport and Road Research Laboratory's (TRRL) Department of the Environment, Department of Transport, Accident Investigation Division's Safety Department; **R. G. Chapman:** Researcher for TRRL

In an effort to reduce glare from opposing traffic, an anti-dazzle screen was installed on the M6 Motorway on the Midlands Link. After the 19 km screen was installed, accident rates were tabulated and categorized as non-injury or injury accidents. The initial idea was to do a before and after study by putting the screen up on a length of highway that allowed for a control section; however, there were no highways suitable in length. Therefore, the control length used was only 10 km instead of the full 19 km stretch.

The anti-dazzle screen used the accepted optimum design of the expanded metal screen. Angles ranging from 15 to 20 degrees worked best in preventing light passing through the median. The necessary height was 1.73 m. After consultation with the Landscape Advisory Committee it was agreed to use plastic vanes mounted vertically on a horizontal tube attached just above the guardrail—a design in use in other European countries. The cost averaged the equivalent of 87,000 euros, which is about 4,600 euros per km, with an additional 150 euros per km for maintenance cost annually.

Throughout the experiment, data was collected for each accident and the type of accident that occurred. In addition, the traffic on both sides was closely monitored. The results are summarized in the table below. Comparing the dark/daylight ratio of accident rates for all accidents on the screened sections with the control indicates that the dark accident rate relative to the daylight accident rate on the screened sections was lower than expected from the control data. The patterns between non-injury and injury varied; therefore, the analysis was done separately. With the results presented, the authors concluded that the anti-dazzle screen aided in the prevention of glare without affecting traffic flow.

Summary of accident data over 3-year period

Section		Dark			Daylight		
		Non-injury	Injury	Total	Non-injury	Injury	Total
Control	Accidents	21	15	36	29	14	43
	Veh x km x 10^7		8.73			28.38	
	Accident rate	2.41	1.72	4.12	1.02	0.49	1.52
Anti-dazzle screen	Accidents	13	18	31	57	13	70
	Veh x km x 10^7		9.79			33.30	
	Accident rate	1.35	1.84	3.17	1.71	0.39	2.10

"Car Headlamps" (1980) - P. Soardo: sponsored by the International Association for Accident and Traffic Medicine, International Road Federation, and La Prevention Routiere

The author states that lighting requirements for a vehicle should accomplish the following:

1. Assure the visibility of the car to other vehicles or pedestrians (the so called conspicuity)
2. Signal the intentions or the actions of the driver (change of direction, braking)
3. Assure the visibility of the road and of the possible obstacles on it sufficiently in advance to enable an appropriate action.

The main purposes of headlights are to light the road ahead of the driver and to improve the visibility of the vehicle to other drivers. Although a driver may see better with a higher level of illumination, glare from his own headlights prevents safe use of too high an intensity. According to the author, glare can be limited only by the following methods: global limitation of the luminous intensity, restrictions to the luminous intensity distribution, control of the luminous intensity based on the distance between the opposing cars, and/or use of the polarized light.

The author focuses on two aspects of glare: the reduction of visibility for oncoming drivers and the discomfort, which may cause tiredness and result in accidents. A formula scale, from 1 (unbearable) to 9 was used to estimate the severity of glare for drivers. Overall, the author's intent was to remind us of the problem and update us on the current solutions. The goal is to obtain more visibility with less glare; however, the final conclusion is that a compromise is necessary to maximize safety for all drivers.

"Efficient Method of Visual Screening for Night Driving" (1980) - H. M. Haddad: sponsored by the International Association for Accident and Traffic Medicine, International Road Federation, and La Prevention Routiere

Due to the nighttime driving hazard presented by glare, the author was concerned with the "dazzle recovery time" (DRT) of drivers. The DRT refers to the time required for a driver to be able to regain visibility after a bright light was shone in his eye. Since it is not feasible to have an ophthalmologist test every driver's night driving abilities, a new method was proposed.

In order to test drivers' DRT, 150 watt low beam and 650 watt high beam lights were used. The subjects began by reading a Snellen chart. Then, they received a second of dazzle spark. After the light, the subjects were asked to read the Snellen chart as soon as they were able to perceive the letters. The time from the dazzle until the time they were able to read the line was recorded as DRT.

The ranges varied quite a bit among the low beam and high beam. The low beam's DRT was between 3 to 50 seconds, while the high beam's DRT was between 10 to 80 seconds. Out of a total of 42 subjects, 4 were aphakic (absence of optical lens), 9 had glaucoma (on miotics), and 6 had macular degeneration. Excluding those particular cases, the ranges dropped to 3 - 10 seconds for low beam, and 10 - 38 seconds for high beam, with a mean of 6 seconds for low beam and 18 seconds for high beam. Based on the results, drivers should not only be tested for their visual acuity during license renewal, but also be tested for their DRT. The authors states

that if the recovery time is longer than 30 seconds, restrictions on night driving should be imposed."

"Human Factors: Effect of Prior Headlighting Experience on Ratings of Discomfort Glare" (1989) – Michael Sivak: Research Professor and Head of University of Michigan Transportation Research Institute's (UMTRI) Human Factors Division; Creator of the Industry Affiliation Program for Human Factors in Transportation Safety; **Paul L. Olson:** Researcher for University of Michigan, Ann Arbor, Michigan; **Kristine A. Zeltner:** Researcher for University of Michigan, Ann Arbor, Michigan

Sivak and his team investigated the effect of prior experience on the level of discomfort glare experienced by observers. Discomfort glare is described as "a subjective impression of discomfort from bright lights." The headlighting standards between Europe and the United States differ due to the ratings from subjects in their respective countries. Europeans' concern with discomfort glare results in low-beam headlights, which decreases illumination toward the top and left of the lamp; therefore, approximately only one-half or one-third of the light of U.S. headlights is transmitted to the oncoming drivers' eyes.

To test whether Europeans are more sensitive to discomfort glare in the U.S., Sivak and his associates experimented with two types of subjects, 9 U.S. born citizens and 9 West Germans. Four types of glare stimuli were used, high beams or low beams, each either unfiltered, or filtered with neutral-density filters having transmissivity of 18%. Three subjects were tested at one time. All three sat in the front of the car driving at 40 mph, while an experimenter sat in the backseat to notify another experimenter every time a cone was passed at specific distances. All the subjects were instructed to look straight ahead but not directly into the stationary car's headlights which were causing the glare (and where the other experimenter was seated).

The results showed a statistical significant correlation between glare stimulus and country. A correlation was seen between glare ratings and illuminance. The effect of glare angle/vehicle separation on glare sensitivity was found to be statistically significant only when controlling for the effect of (the logarithm of) illuminance. The authors conclude that recently arrived West German subjects experience significantly higher levels of discomfort than the U.S. born subjects.

"Night Driving: Effects of Glare from Vehicle Headlights on Motion Perception" (1994) - Stephen J. Anderson: Department of Vision Sciences, Aston University, Birmingham, UK; **Ian E. Holliday:** Department of Vision Sciences, Aston University, Birmingham, UK

The authors studied the effects of glare in night driving. Their main objective was to test the ability of older drivers to overcome disability glare from oncoming headlights. The experiment consisted of observers attempting to notice moving targets on a dimly lit road. Observers were asked to sit in a stationary vehicle and view a computer-generated stimulus display at a distance of 23 meters, which is the average stopping distance of a vehicle traveling 50 kilometers per hour. Another vehicle was stationed as an oncoming vehicle with the display two meters to its side. Display luminance of 50 candela per meter squared (cd/m^2), which is photopic, and 0.5 cd/m^2, which is low mesopic, were used. Three conditions were tested: no beam (control condition), low beam, and high beam. The observer's vehicle always had low beams on. The

observers were allowed to use their binocular vision, with correction, and no head restraints. A stimulus was shown for each trial and observers were required to judge its direction of motion.

The experiment with a photopic display screen showed similar results for the various beam conditions between normal corrected vision and artificially blurred vision; it was concluded that the angle of the headlight beam was irrelevant for that particular comparison. However, with high-beam glare and simulated lens opacities, maximal contrast sensitivity was an order of magnitude less than that obtained with normal vision. In mesopic display screen experiments, simulated lens opacities severely impaired visual performance for detecting moving targets. Even in the so-called perfect observers' vision, headlight glare caused a reduction in detection of moving targets. Observers with simulated lens opacities had a greater significant reduction in visual performance. Mesopic display resulted in a greater reduction in motion sensitivity. He authors concluded that simulated lens opacities behave like age-related cataracts in that they have little effect on standard measures of Snellen acuity; however, glare significantly reduces sensitivity to low contrast targets. Based on the results, sight re-testing, driver re-training, improved road lighting, and vehicle modifications were recommended to prevent the reduction of visual performance.

"Conspicuity and Glare Properties of Daytime Running Lights: Effects of Lamp Separation and Intensity" (1998) - Michael Sivak: Research Professor and Head of UMTRI's Human Factors Division; Creator of the Industry Affiliation Program for Human Factors in Transportation Safety; sponsored by the University of Michigan Transportation Research Institute (UMTRI); **Michael J. Flannagan:** Research Associate Professor UMTRI's Human Factors Division; **Eric C. Traube:** Researcher for UMTRI; **Toshio Miyokawa:** Researcher for UMTRI

In this particular study by UMTRI, daytime running lights were evaluated based on lamp separation and lamp intensity. Daytime running lights were the solution presented for the improvement in daytime conspicuity of vehicles. Each subject rated the level of discomfort glare as well as the conspicuity of the lamps. Nine different stimuli were used for both portions of the study. These stimuli were obtained by the orthogonal combination of three levels of luminous intensity directed to the subject's eyes from the two lamps (14,000, 3,500, and 875 cd), and three levels of lamp separation (1.05, 0.65, and 0.25 m- edge to edge).

Subjects were seated in a car 20 meters away from the lamps. In order to shield the experimenters, another car was parked directly in front of the car in which the observers were seated. To the right of that car, they placed a comparison lamp on a tripod, which illuminated at 36,820 cd at a voltage of 14.7. To the left of that car, a rack of six lamps was placed, which illuminated 7,000 cd when at 12.8 V. All of the 7 lamps were high-beam, tungsten-halogen sealed beams. To obtain the different intensities necessary, filters were used to control the amount of light shone. The De Boer response scale was used to evaluate the level of glare on a scale of 1 to 9, 1 being unbearable. For determining conspicuity of the lamps, the observers were told to adjust the brightness of the comparison lamp to match the lamp on the rack. The data for conspicuity is in voltages; therefore, the experimenters must convert the voltages into luminous intensities.

The results are listed in the tables below. Lamp intensity was the only statistically significant variable analyzed in the glare portion. A positive correlation exists between lamp intensity and discomfort levels: as one increases, the other increases as well. The remainder of the independent variables, such as age, separation, or order of tasks did not show statistically significant correlations. However, the conspicuity portion varied slightly from the discomfort glare results, with both lamp intensity and lamp separation showing statistically significant correlations with conspicuity. No other variables proved to be significant. The authors thus state that if the possible increase in discomfort from narrowly separated lamps is counteracted by a slight reduction in intensity, there is still a net benefit for narrowly separated lamps in terms of conspicuity. Conversely, narrowly separated lamps that are as noticeable as widely separated lamps of higher intensity would be less glaring. Therefore, the final results imply a small net benefit overall in using narrowly separated daytime running lights.

Table 1
The effect of lamp intensity on de Boer ratings of discomfort glare.
(Lower de Boer units indicate more discomfort.)

Combined intensity of two lamps (cd)	Discomfort glare (de Boer units)
14,000	3.9
3,500	6.2
875	7.9

Table 2
The effect of lamp separation on de Boer ratings of discomfort glare.
(Lower de Boer units indicate more discomfort.)

Lamp separation (m)	Discomfort glare (de Boer units)
0.25	5.8
0.65	6.0
1.05	6.1

Table 3
The effect of lamp Intensity on conspicuity.

Combined intensity of two lamps (cd)	Conspicuity (intensity of the comparison lamp (cd))
14,000	15,410
3,500	6,495
875	2,973

Table 4
The effect of lamp separation on conspicuity.

Lamp separation (m)	Conspicuity (intensity of the comparison lamp (cd))
0.25	9,002
0.65	8,512
1.05	7,364

"Headlamp History and Harmonization" (1998) - David W. Moore: researcher of UMTRI

David Moore of UMTRI performed extensive research on the history of headlamps. He went through numerous sources to compile a complete briefing of headlamps beginning at the 19th century. We will summarize his chronology to show how the modern day headlamps came into being. In the 19th century, horse drawn carriages were the primary mode of transportation. The carriages carried lamps with candles and oil burning lanterns. Automobiles were not invented until late 1880s. Although the electric light bulb was invented just prior to that, it was not implemented into the vehicles until much later. Due to the lack of lighting on vehicles, no nighttime driving was possible until oil burning (kerosene) lanterns were used.

As the country headed into the first decade of the 20th century, electric lighting was implemented with a small dynamo driven by the motor flywheel (in 1901); however the cost of the installation was almost as expensive as the car itself. A more efficient method employing acetylene headlamps came into use in 1906. Gas to power these lamps was generated by water dripping slowly onto calcium chloride, but the decrease in temperature caused the water to freeze over. The addition of alcohol to the water alleviated the situation a little bit, but frequent cleaning of the nozzle was required. The switch to a pressure tank containing acetylene gas dissolved in acetone solved the freezing issue, but the gas flame repeatedly extinguished due to winds and rain. The large size and instability provided poor beam pattern control. Because of the minimal number of cars on the road, glare was not a significant problem until near the end of the decade. In 1908, automotive headlamp bulbs in the U.S. using a carbon filament, and containing a vacuum, were introduced. However, soon after that, the advantages of tungsten were quickly realized.

By 1911, electric headlamps were routinely installed. At this particular time, headlamps used a 21-candlepower bulb. European vehicles started mimicking the U.S. automobile installations. Tungsten filament bulbs filled with nitrogen gas were used around 1915. Then, the first lighting regulation was passed by the state of Massachusetts on October 27, 1915, presented as follows:

> "This regulation provided that wherever there was not sufficient light on the highway to make all substantial objects visible for a distance of at least 150 feet (45.7 meters), the lamps which a motor vehicle was required to display, should throw sufficient light ahead to make clearly visible any such object within the specified distance. They provided further that any light thrown ahead or sidewise should be so directed that no dazzling rays should at any time be more than 3.5 feet (1.1 meter) above the ground 50 feet (15 meter) or more ahead of the vehicle, and that such light should be sufficient to show any substantial object 10 feet (3 meter) on each side 10 feet (3 meter) ahead of the vehicle."

Drivers started noticing the glare issue and attempted to diffuse glare sources by attaching pieces of frosted glass. Baltimore, Maryland, passed an ordinance which limited glare but did not control visibility. A progression of light bulbs included simple transverse filaments, coiled-coiled spiral axial designs, and center supported V-shaped coils. The output ranged from 135 to 584 lumens. During this decade, headlamps were approximately 107 cm above the road, and driver's eyepoint was 137 cm above the road. These numbers tended to lower in time, as automobile styles underwent changes. While the headlamps were evolved, glare reduction was

taken into account. Some methods that were used include the following: switching a resistor into the headlamp circuit to reduce the current to the headlamp bulb filament, introducing reflectors that tilt with approaching vehicles, and installing a vacuum connection from the intake manifold. Ironically, instead of reducing glaring effects, each of these methods contributed to the glare. In addition to all the new innovation, standards and regulations were being written to improve the conditions. The first joint Illuminating Engineering Society (IES) and Society of Automotive Engineers (SAE) completed the following specification in 1918:

> "Measurements shall be made at the following positions at a distance of 100 feet (30.5 meters) ahead of the headlamps:
>
> Position 1. Directly ahead and at a height not less than one-half the distance of the center of the headlamps above the level surface. The indication of the foot-candle meter shall be not less than 0.48 ft-c (5.2 lux) for a motor vehicle and not less than 0.24 ft-c (2.6 lux) for a motorcycle.
>
> Position 2. Seven feet (2.1 meters) to the right of Position 1 at any point not above the level of the headlamps. The indication of the foot-candle meter shall be not less tan 0.12 ft-c (1.3 lux) for a motor vehicle and not less than 0.06 ft-c (2.6 lux) for a motorcycle.
>
> Position 3. Directly in front, 5 feet (1.5 meter) above the level surface. The indication of the foot-candle meter shall be not more than 0.24 ft-c (2.6 lux).
>
> Position 4. Five feet (1.5 meter) above the level surface and 7 feet (2.1 meter) to the left of the axis of the vehicle. The indication of the foot-candle meter shall be not more than 0.08 ft-c (0.9 lux).
>
> Note: In order to allow for any possible inaccuracies of a test of this character, a tolerance of 20 per cent may be allowed on the above values."

The authors claim that the first documented study of headlamp performance was conducted in 1920. In the experiment, thirty headlamps were used, tested by laboratory photometry as opposed to on-road performance. These particular headlamps used 1 3/8 inch (35 mm) focal length parabolic reflectors and were 9 inches and 9 ¼ inches in diameter. Glare levels were found to be generally acceptable. The researchers also agreed that additional lighting was needed to make road objects adequately visible.

The studies continued into the 1920s. During this decade, inspections were made throughout the country that required drivers to have a certificate verifying the proper usage of headlamps. The criteria included: proper aim, sufficient light output, and control of excessive glare. With the rapid increase in numbers of automobiles, two different philosophies evolved:

1. Primary emphasis: Develop as much light as possible to maximize seeing ahead of the vehicle. Secondary emphasis: Consider the other driver and try to do something to minimize glare.
2. Primary emphasis: Do whatever is necessary to minimize glare in the other driver's eyes. Secondary emphasis: Try to make sure there is available light to drive.

The first approach is the one the United States has adopted, while the second approach is the one the European countries have adopted. The priorities vary internationally even though the International Commission on Illumination has passed regulations to promote uniformity of

headlamps worldwide. In the mid-twenties, the first two-beam system was developed, which was practiced until the mid-fifties.

In the United Kingdom in the 1930s, a movable reflector assembly was used to control glare toward opposing vehicles. An electromagnet operated by a switch under the driver's control allows the assembly to be tilted down and toward the side of the road to alleviate the glare to the approaching driver. Various types of patterns were developed in the U.S. to help control the glare, which includes the following: three-filament bulbs with a regular high beam, a regular low beam, a meeting beam, and a super high beam, and ranges from a single beam up to four beams as well as side shifting beams. Throughout the decade, engineers, researchers, and manufacturers all tried over and over again to control glare conditions. Due to dissatisfaction with the current headlamps, new headlamps were invented to improve efficiency. Various schemes were tried. Ultimately, the glass sealed beam headlamps satisfied most of the desired criteria. The glass sealed beam was made of two pieces of glass, a lens with optics, a parabolic aluminized reflector, and tungsten filaments supported by metal lead wires. Within a space of several years, automotive manufacturers adopted use of two seven-inch round headlamps per vehicle. After this major advance, the following decade (1941-1950) did not see the introduction of any significant changes to headlamp design.

In the 1960s, there was a transition to halogen headlamps. Europe adapted to this advantageous method faster and almost immediately, while the U.S. did not implement halogens until the 1970s. Also during this decade, other improvements in headlight technology included the fabrication of a better headlamp which included aim tips or aim pads, reflector axis tilted down, and external shield or fog cap installed.

In 1970s, another headlamp size was legalized and promoted by the newly created National Highway Traffic Safety Administration (NHTSA). Now two sizes, 7 inch round (two per vehicle) and 5 ¾ inch round (four per vehicle), were being used. Over the decade, the gradual increase of intensity per vehicle from 75,000 cd to 150,000 cd, greatly improved visibility on the road. The use of halogen light sources obviated the need for the all-glass sealed beam.

A major breakthrough occurred in 1984 with the first aerodynamic/composite/replaceable-bulb headlamp. Plastic materials allowed improved performance and increased styling flexibility, unachievable with glass materials. As the nation began to adopt these headlamps, research on high-intensity discharge (HID) lighting was being conducted. European engineers, using predominantly the H4 light source, began to employ a segmented reflector, but the basic surfaces were still parabolic. The researchers next aimed to develop multisegmented surfaces and to further smooth computer-generated surfaces. Advantages were seen in ellipsoidal surfaces, which allowed a smaller vertical dimension, more uniformity in the beam pattern, and the ability to make a sharper cutoff, or gradient, thus allowing more accurate visual headlamp aim.

In the 1990s, new methods for mechanical aiming were developed. A vehicle headlamp aiming device (VHAD) installed on each headlamp allowed the new headlamps, originally too small (55 mm by 135 mm), to achieve mechanical aim. Due to VHAD, aiming tips on lenses were not required. Soon, VHAD was installed on all headlamps. HID provided the most advantageous benefits for the upcoming decade. With HID, headlamps lasted longer, had increased light-source lumens, higher intensity beam patterns, increased color temperature of light source, and

greater durability of light source, their only disadvantage being increased cost (no mention was made of the glare from HID headlamps that has become the subject of many complaints). In regards to regulations, NHTSA revised a rule changing it to allow visual/optical aim for headlamps as long as they meet a certain minimum vertical gradient of the beam pattern. Now the beam pattern itself could be accurately positioned in the aiming process. Harmonization of headlamp beam pattern continued with many being investigated at UMTRI. As manufacturers of automobiles and lighting became more international, a worldwide harmonized beam pattern was predicted.

"Subjective and Objective Aspects of Headlamp Glare: Effects of Size and Spectral Power Distribution" (1999) - Michael J. Flannagan: Research Associate Professor UMTRI's Human Factors Division

In this study, particular aspects of subjective and objective glare were compared. Subjective glare refers to discomfort glare, while objective glare refers to disability glare. The author wanted to know if size and spectral power distribution affected either one or both types of glare. Disability glare was measured by the luminance threshold for detecting a pedestrian silhouette presented near glare sources. Discomfort glare was based upon the subjects' numerical ratings. Twelve individuals, representing females and males as well as younger and older age groups, participated. The subjects sat in a chair at one end of the room, while all the stimuli and equipment were at the other end. The stimuli were 7.6 meters from the subjects' eye position. The area around the stimuli was black to simulate dark areas beyond lighted pavement in real driving conditions. A rectangular white area was placed below the glare stimuli and pedestrian silhouette to represent the lighting effects of a road surface. The surface was evenly illuminated to a luminance of 1.0 cd/m^2 by a tungsten lamp. A representation is shown in the figure below. The glare stimuli were four degrees of visual angle to the left and right of the pedestrian, and their diameters were 0.6 and 0.3 degrees. On either side were tungsten halogen (TH) or high intensity discharge (HID) headlamps. The simulated pedestrian was one degree of visual angle in height and had a luminance of 0.50 cm/m^2 due to ambient light. The subjects made observations for all twelve combinations of glare conditions. The disability task was always performed before the discomfort task. Shutters controlled the beginning of the trials. Observers were asked to look down at the white panel until each trial was ready to begin. Once told, the observers looked up and announced when the image was no longer visible to them.

The discomfort task was similar, but the simulated pedestrian figure not used. The white panel was still used between trials. The shutter was also used to begin the trial, but only opening for an interval of two seconds. During that time, the observers were asked to rate the level of discomfort.
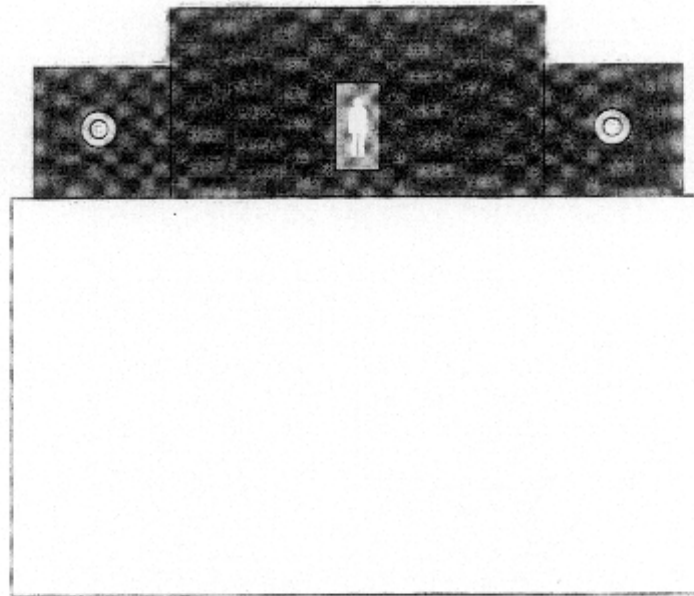
Figure 1. The subject's view of the glare sources and pedestrian silhouette. The glare sources appeared, as shown, to the right or left of the pedestrian. The larger glare stimuli are represented by the outer circles and the smaller glare stimuli are represented by the inner circles. The pedestrian appeared, as shown, in positive contrast against a neutral background within a small rectangular frame. The large white area below the pedestrian and glare stimuli was illuminated to a dim level representative of pavement illuminated by typical low-beam headlamps. The areas surrounding the glare stimuli and pedestrian were black.

For disability glare, threshold luminance was found not to be affected by size, spectral power distribution, or the interaction of those two variables. For discomfort glare, the effect of size was not statistically significant, but the effect of spectral power distribution was. Discomfort ratings for HID were higher than those for TH. The researchers were surprised not to find an effect of size on discomfort ratings in view of previous studies. The author concluded that conditions which give rise to certain effects on discomfort glare do not necessarily imply similar effects on disability glare.

"Assessing the Potential Benefit of Adaptive Headlighting Using Crash Databases" (1999) - John M. Sullivan: Assistant Research Scientist in the University of Michigan Transportation Research Institute's Human Factors Division; sponsored by the University of Michigan Industry Affiliation Program for Human Factors in Transportation Safety; **Michael J. Flannagan:** Research Associate Professor UMTRI's Human Factors Division

The authors investigated the advantages of adaptive headlighting. Adaptive headlighting is a type of installed headlight that modifies the beams to aim directly at the road in front of the car. Since the headlights are able to adjust illumination toward the road, adaptive headlighting may eliminate some glare for oncoming drivers. They found this method to be a good compromise between a driver's control of his/her vehicle without compromising the vision of others who share the road.

Previous studies had found that, in most cases, increased illumination lowered accident rates; therefore, adaptive lighting can act to increase the amount of illumination available at a particular section of the road, especially when pedestrians are involved. Pedestrians were found

to be more vulnerable when there were time changes (daylight savings time and British summer time).

The authors used crash statistics from the databases available through the National Highway Traffic Safety Administration (NHTSA). They took time changes throughout the day (twilight) and the year (DST) into account. There were three scenarios for the comparisons. The first focused on pedestrian crashes at intersections, which mainly involved crashes due to limited lighting at corners of the streets. A similar study had been conducted by Owens and Sivak in 1993. The results were consistent with those of the prior study and showed no seasonal trends.

The second scenario was pedestrian crashes on dark, straight, high-speed roads. Pedestrians were singled out for the study due to the fact that they are unlit and usually unexpected. Different levels of lighting during twilight seemed to vary the accident rates during that particular period of the day. The crashes were at a maximum during December for twilight, October for daylight, and July for nighttime. The exposure effect may have influenced the data in December. Sullivan and Flannagan believe adaptive lighting will help in spotting pedestrians more efficiently on dark, straight roads.

The third scenario was based on single-vehicle off-road crashes. The authors think fixed lighting on curves created glare, which in turn contributed to the incidence of run-off-road accidents. A huge percentage of night accidents was due to alcohol influence, making the day and night accident rates based on illumination harder to differentiate.

The authors claim that adaptive headlighting that mitigates pedestrian vulnerability in darkness is likely to prevent fatal crashes and reduce the number of accidents.

"Blue Content of LED Headlamps and Discomfort Glare" (2005) - Michael Sivak: Research Professor and Head of University of Michigan Transportation Research Institute's (UMTRI) Human Factors Division; Creator of the Industry Affiliation Program for Human Factors in Transportation Safety; sponsored by UMTRI; **Brandon Schoettle:** Researcher for UMTRI; **Takako Minoda:** Researcher for UMTRI; **Michael J. Flannagan:** Research Associate Professor UMTRI's Human Factors Division

The authors wished to replicate and enlarge upon previous research that showed that an increase in the color temperature of headlights of an opposing vehicle was associated with an increase in discomfort glare. As correlated color temperature increases, so does the blue content within headlamps.

The researchers gathered a wide range of subjects, 6 younger and 6 older with a 50-50 split between males and females. Subjects viewed 5 different lamps placed 0.66 m above the ground to mirror actual car headlamps. Each of the 5 headlamps displayed a different light source, tungsten-halogen, HID, and 3 types of LEDs with nominal color temperatures of 4000, 4800, 6600 K. One lux was produced toward each subject pair at night and they used a Minolta T-10 illuminance meter, which was located inside the vehicle. A black board was used to shield the lamps to ensure only one lamp was shown at a time. When the light source was not being shown, a white dot marked the focal point to guide the subjects in the proper staring direction.

The De Boer 9-point response scale (1 being unbearable) was used to rate the level of discomfort glare. The results are shown in the tables below. Both the effects of illuminance and lamp type on the level of discomfort glare were found to be statistically significant. Overall, the bluish light results in more discomfort than white light. The authors state that it is not clear exactly what aspects of the spectral power distribution of light determine whether the average person will subjectively rate it as more or less glaring. The closely related issue of what visual mechanism or mechanisms may be responsible for the effect is also unclear.

Table 2
The effect of illuminance on de Boer ratings of discomfort glare.
(Lower de Boer units indicate more discomfort.)

Illuminance (lux)	Discomfort glare (de Boer units)
0.25	5.8
0.5	4.1
1	2.9

Table 3
The effect of lamp type on de Boer ratings of discomfort glare.
(Lower de Boer units indicate more discomfort.)

Lamp type	Discomfort glare (de Boer units)
Tungsten-halogen	5.3
HID	4.7
LED-4000	4.2
LED-4800	3.7
LED-6600	3.3

To further try to explain discomfort glare, an analysis was performed, where spectral power distributions of each lamp was weighed by the blue-cone sensitivity function, integrated over wavelength. The output calculations were then compared to the discomfort glare ratings. A strong linear relationship was seen and the spectral power weighted by the blue-cone sensitivity function accounted for 99% of the variance in discomfort-glare ratings.

Literature Review Reference List

This list is divided into two portions, references which proved useful in the review and references which were investigated but proved irrelevant to the subject of this report. All references listed were photocopied, converted to PDF format, and compiled on DVD.

Relevant Sources:

Adrian W. On the Reduction of Disability Glare Under Night Driving Conditions. La Prevention Routiere Internationale; Bertrange, Luxembourg: 250-259.

Anderson SJ, Holladay IE. Night Driving: Effects of Glare from Vehicle Headlights on Motion Perception. Ophthalmic and Physiological Optics 1995; London, United Kingdom: 545-551.

Bjorkman B. A summary of papers and discussions on Lighting Problems in Road Traffic. The Official Swedish Council on Road Safety Research October 1962; Stockholm, Sweden: 4-6.

Capelli JT. Effectiveness of Glare Screens. U.S. Department of Transportation Federal Highway Administration, Engineering Research and Development Bureau March 1973; Albany, New York: 1-20.

Flannagan MJ. Subjective and Objective Aspects of Headlamp Glare: Effects of Size and Spectral Power Distribution. The University of Michigan Transportation Research Institute November 1999; Ann Arbor, Michigan: 1-13.

Haddad HM. Efficient Method of Visual Screening for Night Driving. La Prevention Routiere Internationale; Bertrange, Luxembourg: 186-188.

Moore DW. Headlamp History and Harmonization. The University of Michigan Transportation Research Institute June 1998; Ann Arbor, Michigan: 1-17.

Musick JV. Accident Analysis Before and After Installation of Expanded Metal Glare Screen. Ohio Department of Public Safety Division April 1969; Columbus, Ohio: 1-18.

National Research Council (U.S.) Transportation Research Board. Glare Screen Guidelines. American Association of State Highway and Transportation Officials, Federal Highway Administration December 1979; Washington, D.C.: 1-16.

Road Research Laboratory. Interim Measures for the Prevention of Dazzle on Roads. Department of Scientific and Industrial Research 1948; London, United Kingdom: 1-6.

Roper VJ. Headlighting with Minimum Glare. Society of Automotive Engineers, General Electric Company's Lamp Department March 1948; New York, New York: 1-7.

Sivak M, Flannagan MJ, Traube EC, Miyokawa T. Conspicuity and Glare Properties of Daytime Running Lights: Effects of Lamp Separation and Intensity. University of Michigan Transportation Research Institute August 1998; Ann Arbor, Michigan: 1-17.

Sivak M, Olson PL, Zeltner KA. Effect of Prior Headlighting Experience on Ratings of Discomfort Glare. Human Factors 1989; Ann Arbor, Michigan: 391-395.

Sivak M, Schoettle B, Minoda T, Flannagan MJ. Blue Content of LED Headlamps and Discomfort Glare. University of Michigan Transportation Research Institute February 2005; Ann Arbor, Michigan: 1-15.

Soardo P. Car Headlamps. International Association for Accident and Traffic Medicine, International Road Federation, La Prevention Routiere 1980; Bertrange, Luxembourg: 161-172.

Sullivan JM, Flannagan MJ. Assessing the Potential Benefit of Adaptive Headlighting Using Crash Databases. University of Michigan Industry Affiliation Program for Human Factors in Transportation Safety September 1999; Ann Arbor, Michigan: 1-62.

Walker AE, Chapman RG. Assessment of anti-dazzle screen on M6. Transport and Road Research Laboratory's Department of the Environment, Department of Transport, Accident Investigation Division's Safety Department 1980; Crowthorne, Berkshire: 1-6.

Wolbarsht ML. Field Trials of Tests to Determine Susceptibility to Glare and Defects in Peripheral Vision. La Prevention Routiere Internationale 1980; Bertrange, Luxembourg: 246-248.

Irrelevant Sources:

American Association of State Highway and Transportation Officials. 2002 Interim to Standard Specifications for Structural Supports for Highway Signs, Luminaires and Traffic Signals. American Association of State Highway and Transportation Officials 2002; Washington, D.C.: 1.1-13.11.

Andre J. The Twilight Envelope: A User-Centered Approach to Describing Roadway Illumination at Night. Human Factors 2001; Harrisonburg, Virginia: 620-630.

Assum T, Bjornskau T, Fosser S, Sagberg F. Risk Compensation-the Case of Road Lighting. Accident Analysis & Prevention 1999; Oslo, Norway: 545-553.

Christie AW. Some Investigations Concerning the Lighting of Traffic Routes. Public Lighting December 1962; 189-199.

Frederiksen E, Jorgensen NO. Glare on Motorways. Kobenhavn 1972; Denmark: 1-78.

Graf CP, Krebs MJ. Headlight Factors and Nighttime Vision. National Highway Traffic Safety Administration Department of Transportation November 1976; Washington, D.C.: 1-88.

Hellriegel EJ. An Evaluation of Expanded Metal glare Screen on the New Jersey Concrete Median Barrier. New Jersey Department of Transportation Diveision of Research and Development February 1978; New Jersey: 1-20.

Helmers G, Rumar K. High Beam Intensity and Obstacle Visibility. University of Uppsala Department of Psychology 1974; Uppsala, Sweden: 1-15.

Hermion RH. A Preliminary Cost-Benefit Study of Headlight Glare Reduction. Southwest Research Institute March 1969; San Antonio, Texas: 1-24.

Hermion RH. Night Visibility Improvement Through Headlight Glare Reduction. Southwest Research Institute September 1969; San Antonio, Texas: 1-32.

Horberg U, Rumar K. Running Lights Conspicuity and Glare. University of Uppsala Department of Psychology 1975; Uppsala, Sweden: 1-21.

Huculak P. The Influence of Glare on the Detection of Hazardous Objects in Automobile Night Driving. National Research Council of Canada National Aeronautical Establishment June 1978; Ottawa, Canada: 1-13.

Jehu VJ. Developments in Vehicle and Street Lighting. Road Research Laboratory Department of Scientific and Industrial Research 1962; London, United Kingdom: 1-8.

OECD Research Group. Lighting, Visibility and Accidents. OECD Research Group March 1971; 11-85.

Reid KM, Chanon HJ. Evaluating Visibility on Lighted Streets. 1952.

Rompe K, Tupova J, Engel G. The Influence of Tinting the Windscreens on Visibility During Night Driving. La Prevention Routiere Internationale 1980; Bertrange, Luxembourg: 238-239.

Rowhani P, Hawatky SM, Glauz DL, Stoughton RL. Vehicle Crash Tests of a Concrete Median Barrier Retrofitted with a Concrete Glare Screen. California Department of Transportation 1992; Sacramento, California: 1-31.

Schiflett SG, Cadena DG, Hemoin RH. Headlight Glare Effects on Driver Fatigue. Southwest Research Institute September 1969; San Antonio, Texas: 1-68.

Schoettle B, Sivak M, Flannagan MJ, Kosmatka WJ. A Market-Weighted Description of Low-Beam Headlighting Patterns in the U.S.: 2004. University of Michigan Transportation Research Institute September 2004; Ann Arbor, Michigan: 1-10.

Sivak M, Olson PL. Nighttime Legibility of Highway Signs. La Prevention Routiere Internationale 1980; Bertrange, Luxembourg: 139-150.

Texas A&M University. 1st Annual Symposium on Visibility in the Driving Task. Highway Research Board, Illuminating Engineering Research Institute, Texas A&M University May 1968; Texas: 1-164.

Texas A&M University. 2nd Annual Symposium on Visibility and Driving. Highway Research Board, Illuminating Engineering Research Institute, Institute of Transportation and Traffic Engineering, University of California Extension December 1969; Berkeley, California: 1-99.

Traffic Engineering Division. Handbook of highway Illumination Practice. Traffic Engineering Division 1952; Washington: 1-56.

Watson RL. A Modified Formula for Calculating the Disability Glare Effect From Street Lighting Lanterns. Road Research Laboratory 1968; Crowthorne: 1-7.

Appendix B: Notes on the Luminance Values of the Concentric Disks in the Disability (Contrast) Test

The *Radiant Imaging* (RI) photometer was focused onto the computer monitor with the disability glare (contrast) test displayed. Its distance to the screen and the ambient lighting conditions were both the same as if an observer were undergoing the test.

When the luminance of the inner disk was determined (see below) it was recorded along with the corresponding number of grayscale steps (up arrow button pushes) necessary to reach that luminance. The result was Table 1.

1. Grayscale Steps	Luminance (cd/m²)	2. Grayscale Steps	Luminance (cd/m²)
0	0.305	50	8.88
1	0.314	55	10.78
2	0.317	60	12.87
3	0.32	61	13.40
4	0.33	62	13.91
5	0.34	63	14.38
6	0.35	64	14.89
7	0.36	65	15.41
8	0.38	70	18.34
9	0.40	75	21.25
10	0.42	80	24.3
15	0.63	85	27.6
20	1.08	86	28.1
21	1.22	87	28.7
22	1.38	88	29.5
23	1.56	89	30.1
24	1.75	90	30.8
25	1.96	95	34.6
26	2.19	100	37.8
27	2.44	120	54.7
28	2.69	150	88.4
29	2.88	175	119.7
30	3.13	200	158.3
35	4.26	225	197.3
40	5.59	250	239.5
45	7.07	255	250.0

Table 1. Luminance in cd/m² versus the number of grayscale steps above zero ("pure" black). This "pure" black (zero steps) was the luminance of the surrounding annulus (or outer disk). Grayscale steps of 255 represent "pure" white. The gray field on the rest of the monitor was 1.11 cd/m².

Since the RI photometer is an *imaging* photometer, as opposed to a *spot* or averaging photometer, a few words are in order as to how the luminance numbers in Table 1 were obtained. The RI photometer software (*ProMetric*) comes with quite a few analysis features. One of these is a histogram feature. This is seen in the Figure 1.
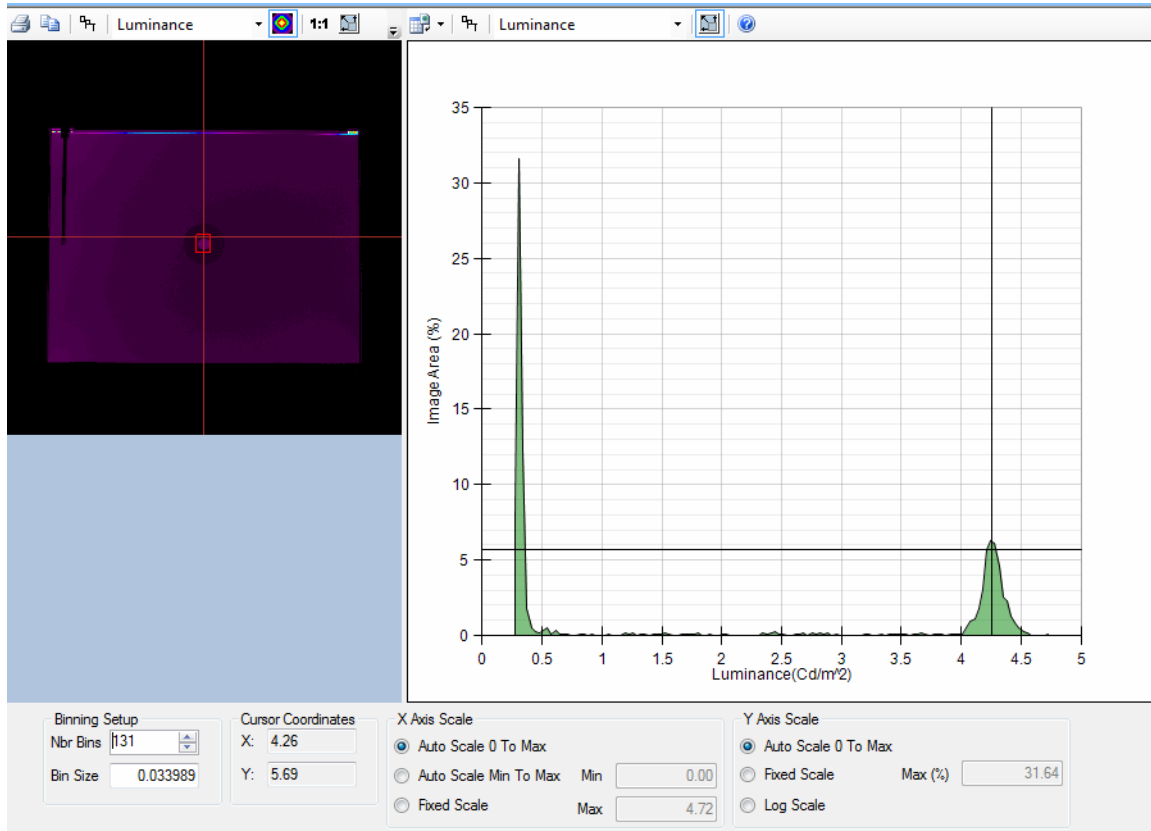
Figure 1. The histogram of the luminance in the small selected rectangle in the false color luminance image in the upper left. (This image corresponds to 35 grayscale steps in the table.)

In the upper left is a false color luminance image of the screen. The crosshairs are very nearly centered on the inner disk in that image. (It being <u>very</u> difficult to get them perfectly centered.) If the photometer operator then selects a *portion* of the screen (small red rectangle near the center of the crosshairs), then *that portion*, rather than the entire image is histogrammed.

If the operator gets most of the selected area to cover a good portion of the inner disk and a small portion of the outer disk (annulus) (with none of the gray background field selected) and *if there is sufficient contrast (luminance differential) between the inner and outer disks*, then we have the situation prevailing in the figure. The histogram of the selected area is (essentially) comprised of two separated Gaussian-like curves. The lower curve represents the outer disk or annulus pixels while the upper curve represents the luminance of the inner (and therefore brighter) disk.

For all but the lowest luminance values (fewest grayscale steps) the two curves are readily distinguishable (but see below) and the upper curve is reasonably symmetric about its peak. *Thus the peak value of the upper curve is taken as the luminance of the inner disk at that grayscale value.*

Note that here is the difference between an imaging photometer and a spot photometer. The spot photometer assigns a single number (an average) to the field of view falling within its spot or imaging circle. An imaging photometer will (usually) have many pixels fall within the equivalent spot. Thus there are *many* values for the luminance (one for each pixel) of the inner disk. If one got really lucky these would all be the same value, but given the vagaries of the real world this is seldom the case and consequently there is a range of values, especially given a photometer with good discrimination and dynamic range like the RI photometer.

To determine where the peak is on the upper curve, the software comes with movable crosshairs on the histogram. These can be seen in Figure 1. A "readout" from the crosshairs then determines the peak luminance value to a high degree of accuracy.

Additionally, the histogram itself can be windowed or "zoomed" to even further hone in on the peak. This is shown in Figure 2.
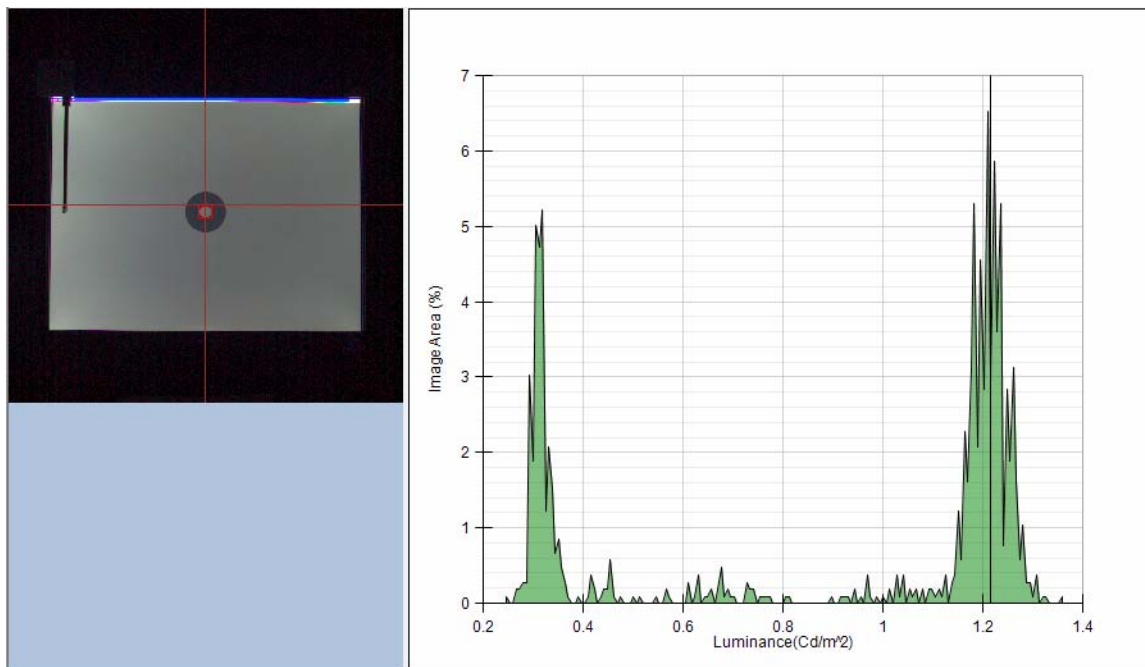
Figure 2. At 21 grayscale steps we have the following histogram for the inner disk plus some of the outer disk. The histogram has been enlarged or "zoomed" to better select the peak. Unlike the previous figure, the image from the screen is "true color" rather than false color luminance (the choice makes no difference to the histogram).

As was mentioned, the peaks are easy to distinguish in the histogram when there is sufficient contrast between the inner and outer disks, which corresponds to enough grayscale steps to make the inner disk much brighter than the outer one.

Thus this procedure just outlined is best done from higher grayscale steps and then moving down in contrast for the next value. This allows the operator to see how the upper peak moves within the histogram with decreasing contrast.

Below five grayscale steps there is difficulty. This can be seen in Figure 3. The "Gaussians" begin to merge. The value of the upper peak is then lost and must be estimated from where the upper peak is at five grayscale steps to where the (single) peak is at zero steps. As can be seen in the figure, a value like 0.008 or 0.01 cd/m² or even bigger is a reasonable estimate for a "standard deviation" on these curves. Thus this estimation process has a lot of uncertainty to it and the numerical value in the third decimal place (for grayscale steps 0, 1, and 2) is less than this uncertainty.
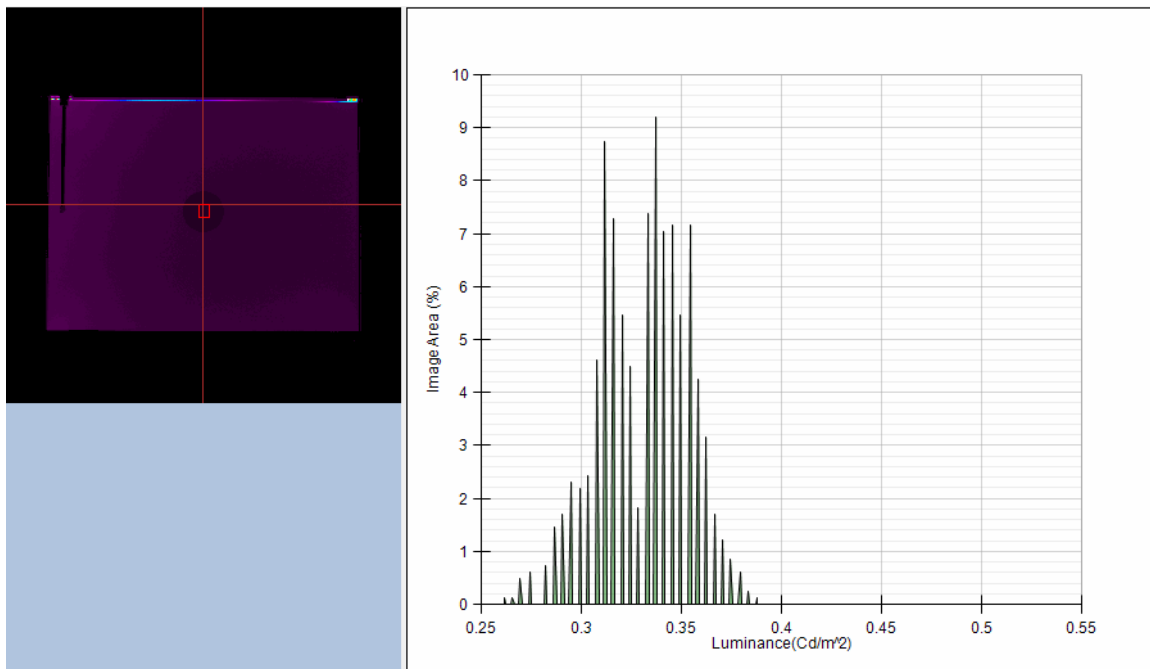
Figure 3. "Gaussians" begin to merge at 5 grayscale steps (histogram shown here) and become unresolvable below this. Thus the luminance values for grayscale steps 1 through 4 involve some educated guessing.

Since many observers in the testing could distinguish the inner disk (no glare source) at two or three steps (one person even resolved the inner disk at one step), it is clear that the eye is (quite often) better than the photometer at contrast resolution at these luminance levels, at least when there is no glare source.

In order to provide a check on the RI photometer, a handheld spot photometer[1] was mounted securely on a tripod and had its imaging circle focused solely on the inner disk of the contrast test. The (near) limit of focus of the device was just at the viewing distance of the test. The following values provide a spot check (pun intended) for the imaging photometer.

---

[1] *Konica-Minolta* Luminance Meter LS-110.

Grayscale Steps	Luminance (cd/m²)
0	0.28
5	0.31
10	0.41
25	2.11
30	3.37
50	9.17
80	23.88
100	36.54
255	233.60

(Gray background = 1.11 cd/m²)

Table 2. Luminance values for various grayscale steps as measured by the spot photometer. These provide an independent check on the values in the table for the RI photometer.

The spot and RI photometer values compare favorably as can be seen in Figure 4.
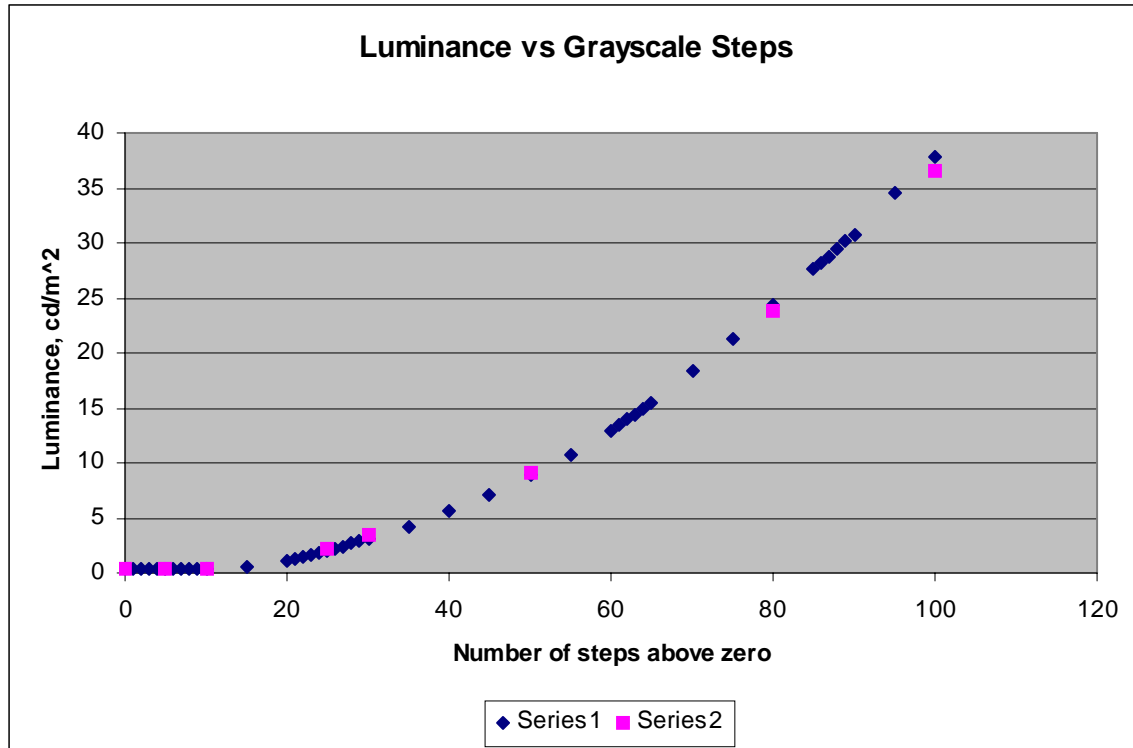
Figure 4. A comparison of the luminance values as measured by the RI photometer (blue) and the spot photometer (pink).

With both photometers giving very close numbers, we can just use those from the RI photometer. These values over the full range are shown in Figure 5.
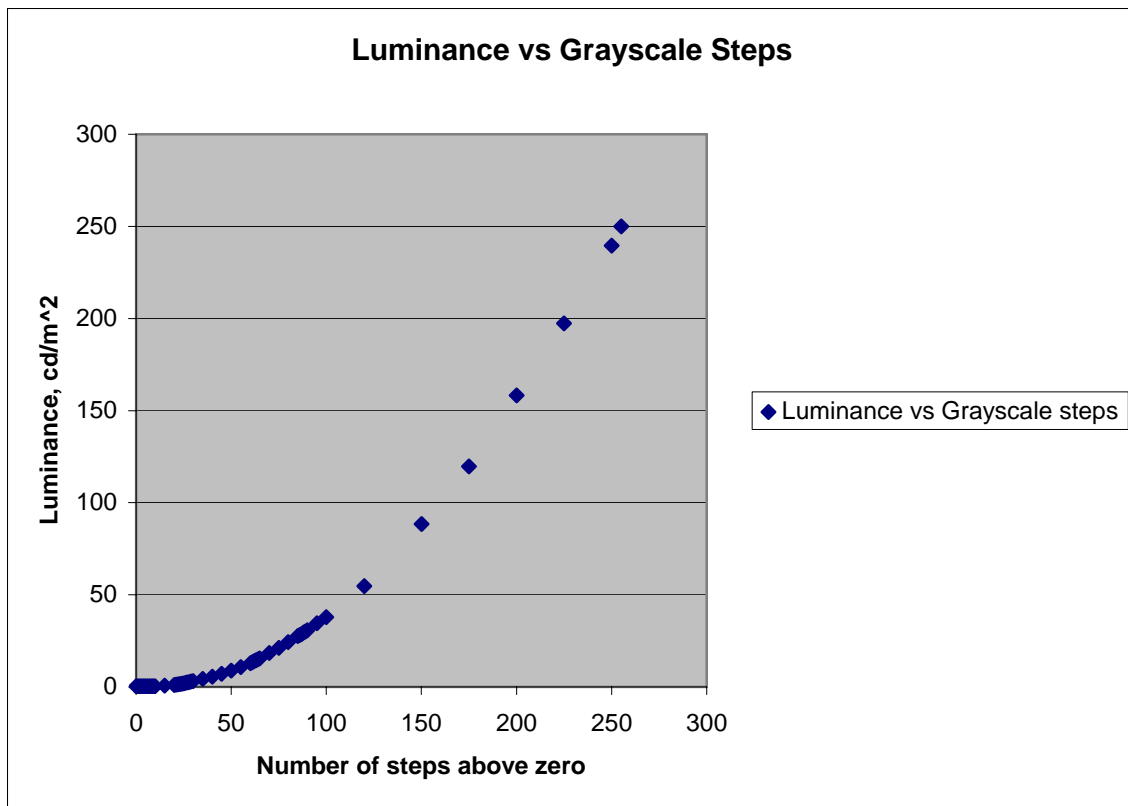
Figure 5. Luminance vs. grayscale steps for the inner disk in the contrast (disability) test over the full range, as determined by the RI photometer.

Since the upper part of the range was not needed for any observer tested, an enlarged version of this last figure, only going up to 90 grayscale steps is shown below. Here the data points are joined to show a smooth curve.

Since this curve looks very parabolic, it was (*least squares*) fit with a second order polynomial over the range 0 to 90 grayscale steps. The result is,

$$Lum = 0.409201 - 0.0435403\ x + 0.00424794\ x^2$$

where x is the number of grayscale steps and *Lum* is the luminance of the inner disk in cd/m^2. The closeness of the fit can be seen below. This fit can be compared to the values from linear interpolation when estimating the luminance values at a grayscale step that is not in the table.

A *third* set of luminance versus grayscale step data was taken with a *Pritchard* photometer but these numbers are not displayed, as they are not reliable in absolute terms since that photometer is quite out of date in its calibration.
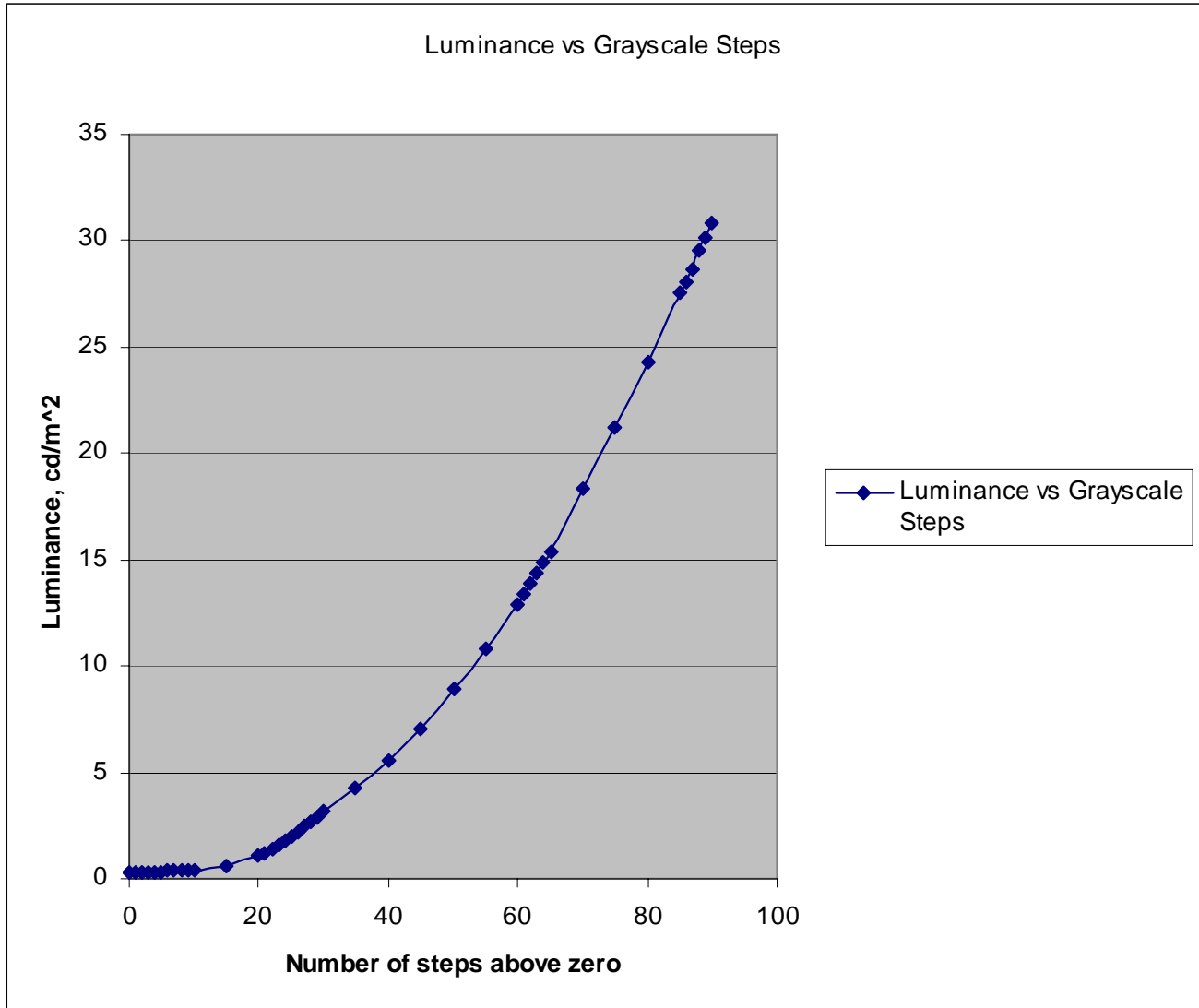
Figure 6. This figure is the same as the Figure 5 but only going up to 90 grayscale steps (the relevant range for our disability test). The points are joined to provide a smooth curve.
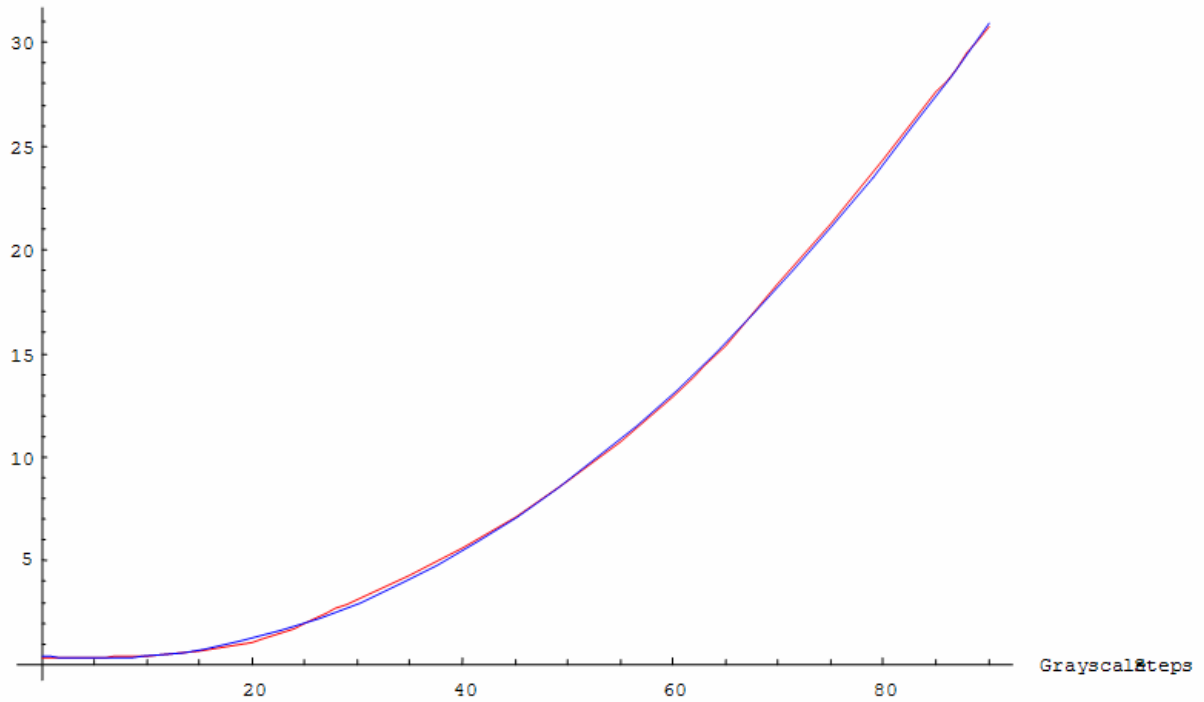
Figure 7. The fit (red curve) 0.409201 – 0.0435403 x + 0.00424794 x^2 compared to the data (blue with points joined) where x is the number of grayscale steps above zero. The ordinate is luminance in cd/m^2. Obviously the fit is very good.

Appendix C: Measured Current in the Disability Glare Test LED for the Three Settings and Other Data

The three settings for the disability and discomfort glare tests corresponded to one of three different resistors put in series with a *Coast High Output White LED* [TT7803] and 5 volts from a power supply (actually 5.04 volts as measured).

1. Low	2. Medium	3. High
R = 6,490 Ω (nominal)	R = 432 Ω (nominal)	R = 51.1 Ω (nominal)
I = 317 µA (measured)	I = 5.19 mA (measured)	I = 31.80 mA (measured)
L = 21,000 cd/m² (approx.)	L = 461,000 cd/m² (approx.)	$L = 2.7 \times 10^6$ cd/m² (approx.)[1]

Table 1. Electrical and luminance values for the glare LED setup. The luminance values shown are with the LED aimed at and *directly opposite* the photometer at the same distance as the observers during the test. The luminance varied over the face of the LED hence the approximate value.

The rule-of-thumb used in choosing the resistors was that the LED would drop 3 volts in forward operation. Various resistors were then tried with the measured currents close to the estimated currents. The final choice of resistors was made based on the visual appearance of the LED. The currents shown in Table 2 were then measured.

Intensity	10,000 mcd (= 10 cd)
Directivity	15°
Wavelength	470-600 nm
Forward Current (*continuous*)	30 mA
Forward Current (*peak*)	100 mA
Reverse Voltage	5 V
Power Dissipation	120 mW

Table 2. Technical Data for the *Coast High Output White LED* [TT7803CP]. These are the maximum allowed values except for (obviously) directivity and wavelength.

The monitor dimensions are shown in Figure 1. Except for the one labeled "0", the red lines point to where the LED holder's right edge was placed at various times during the test. The red line labeled zero points to the left edge of the whole monitor (not just the screen). With that as a reference point, the other positions are as given in Table 3.

We note that marks 1 and 2 were used for both *disability* and *discomfort* glare tests. Mark 3 was used for *discomfort* tests only and mark 3c was only used for *disability* tests. After the bulk of the observers had been tested, two more positions were added; for details on those positions see appendix E.

---

[1] The values of the LED's luminance at the highest setting no longer look like a Gaussian when histogrammed. This is an estimate and the numbers range from about one million to 3.3 million cd/m² over the face of the LED when it is set to high.

Mark #	Distance From 0 Mark
1	5.25 cm
2	14.05 cm
3c	21.40 cm
3	22.80 cm

Table 3. Distance for the mark from the zero mark (left edge of monitor).

Now in the computations it must be noted that ***the LED itself was 1.10 cm left of its holder's right edge, which was <u>what was placed at the marks</u>*** (*right* and *left* as seen by the viewer).
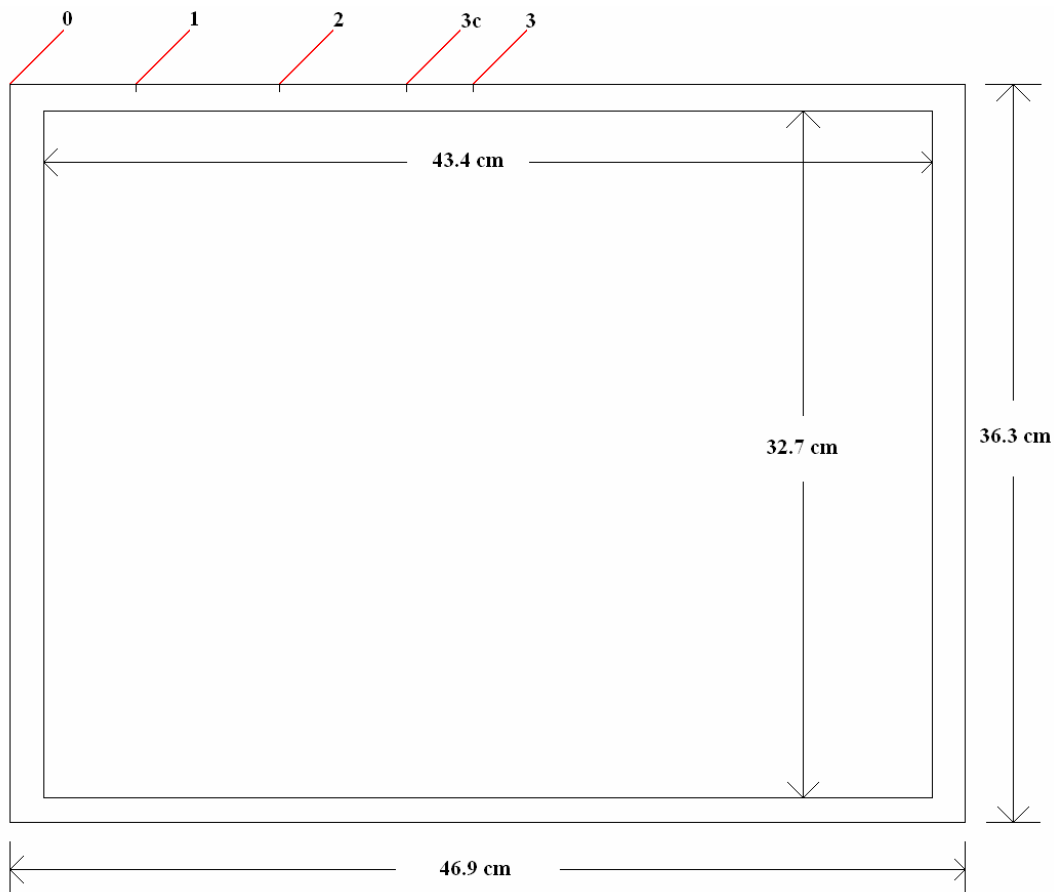
Figure 1. The dimensions of the *SyncMaster 214T* (Samsung) monitor are shown. The screen itself is 43.4 cm by 32.7 cm. The outer dimensions of the monitor[2] itself are 46.9 cm by 36.3 cm. The marks 1, 2, 3c and 3 at the top correspond to where the LED holder's right edge was placed. The zero mark is the outermost left edge of the monitor and is the reference point. (See Table 3.) NOTE: The LED itself was 1.1 cm *to the left* of the holder's right edge.

[2] **Notes on dimensions**: A) The <u>lit area</u> of the screen stops short a fraction of a millimeter before the screen's edge with its borders (all sides). Thus the *viewable* dimensions of the screen are ~ 43.3 cm x 32.6 cm leading to a diagonal of 54.2 cm or 21.3″. B) The outer border of the front face <u>slopes inward</u>—toward the viewer. In other words, viewed from above the top looks like a *trapezoid*. The slope is small but detectable. Our reference or "zero mark" ***is taken from the <u>back</u> left edge of the monitor*** (as are these dimensions).
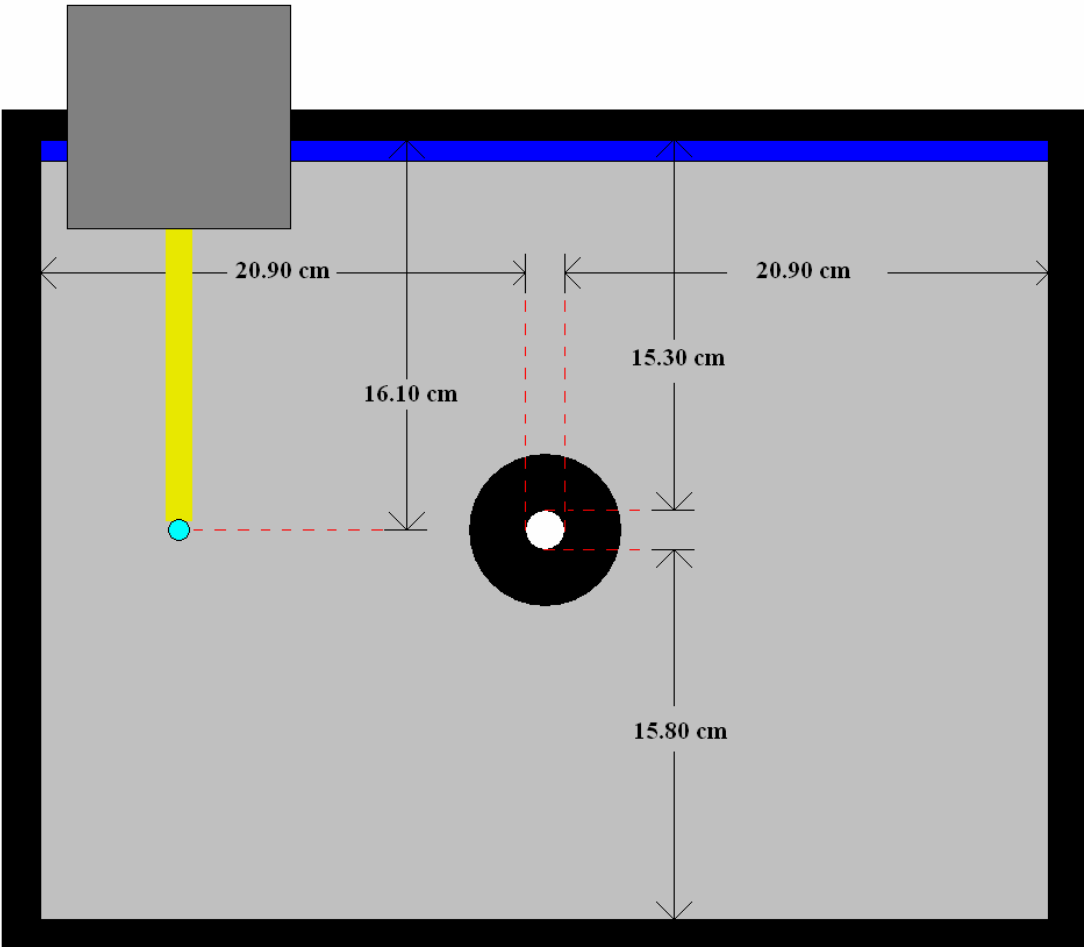
Figure 2. Dimensions for the disability glare test setup. The target disk (white) has a diameter of 1.60 cm. The background disk (black) has a diameter of 5.60 cm. In other words, the black *annulus* has a thickness of 2.00 cm.

Appendix D: Angle-Pixel Scaling and Measurement
for the Radiant Imaging Photometer

The implementation of any "glare score" for a scene saved by the photometer requires that the algorithm processing the image data can compute an angle for a given pixel relative to the center of the image. Rather than trusting any numbers preloaded into the *ProMetric* software, we measured the pixel numbers and angles directly.

Figure 1 shows the setup used. Blue masking tape was used to mark one-foot intervals vertically along the back wall next to the window, and horizontally along the front of the black countertop.
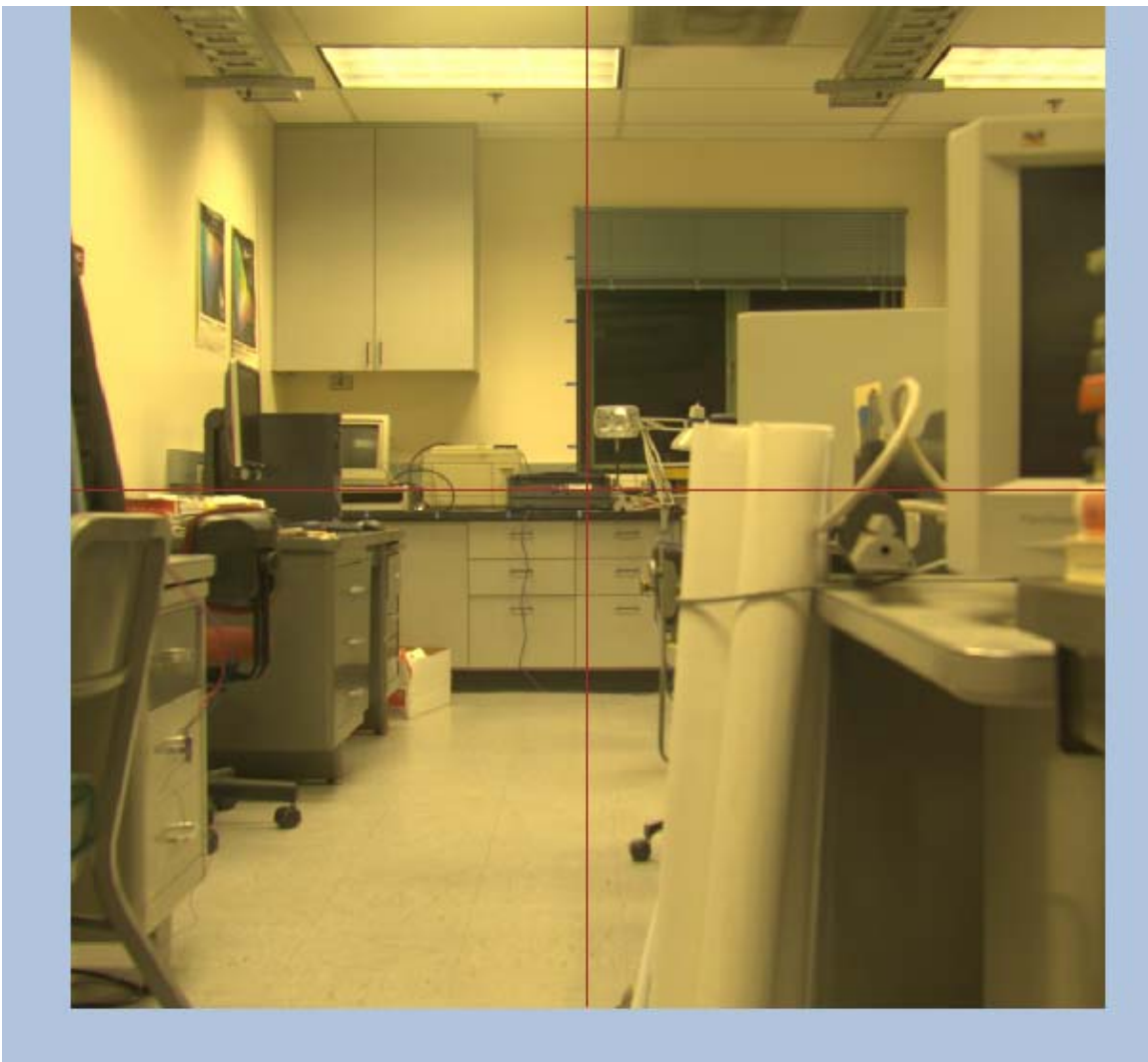
Figure 1. Entire "True Color" image (with superfluous blue border) for the 1020 x 1020 photometer array. The *Nikon* lens was used; it was focused at "infinity" and the f-number was f/8. The *ProMetric* software used "measurement #8", that is ND2 for the three tristimulus values and exposure times of Y = 25 s, X = 100 s, and Z = 300 s along with "dark imaging". The distance from the front surface of the lens to the front of the countertop was 21' 3". There was an additional length of 30.5" from the front of the countertop to the wall.

The tape was further marked with a line of "whiteout" to provide the exact tick marks needed. These can (barely) be seen on some of the tape pieces in the magnified image in Figure 2.

Figure 2. Magnified version of Figure 1.

The piece of tape nearest the crosshairs center served as the origin or reference point. It had a "T" marked on it in white. The point where the arms of the T intersected provided the "exact" reference point—the middle of the tape horizontally and the top surface of the countertop. Unfortunately it couldn't be easily aligned with the exact center of the crosshairs.

This reference piece of tape was 21 feet and 3 inches (or 255 inches) from the photometer lens front surface. The small offset from the crosshairs' center will not make an appreciable difference.

The horizontal crosshair is seen to just "skim" the top of the black recess on the left of the picture just below the computer monitor. This line is 3.5 inches above the countertop. Thus $\sqrt{(255)^2 + (3.5)^2} = 255.024$ and, as claimed no appreciable error is made by taking the reference mark as being 255" from the camera.

The back wall with the vertical tape marks (near the frame of the window) was an additional 30.5" behind the reference tape mark (at the wall's base at the countertop obviously).

The pixel location of each tick mark within the image was noted. The image array consists of pixels in a 1020 by 1020 grid. The pixels are labeled by their column and row location. Each

index runs from 0 to 1019 rather than 1 to 1020 (probably because the software follows computer science conventions). The column number is the x or abscissa value and the row number is the y or ordinate number. Thus the labeling of a particular pixel location takes the form: (column, row). This is what is shown in Figure 3.
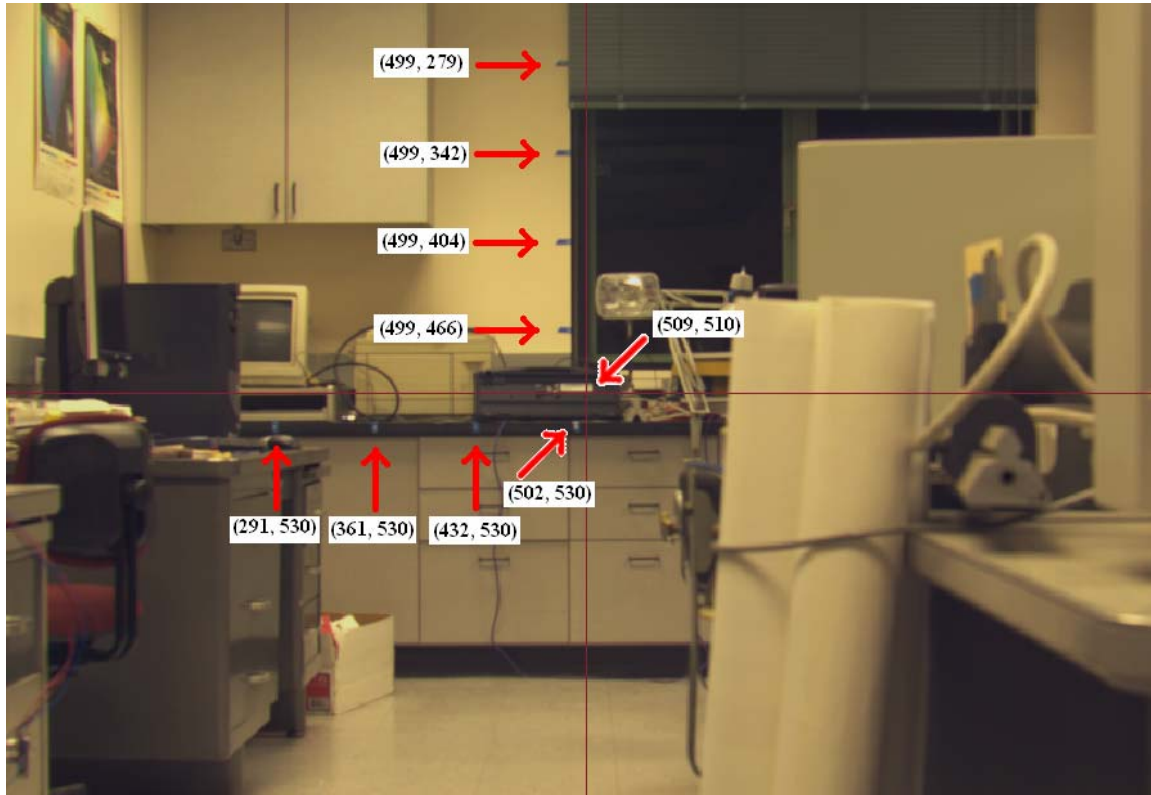
Figure 3. Pixel locations for the tick marks shown in the form (column number, row number).

The pixel locations were found with the *ProMetric* software. The image was magnified ('zoom in') and the "hovering readout" was used to zero in on the white marks on the blue tape and display the pixel's column and row number. Despite being hard to see in these pictures, when magnified the white marks on the blue tape could be read to about ±1 pixel.

In theory the crosshairs' center should be (509.5, 509.5) but, of course, only integer values are allowed. As it turns out the crosshairs' intersection is at (509, 510). The reference tape's white mark at the top of the counter was at (502, 530). The other marks are as labeled in Figure 3. The "tick mark pixel" in the case of the horizontal marks (and reference mark) was taken at the top of the tape/countertop. In the case of the vertical pieces of tape, the mark was taken at the *right* edge of the tape along the wall's edge near the window frame. In other words, the arrows in Figure 3 are shifted somewhat from the actual tick marks for purposes of clarity.

The lateral shift in the reference mark with respect to the crosshairs (502 vs. 509) does not produce a serious error (this can be shown retroactively). Thus we can construct Table 1.

Pixel Deviation	Horizontal Length (Δx)	$\theta = \tan^{-1}(\Delta x/L)$
502 – 432 = 70	12"	$\theta = \tan^{-1}(12/255) = 2.69°$
502 – 361 = 141	24"	$\theta = \tan^{-1}(24/255) = 5.38°$
502 – 291 = 211	36"	$\theta = \tan^{-1}(36/255) = 8.04°$

Table 1. Horizontal change in pixel location and the associated length change and angle.

Here the reference tape mark pixel has a column number of 502; moving out to the 2nd mark to its left, for instance, is a distance of two feet and the corresponding pixel column number is 361. Thus the two-foot change in distance corresponds to a pixel deviation of 141. The distance from the camera/photometer lens face to the reference tape mark was taken as L = 255 inches.

A similar approach to the vertical tape marks can be made and the result is shown in Table 2. Here the additional 30.5 inches to the back wall from the front of the countertop must be taken into account and hence we use D = 255 + 30.5 =285.5 inches for the distance to the camera. In the vertical case though, the position of the horizontal crosshair is used. As mentioned above it is 3.5 inches above the reference tape mark. Thus it is 12" - 3.5" = 8.5" below the next mark.

Pixel Deviation	Height (Δy)	$\theta = \tan^{-1}(\Delta y/D)$
510 – 466 = 44	8.5"	$\theta = \tan^{-1}(8.5/285.5) = 1.71°$
510 – 404 = 106	12" + 8.5"	$\theta = \tan^{-1}(20.5/285.5) = 4.11°$
510 – 342 = 168	24" + 8.5"	$\theta = \tan^{-1}(32.5/285.5) = 6.49°$
510 – 279 = 231	36" + 8.5"	$\theta = \tan^{-1}(44.5/285.5) = 8.86°$

Table 2. Vertical change pixel deviation and the associated length change and angle.

The results of Tables one and two can be combined with the obvious notion that the crosshair center represents both zero pixel deviation and zero length change. Thus:

Pixel Deviation	($\Delta x/L$) or ($\Delta y/D$)
0	0
44	0.0297723
70	0.0470588
106	0.0718039
141	0.0941176
168	0.1138350
211	0.1411760
231	0.1558670

Table 3. Pixel position change from the center and the corresponding tangent to the associated angle.

The results of Table 3 can be plotted with the pixel deviation on the x-axis and the angle tangent on the y-axis. The result is the blue curve in Figure 4. Here the individual points have been joined with straight lines (piecewise linear). The values in Table 3 can also be least-squares fit to

a line with a forced intercept of zero. The result is the aquamarine line in Figure 4. We can see by inspection that the fit is very good and resorting to looking at the residuals or performing a chi-square test would clearly be overkill.
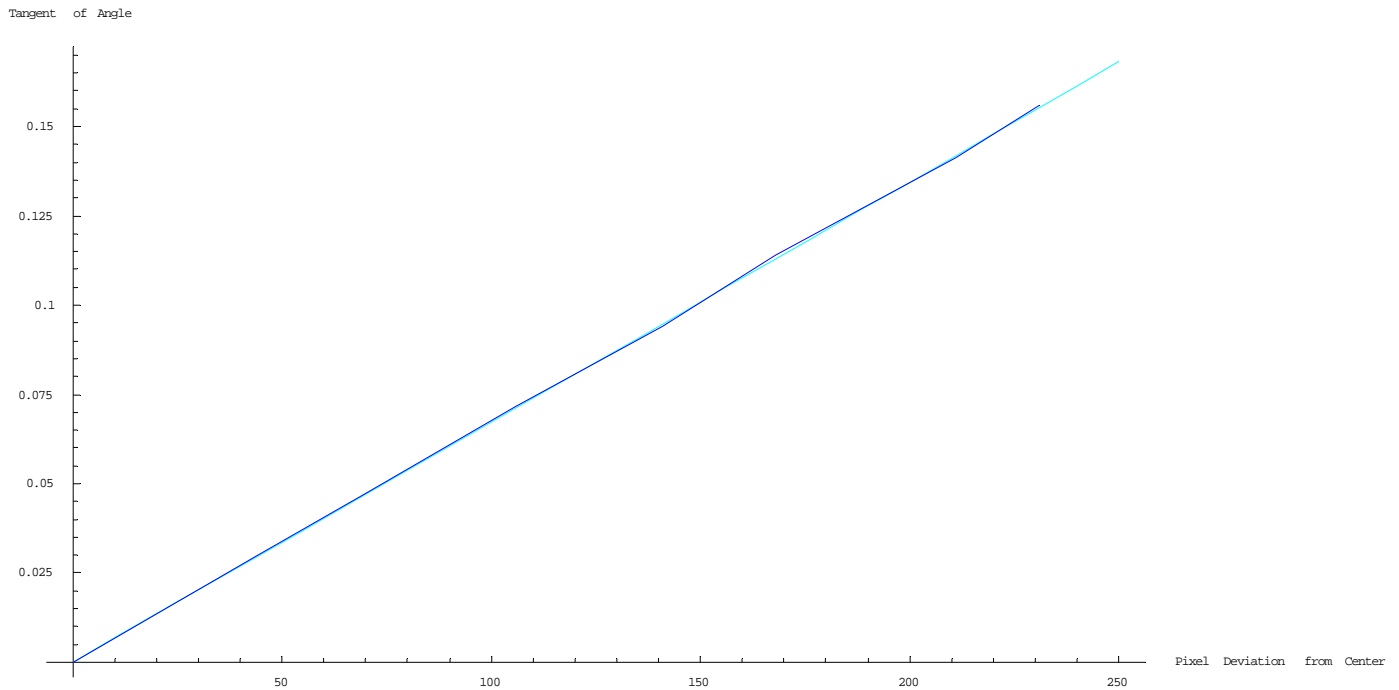
Figure 4. The blue *curve* is formed from table 3 with the points joined by lines (piecewise linear). The aquamarine *line* is the fit line t = 0.0006724374977215244 p, where t is the tangent of the angle ((Δx/L) or (Δy/D)) and p is the absolute value of the pixel deviation from the crosshair center.

Since the maximum deviation on either side of the center of the (square) array is 510 pixels, we see that, barring edge effects, the fit suggests an angular range of:

$$6.72437 \times 10^{-4} \cdot 510 = 0.342943$$
$$\text{and Arctan}\,(0.342934) = 18.93°.$$

The range of viewing angle is thus about ±19° on either side (left/right or up/down) of the (centered) crosshairs (Figure 1).

The linear fit in Figure 4 is quite good, but the function arctangent is, of course, non-linear. On the other hand, for small angles (in radians) $\tan \vartheta \approx \vartheta$. Hence plotting absolute pixel deviation from the center of the array against the corresponding angle should give a fairly linear plot for small angles. This is seen in Figure 5.

Angle (rad.) or its Tangent
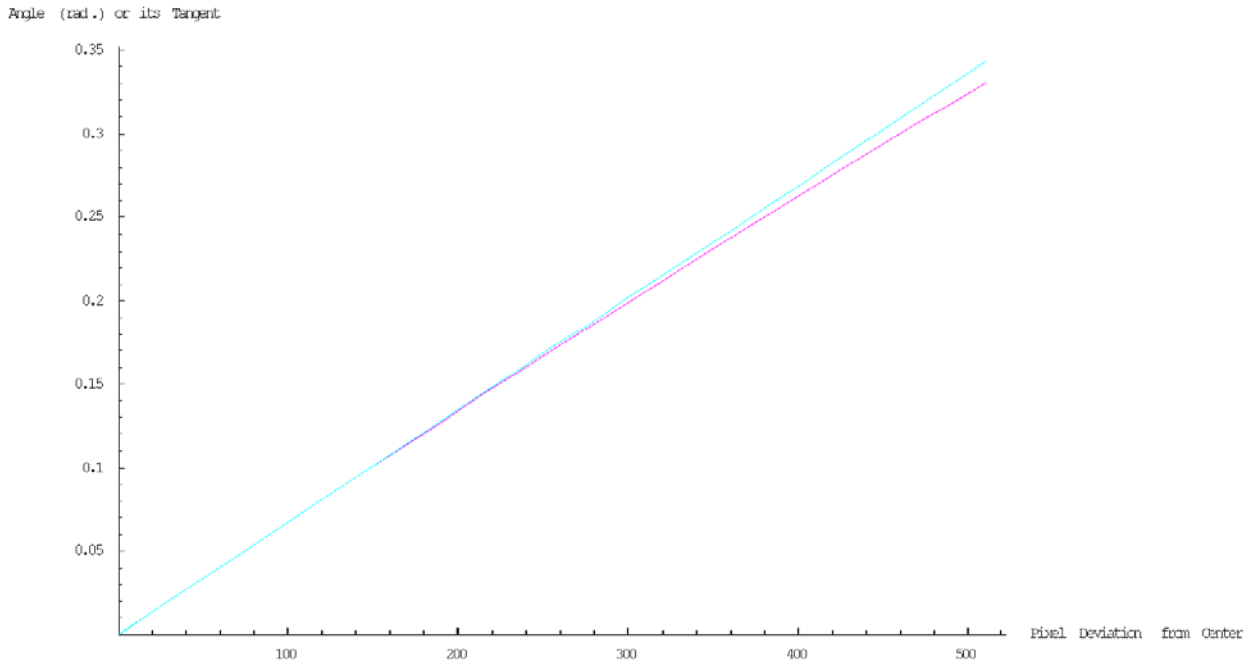
Figure 5. Angle (purple) in radians or its tangent (aquamarine) from linear fit vs. Pixel Deviation [For scale: 0.35 radians is very close to 20 degrees.]

Where the tangent of the angle can be approximated with the angle itself in radians (i.e. where the two curves in Figure 5 overlap) the slope is about 0.038 *degrees* per pixel or roughly **26 pixels for every degree** as a rule of thumb. This seems to be the case for up to about 10°.

Finally we turn (briefly) to the case where the f-stop is f/2.8. This is shown in Figure 6. We do not expect anything to change and it doesn't.[1] Looking at the coordinates for the marks we see that the pixel deviations in table 1 would now read 70, 141, 211 instead of 71, 141, 211 (i.e. identical except for the first value which is within the margin of error for reading the pixel position). Similarly, the values in table 2, namely, 44, 106, 168, 231 would now become 45, 107, 169, 232—all the same as before within the margin of error. Consequently, the angle-pixel relation (Figures 4 and 5) doesn't change when switching between f/8 and f/2.8.[2]

---

[1] The cart holding the photometer was accidentally moved a few inches leftward. This made no real difference in the setup.
[2] At least it doesn't change for pixels near the center of the array. We didn't measure out toward the array edges and there could conceivably be some optical edge effects (unlikely though).
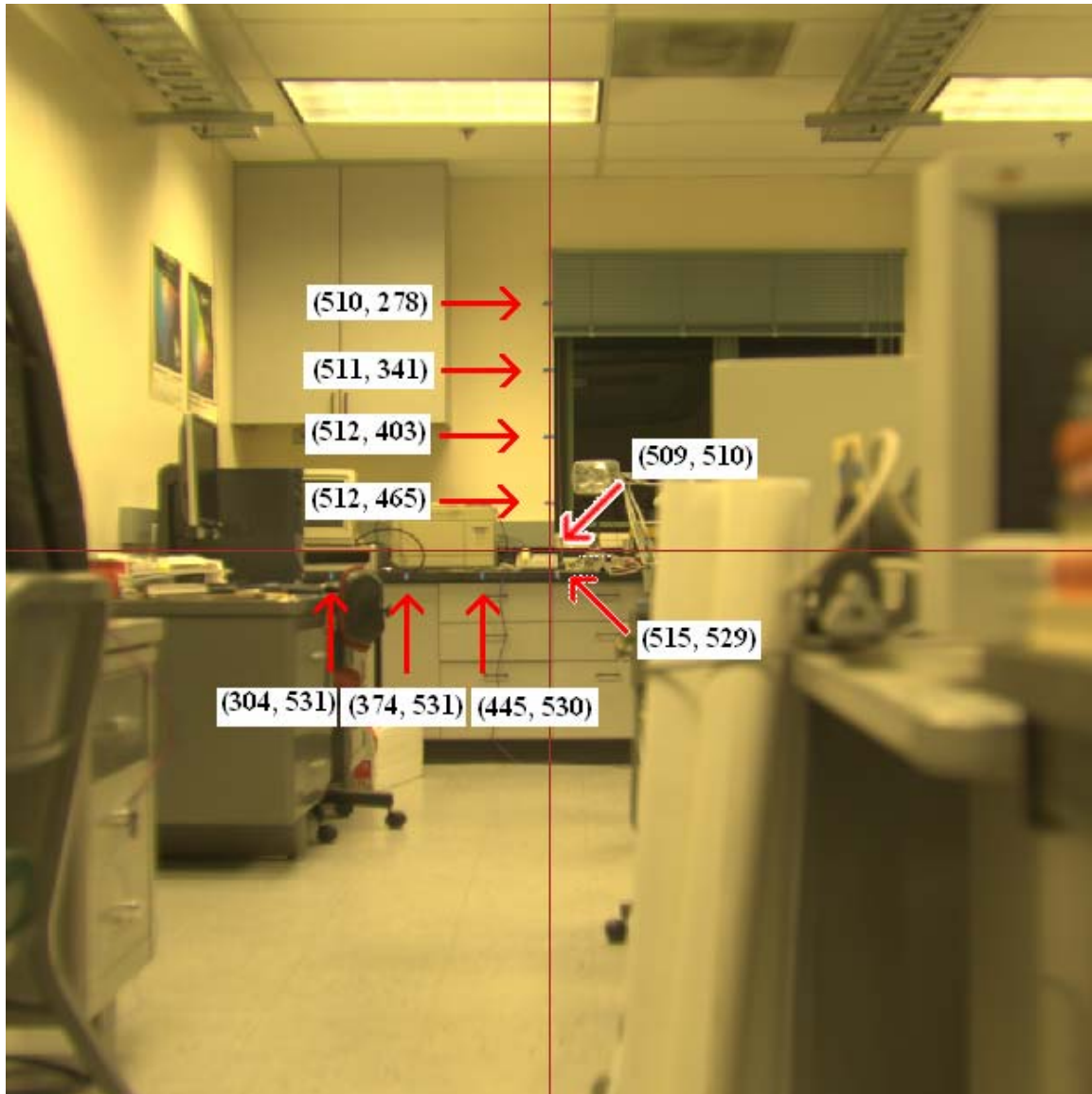
Figure 6. This is the same scene as Figures 1-3 except a) the photometer was very slightly shifted to its left (no change in the distance to the back wall) and b) photometer "measurement #3" was used. This is still the Nikon with ND2 for all filters, but the exposure times are now Y = 3 s, X = 12 s, Z = 40 s and *most importantly* the aperture is now f/2.8.

Figures 4 and 5 along with the fit

$$t = 6.72437 \times 10^{-4}\, p$$

where t is the tangent of the angle and p is the distance in pixels from the center of the crosshairs, constitute the angular relationship with pixel location for both the f/8 and f/2.8 cases (the only ones that we have calibrations for at present).

The above equation is the primary one needed in the report for the angle-pixel relationship.

Appendix E: Notes on the Calculations for Positions α and β

After most of our subjects had completed their testing, VDL decided to supplement the original data set with two additional positions for disability glare tests on three people who were conveniently still available. This was in order to check linearity of the main disability glare equation in a range where the original data was limited. The two additional positions were designated α and β. The mechanical setup remained as detailed in appendix C.

Since "reshooting" the (high intensity) luminance image for the newly created positions of α and β along the disability glare mark line on the SyncMaster 214T was somewhat difficult, and since these positions were used for only three people, two of whom had their other disability glare data taken under different positions, the L_P values were calculated via suitable modifications of the original "high intensity position 2" luminance file. This appendix supplies the needed geometric information to affect those modifications.

From the notes in appendix C, we have the following figure where the new positions α and β have now been added.
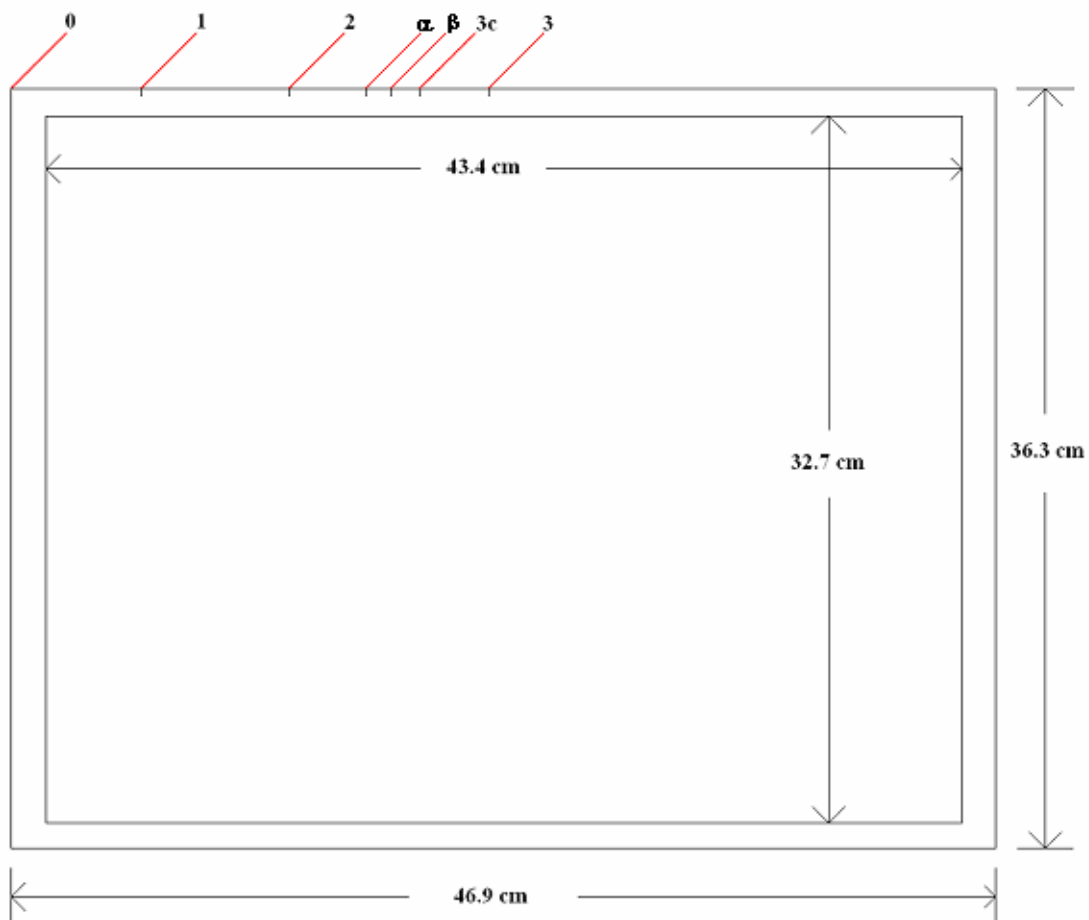
The SyncMaster 214T monitor with new positions α and β shown.

The "α mark" was measured to be 4.21 cm to the right of mark 2 and 3.19 cm to the left of mark 3c. This would suggest a distance of 4.21 + 3.19 = 7.40 cm between marks 2 and 3c, which is 0.05 cm greater than the separation of those marks as inferred from earlier measurements. Half of a millimeter is certainly within the overall measurement uncertainty though. We take the α mark as 4.21 cm to the right of mark 2.

The "β mark" was measured to be 5.68 cm to the right of mark 2 and 1.70 cm to the left of mark 3c. This gives a separation of 5.68 + 1.70 = 7.38 cm between marks 2 and 3c compared to an earlier calculated separation of 7.35 cm. Again, a difference of 0.03 cm is acceptable. We take the β mark as 5.68 cm to the right of mark 2.

The table shown in appendix C now becomes:

Mark #	Distance From 0 Mark
1	5.25 cm
2	14.05 cm
α	18.26 cm
β	19.73 cm
3c	21.40 cm
3	22.80 cm

Table 1: Mark measurements with the new positions added.

Now from *Tables Preparatory to Revision*… [not included in this report] we have the center of the LED spot at CCD pixel position (302.0, 507.0) for LED position 2 on high. We also have LED position 3c on high at (443.5, 506.0). Interpolating using this data and the values in Table 1 we have

$$\alpha \; CCD \; x \; position = \left(\frac{4.21}{7.35}\right) \times (443.5 - 302.0) + 302.0 = 383.05 \approx 383.1$$

and

$$\alpha \; CCD \; y \; position = \left(\frac{4.21}{7.35}\right) \times (506.0 - 507.0) + 507.0 = 506.427 \approx 506.4 .$$

Doing the same thing for the β mark yields,

$$\beta \; CCD \; x \; position = \left(\frac{5.68}{7.35}\right) \times (443.5 - 302.0) + 302.0 = 411.35 \approx 411.4$$

and

$$\beta \; CCD \; y \; position = \left(\frac{5.68}{7.35}\right) \times (506.0 - 507.0) + 507.0 = 506.227 \approx 506.2 .$$

Now if the "high intensity position 2" luminance file (LED spot only) is used, its LED spot center is, as mentioned, at CCD pixel position (302.0, 507.0), but we need to pretend that it is "really" at (383.1, 506.4) for the α case and at (411.4, 506.2) for the β case. Unfortunately, it is difficult to move the center of the LED spot in the luminance data file.

Instead, we "move" the center of the disability glare target. For all CCD luminance images used, the photometer crosshairs at the center of the target were at (507.5, 508.5).

Our new "center" for the α case is

$$(302.0, 507.0) - (383.1, 506.4) + (507.5, 508.5) = (426.4, 509.1)$$

so that

$$(302.0, 507.0) - (426.4, 509.1) = old\ spot - new\ center$$
$$= new\ spot - old\ (real)\ center = (383.1, 506.4) - (507.5, 508.5).$$

Our new "center" for the β case is

$$(302.0, 507.0) - (411.4, 506.2) + (507.5, 508.5) = (398.1, 509.3).$$

Thus entering these new "center" values into the program *GlareScoreDA.exe* along with the "spot" luminance CCD data file for "high intensity at position 2" should yield the correct L_P values for the α and β cases.

Appendix F: Calculations for the Solid Angle Subtended by CCD Pixels in an Imaging Photometer

The various glare formulae typically require knowing the solid angle subtended by a pixel or a group of pixels in the CCD (*charge coupled device*). These notes develop the formula for finding the solid angle occupied by those pixels.

The reader will recall that the vertex of the solid angle is coincident with an observer. A (typically finite) surface S that the observer sees is projected onto a sphere centered about the vertex. The sphere is of sufficient size to encompass[1] S and the projection is done by drawing lines from the sphere's center (the vertex) through the boundary curve of S until those lines intersect the surface of the sphere. The locus of those intersection points forms another boundary curve on the surface of the sphere. The area on the sphere's surface enclosed by *that* curve divided by the square of the sphere's radius is the solid angle subtended by S at the observer's location.

Solid angles are measured in *steradians*; the formal dictionary definition (Merriam-Webster) is:

> **Steradian**: A unit of measure equal to the solid angle subtended at the center of a sphere by an area on the surface of the sphere that is equal to the radius squared: *The total solid angle of a sphere is* 4π *steradians*.

This last example should be obvious since a sphere of radius r has a surface area of $4\pi r^2$, which gives 4π upon division by r^2. Thus an (hypothetical) observer who could see in all directions at once would have a solid viewing angle of 4π steradians.

Another simple example is given by Figure 1. Here the surface S is one face of a cube with the vertex (observation point) at the center of the cube. The red straight lines emanating from the vertex and passing through the corners of the upper cube face show how the projection is done. The red arcs lying on the surface of the (wireframe) sphere form the bounding curve of the projection of S onto the sphere's surface. The area of this projection onto the sphere divided by the square of the radius of the sphere gives the solid angle subtended by the upper cube face.

For this simple case symmetry arguments suffice. There are six faces to the cube, which is centered on the observation point. Hence the solid angle is $\frac{4\pi}{6} = \frac{2}{3}\pi$ steradians.[2]

---

[1] Obviously this is not true of infinite surfaces, but those special cases don't concern us here.
[2] Steradians are dimensionless but sometimes the units, denoted as "sr", are written down after the numerical value so that one is aware of what the number stands for.
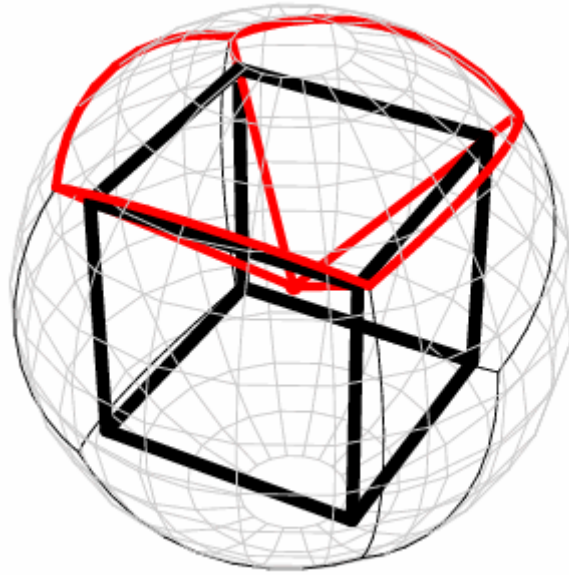
Figure 1. Solid Angle subtended by one face of a cube (from http://mathworld.wolfram.com/SolidAngle.html).

When symmetry arguments don't apply, we can turn to the following, more exact, formulation. A solid angle Ω subtended by a surface S at the origin (observation point or vertex or center of sphere) is given by,

$$\Omega = \iint\limits_S \frac{\vec{r} \cdot \overrightarrow{dS}}{r^3} = \iint\limits_S \frac{\mathbf{n} \cdot \overrightarrow{dS}}{r^2} \qquad (A.1)$$

where $\vec{r}$ is a vector from the origin to an infinitesimal surface element dS. The magnitude of that vector is r, the distance from the origin to the surface element, and **n** is the unit vector having the same direction as $\vec{r}$. The direction of $\overrightarrow{dS}$ is the usual "outward" (away from the origin) surface normal.

Note that r in the above equation is **not** *(usually) the same* "r" *(radius) in the informal discussion of solid angle above*. The two descriptions are, of course, equivalent and both approaches give the same numerical values for the solid angle, but the vector $\vec{r}$ in the equation for Ω has its tail at the origin and its head on S <u>not on the sphere's surface</u>.

(An example using an equation equivalent to (A.1) is done at the URL given in the caption of Figure 1.)

Turning now to our particular problem, we need to find out where the origin (or solid angle vertex or "observation point") is in the case of the imaging photometer. This can be done conceptually with the aid of Figure 2. The imaging or focal plane of the photometer is occupied

by a square CCD array[3]. If that flat array is parallel to a (sufficiently long) wall then vertical lines on the wall will image onto the vertical edges of the CCD. One can then (mentally if not physically) trace planes from the wall to the vertical edges of the CCD and then back until those planes intersect at an "origin". Two planes intersect in a line[4] of course, but a normal from the center of the (square) CCD will intersect this "origin" line (coming out of the page in Figure 2) at a single point. *That point* is the vertex or origin (no quotes now).

The light from the wall being imaged goes through the optics of the photometer (that is how it is imaged!) but that process can be ignored. We can just pretend that straight lines can be "drawn" from points on the wall to the corresponding points on the (parallel) CCD and then continued past the CCD.
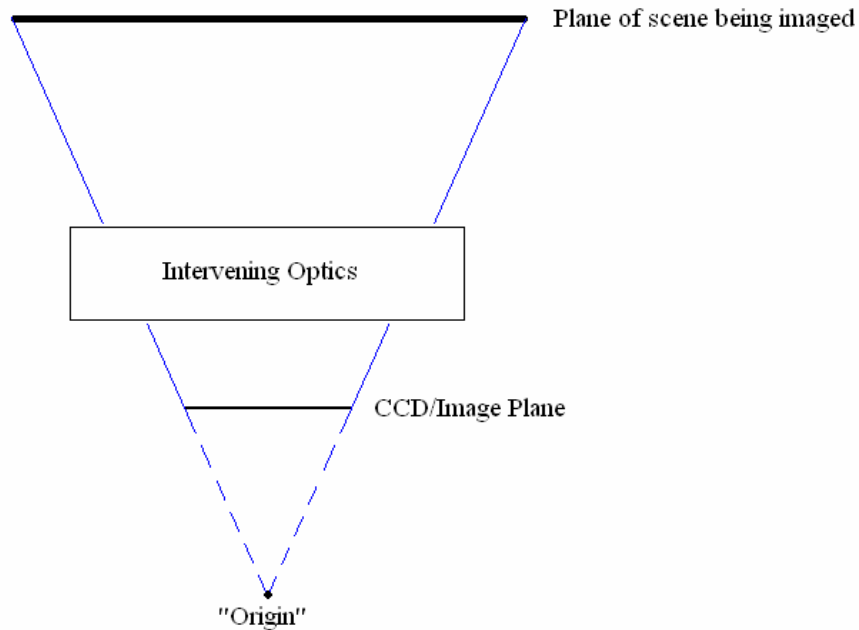
Figure 2. "Bird's eye" view of a scene in a vertical plane (say a wall) being imaged onto a square CCD array which is also in a vertical plane and parallel to the wall. By following the edges of the scene back to the edges of the CCD (ignoring the optics which actually create the image!) and beyond, we can, in principle, find the origin or projection point for subsequent solid angle calculations.

This procedure though just allows us to *conceptually* find the vertex point; in practice a different approach is used. That method is explained below, but first we look at a visualization of our particular problem.

In Figure 3 we have the photometer's CCD displayed as a light blue plane containing the square pixels (obviously not 1020 x 1020 for clarity's sake). It is surrounded by a wireframe sphere whose center is the origin (or solid angle vertex) point "found" in Figure 2. A standard three-dimensional Cartesian coordinate system is shown as well. The x and y axes are parallel to the

---

[3] The photometer from *Radiant Imaging* has its CCD made up of 1020 x 1020 pixels. The CCD actually has 1024 x 1024 elements but the edges of the array are not used for capturing light. Here we call the light capturing elements (somewhat loosely) "pixels".
[4] In three dimensions that is. In 4 dimensions, two-dimensional planes can intersect at a single point!

edges of the square CCD. The x-y plane is parallel to the plane of the CCD and the z-axis represents the "line-of-sight" that passes through the center of the CCD.
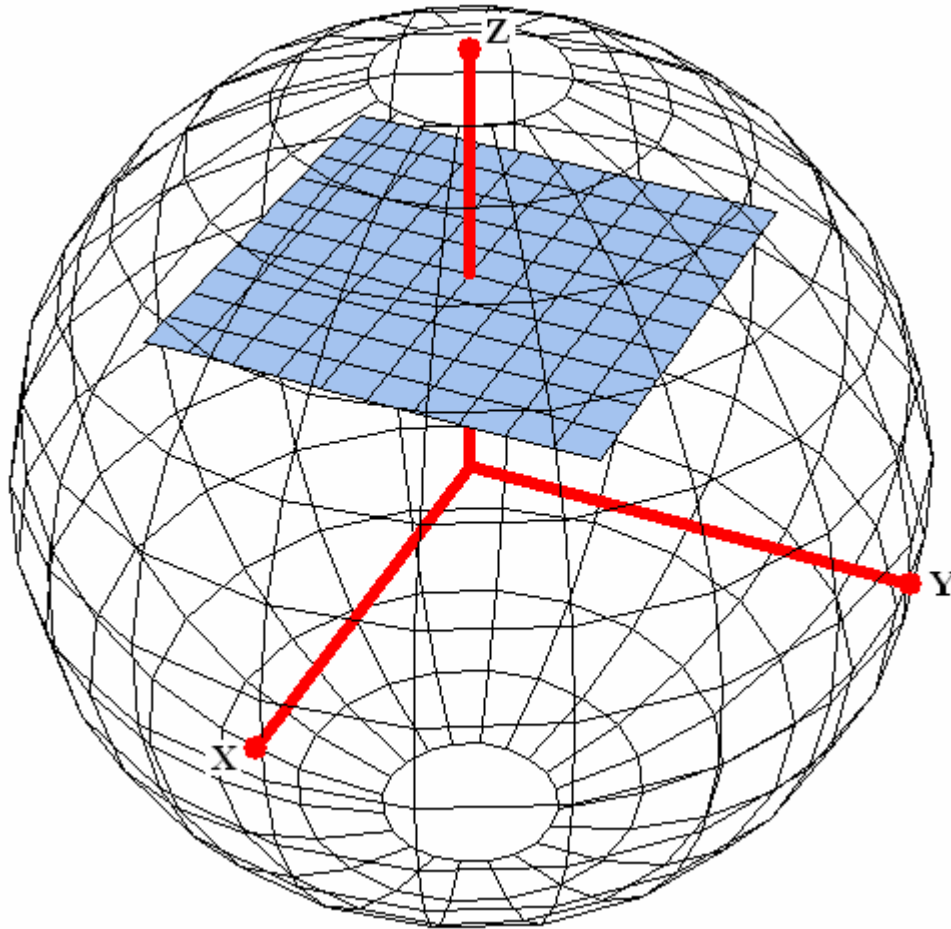
Figure 3. The coordinate system used in these calculations—the z-axis run straight through the middle of the square CCD array. The z-axis is the *line-of-sight*. The center of the sphere is the same origin as found in Figure 2.

What we wish to find is depicted in Figure 4. Here an "arbitrary" pixel (dark blue) is projected onto the sphere. The resulting surface area on the sphere (shown in gold) when divided by the square of the radius of the sphere would give us the solid angle subtended by the (dark blue) pixel at the origin.

To actually perform any computations though, we need a scale or metric. The procedure for doing this comes from Figure 5. Figure 5 also shows how we can "find" our origin as a practical matter.
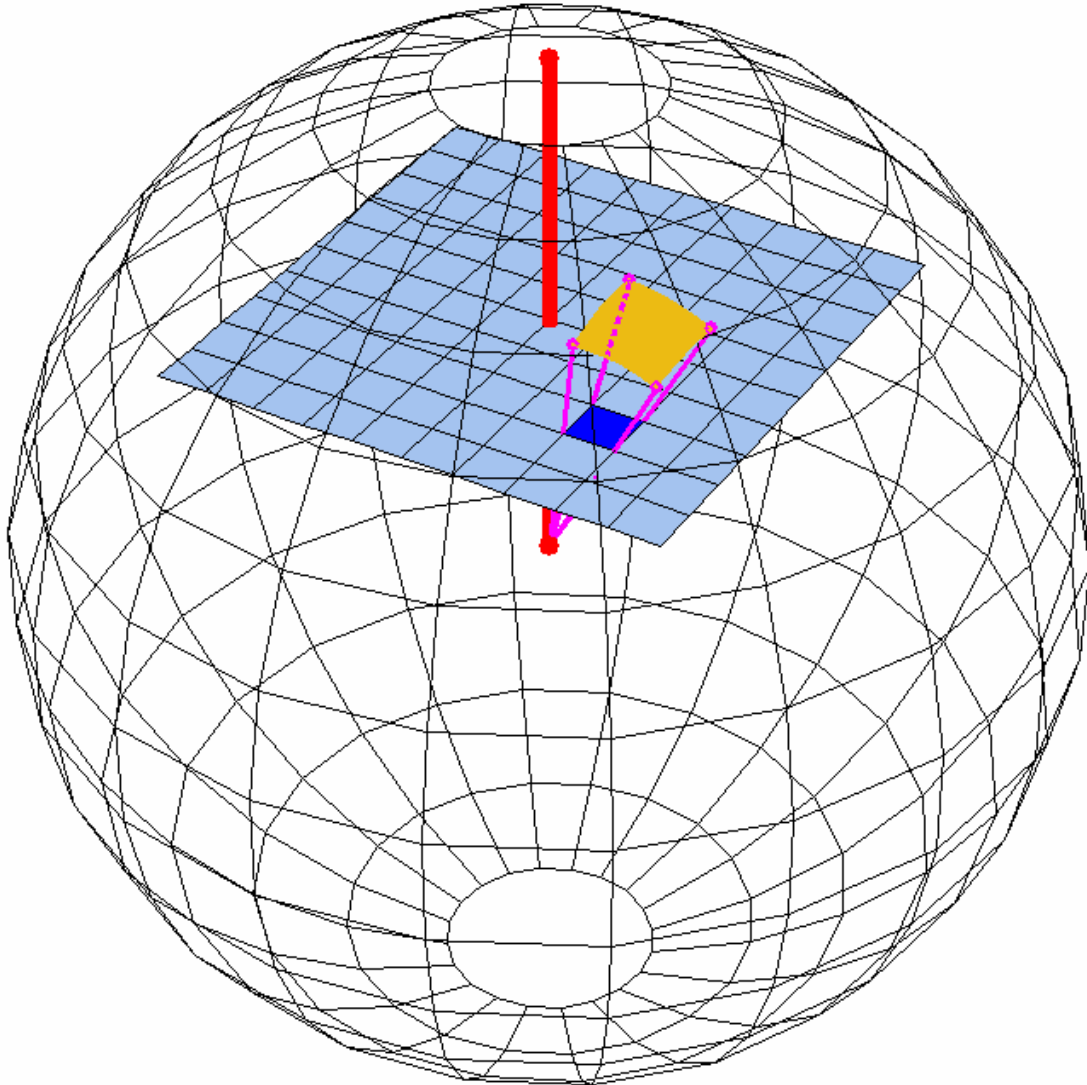
Figure 4. The dark blue square on the CCD plane is projected onto the surface of the sphere. The magenta projection lines start at the origin, run through the corners of the square (pixel) that is being projected, and end on the surface of the sphere. The curvilinear gold square on the sphere's surface represents the projection of the dark blue square (pixel) that is on the CCD. The z-axis or *line-of-sight* is also shown (fat red line).

If the scale of *ordinary* angles[5] has been empirically determined then it is not necessary to know the details of the photometer's optics in front of the CCD. The length of an edge of a square pixel determines the scale. Such an edge is taken as one unit.

For example, the distance 'w' shown in Figure 5 represents the distance from the center of the CCD to the middle of an edge of the CCD (which edge is immaterial since the array is square). Since the photometer's CCD array is 1020 by 1020 pixels, w is half of one CCD edge or 510 pixels[6].

---

[5] See <u>Angle-Pixel Scaling and Measurement for the Radiant Imaging Photometer</u> (Appendix D).

[6] Again, the term "pixel" is used somewhat loosely (see footnote 3). It should be clear that "pixel" in this context means "length of a side of a square pixel" but the latter is too much of a mouthful. In other words, in this sense of use, "pixel" means a length, not an area.
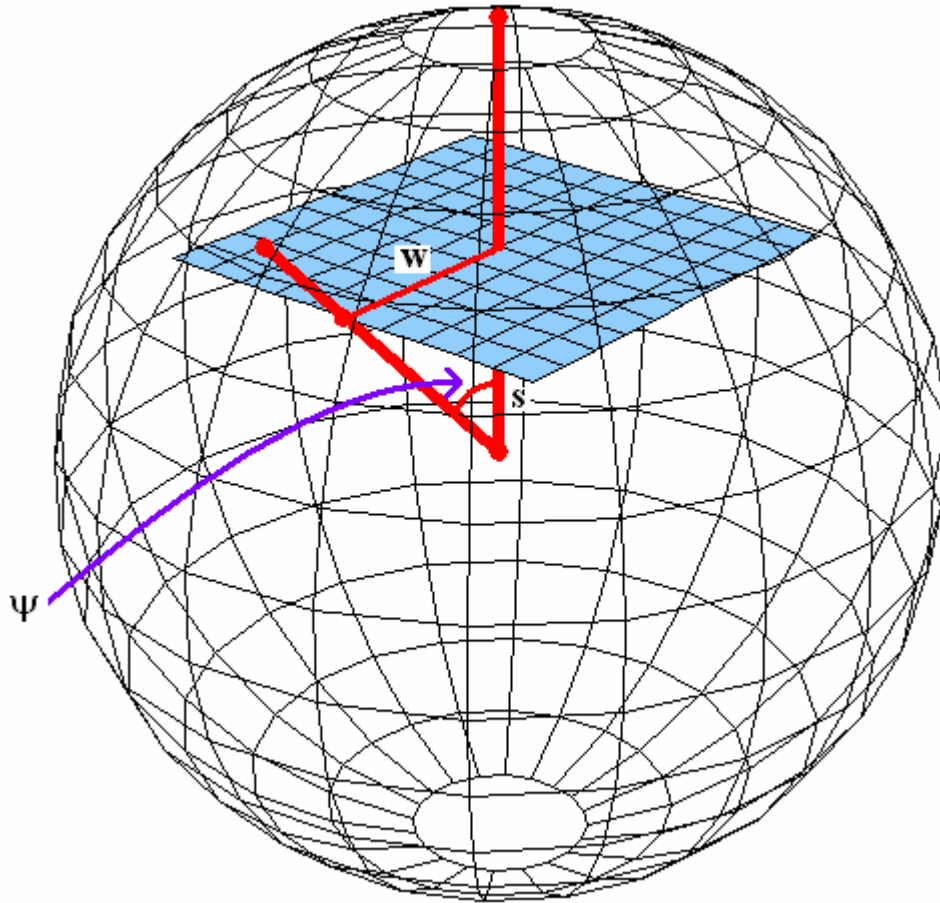
Figure 5. The distance from the origin of the sphere to the plane of the CCD is s. The distance from the center of the (square) CCD to the middle of an edge is w. The angle between that middle of an edge and the CCD center, as subtended at the origin, is Ψ. In other words, w/s is the tangent of Ψ.

As shown in Figure 5, s represents the distance from the origin to the center of the CCD. Put another way, the coordinates of the CCD center, based on the coordinate system of Figure 3, are $(x, y, z) = (0, 0, s)$. Hence, referring to Figure 5, the tangent of the angle shown as Ψ is,

$$tan\,\psi = \frac{w}{s}. \tag{A.2}$$

This tangent value can be measured however (footnote 5). In the case of the *Radiant Imaging* photometer, that number comes out to be 0.342934. Equating this to w/s above and putting w equal to 510 gives $s = 1487.17$. Thus we know the distance in "pixels" from our CCD center point to the origin. This is how we can "locate" the origin (the center of the sphere) as a practical matter.

Returning to the situation in Figure 4, we generalize somewhat. Instead of the solid angle of a single pixel, we determine the solid angle for any rectangular region on the CCD.

This is shown in Figure 6. Here the rectangular region (dark blue) for which we want the solid angle has its corners labeled as (a, c), (b, c), (b, d) and (a, d). These are the x-y coordinates—the z value being understood as s, the height of the CCD plane. In the case of a single pixel, we would have b = a + 1 and d = c + 1.
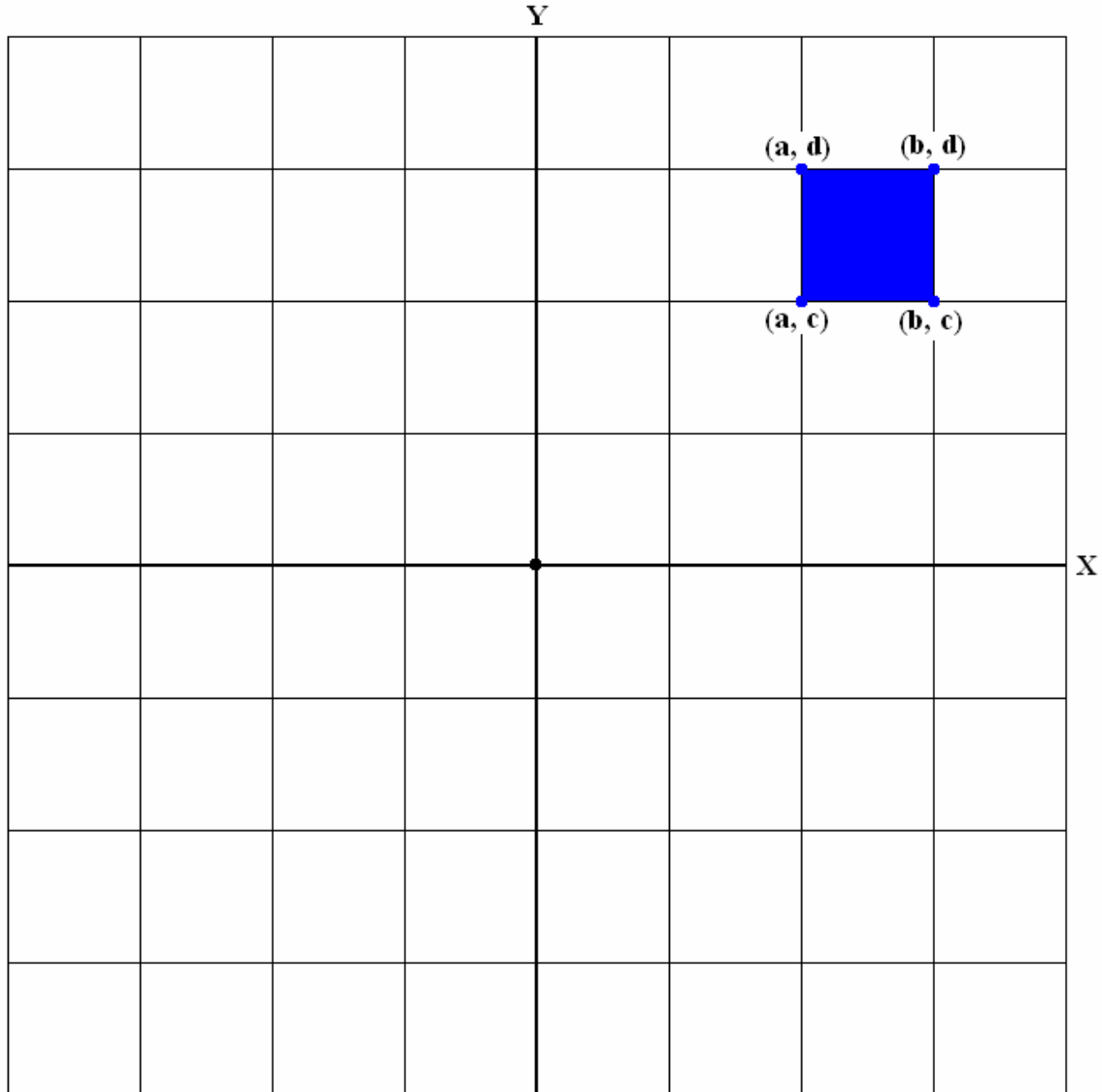
Figure 6. The x-y plane of the CCD. The third (suppressed) coordinate is understood to be z = s. The x and y coordinates of corners of the selected rectangular region (dark blue) are shown.

Applying equation (A.1), it is clear that the normal to S is simply $\hat{z}$ and dS is just dx dy. Thus $\vec{r} \cdot \overrightarrow{dS} = r \cos \theta \, dx \, dy = s \, dx \, dy$, where hopefully s (lower case—distance) isn't confused with S (upper case—surface).

Putting these results into equation (A.1) gives,

$$\Omega = \int_{c}^{d} \int_{a}^{b} \frac{s}{\left(x^2 + y^2 + s^2\right)^{3/2}} \, dx \, dy \,. \tag{A.3}$$

Doing the inner integral above yields,

$$\Omega = \int_{c}^{d} \left[\frac{sx}{\left(s^2 + y^2\right)\sqrt{x^2 + y^2 + s^2}} \right]_{a}^{b} dy$$

$$= \int_{c}^{d} \frac{sb}{\left(s^2 + y^2\right)\sqrt{b^2 + y^2 + s^2}} \, dy - \int_{c}^{d} \frac{sa}{\left(s^2 + y^2\right)\sqrt{a^2 + y^2 + s^2}} \, dy. \tag{A.4}$$

This last type of integral can also be done to yield,

$$\Omega = \left[arctan\left(\frac{by}{s\sqrt{b^2 + s^2 + y^2}} \right) - arctan\left(\frac{ay}{s\sqrt{a^2 + s^2 + y^2}} \right) \right]_{c}^{d}$$

$$= arctan\left(\frac{bd}{s\sqrt{b^2 + s^2 + d^2}} \right) + arctan\left(\frac{ac}{s\sqrt{a^2 + s^2 + c^2}} \right)$$

$$- arctan\left(\frac{ad}{s\sqrt{a^2 + s^2 + d^2}} \right) - arctan\left(\frac{bc}{s\sqrt{b^2 + s^2 + c^2}} \right), \tag{A.5}$$

which is the final answer to the problem.

Here it was assumed that $b > a \geq 0$ and $d > c \geq 0$. In other words, the rectangle in Figure 6 was in the positive quadrant (in 2D) or in the positive octant if we consider the three-dimensional coordinate system of Figure 3. Clearly the geometry of the solid angle is indifferent to which quadrant the rectangle occupies, but one must be wary of how the arctangent function is implemented when using equation (A.5) in a computer program.

Equation (A.5) can be rewritten as,

$$\Omega = arctan\left(\frac{\left(\frac{b}{s}\right)\left(\frac{d}{s}\right)}{\sqrt{\left(\frac{b}{s}\right)^2 + 1 + \left(\frac{d}{s}\right)^2}}\right) + arctan\left(\frac{\left(\frac{a}{s}\right)\left(\frac{c}{s}\right)}{\sqrt{\left(\frac{a}{s}\right)^2 + 1 + \left(\frac{c}{s}\right)^2}}\right)$$

$$- arctan\left(\frac{\left(\frac{a}{s}\right)\left(\frac{d}{s}\right)}{\sqrt{\left(\frac{a}{s}\right)^2 + 1 + \left(\frac{d}{s}\right)^2}}\right) - arctan\left(\frac{\left(\frac{b}{s}\right)\left(\frac{c}{s}\right)}{\sqrt{\left(\frac{b}{s}\right)^2 + 1 + \left(\frac{c}{s}\right)^2}}\right),$$

(A.6)

thereby showing how the distance s sets the scale.

Finally it is worth noting that previous pictures were not typically at the right scale, in order to make the geometry clear. Figure 7 is a more realistic depiction of the size of the CCD relative to the distance to the origin. (The pixel size while reduced is clearly not at the right scale since there are over a million pixels on the real CCD.)
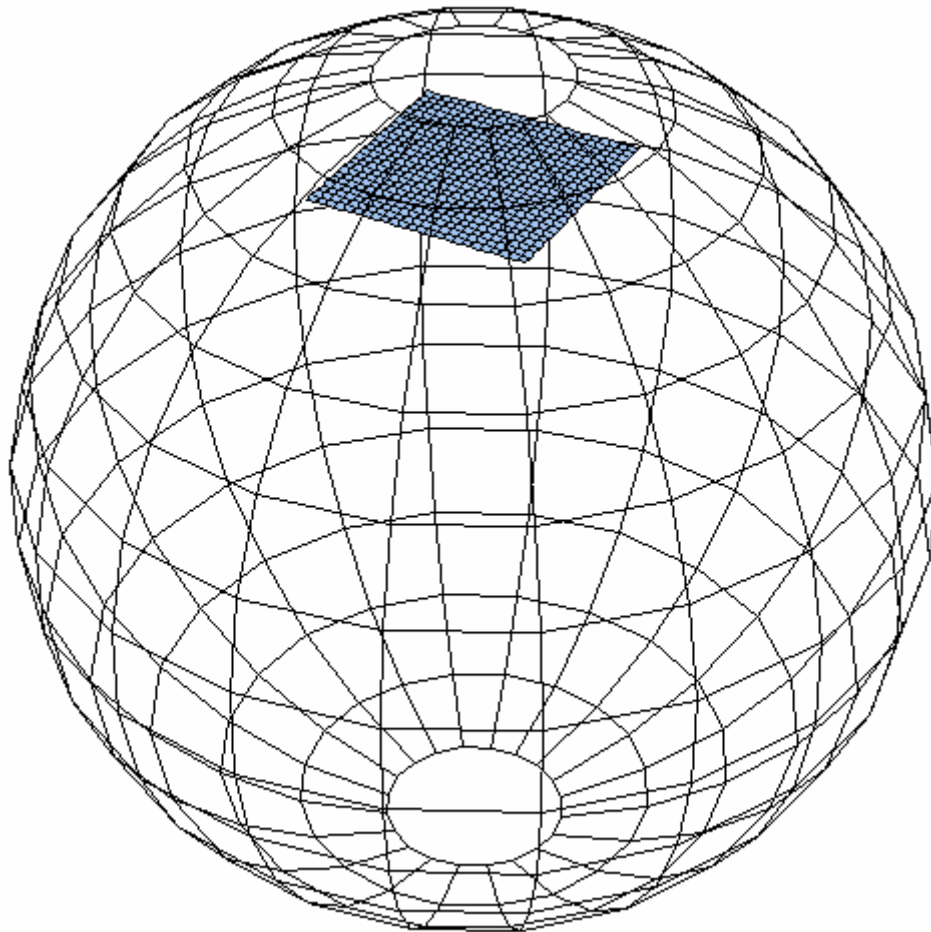
Figure 7. A *somewhat* more realistic depiction of the scale of the CCD (image) in terms of the scale of the projecting sphere.

[Note: the result in equation (A.5) could also be derived using spherical trigonometry, but that requires more effort.]

Appendix G: Disability Glare Raw Data Tables

Subject	Age (yrs)	Lb [all cases - in cd/m^2]	Lt - No LED [steps]	Lt - No LED [cd/m^2]	(Lt - Lb)/Lb - No LED	Lp [program output - arb. Units] - No LED
# 1	61	0.305	3	0.320	0.0492	not taken
# 2	28	0.305	4	0.330	0.0820	
# 3	53	0.305	4	0.330	0.0820	
# 4	25	0.305	3	0.320	0.0492	
# 5	27	0.305	4	0.330	0.0820	
# 6	53	0.305	2	0.317	0.0393	
# 7	45	0.305	3	0.320	0.0492	
# 8	68	0.305	6	0.350	0.1475	
# 9	53	0.305	6	0.350	0.1475	
# 10	60	0.305	3	0.320	0.0492	
# 11	52	0.305	5	0.340	0.1148	
# 12	29	0.305	5	0.340	0.1148	
# 13	71	0.305	8	0.380	0.2459	
# 14	71	0.305	8	0.380	0.2459	
# 15	39	0.305	4	0.330	0.0820	

Subject	Age (yrs)	Lb [all cases - in cd/m^2]	Lt - LED Low Pos. 1 [steps]	Lt - LED Low Pos. 1 [cd/m^2]	(Lt - Lb)/Lb - LED Low Pos. 1	Lp [program output - arb. Units] - LED Low Pos. 1
# 1	61	0.305	4	0.330	0.0820	6.376E-02
# 2	28	0.305	4	0.330	0.0820	3.674E-02
# 3	53	0.305	4	0.330	0.0820	5.160E-02
# 4	25	0.305	4	0.330	0.0820	3.628E-02
# 5	27	0.305	5	0.340	0.1148	3.657E-02
# 6	53	0.305	2	0.317	0.0393	5.160E-02
# 7	45	0.305	3	0.320	0.0492	4.386E-02
# 8	68	0.305	8	0.380	0.2459	7.910E-02
# 9	53	0.305	4	0.330	0.0820	5.160E-02
# 10	60	0.305	4	0.330	0.0820	6.195E-02
# 11	52	0.305	5	0.340	0.1148	5.042E-02
# 12	29	0.305	5	0.340	0.1148	3.693E-02
# 13	71	0.305	9	0.400	0.3115	8.738E+00
# 14	71	0.305	7	0.360	0.1803	8.738E+00
# 15	39	0.305	3	0.32	0.0492	4.021E-02

Subject	Age (yrs)	Lb [all cases - in cd/m^2]	Lt - LED Med Pos. 1 [steps]	Lt - LED Med Pos. 1 [cd/m^2]	(Lt - Lb)/Lb - LED Med Pos. 1	Lp [program output - arb. Units] - LED Med Pos. 1
# 1	61	0.305	5	0.340	0.1148	1.559E+00
# 2	28	0.305	5	0.340	0.1148	8.984E-01
# 3	53	0.305	5	0.340	0.1148	1.262E+00
# 4	25	0.305	4	0.330	0.0820	8.872E-01
# 5	27	0.305	6	0.350	0.1475	8.942E-01
# 6	53	0.305	3	0.320	0.0492	1.262E+00
# 7	45	0.305	5	0.340	0.1148	1.072E+00
# 8	68	0.305	12	0.504	0.6525	1.935E+00
# 9	53	0.305	7	0.360	0.1803	1.262E+00
# 10	60	0.305	7	0.360	0.1803	1.515E+00
# 11	52	0.305	7	0.360	0.1803	1.233E+00
# 12	29	0.305	6	0.350	0.1475	9.030E-01
# 13	71	0.305	10	0.420	0.3770	2.137E+00
# 14	71	0.305	9	0.400	0.3115	2.137E+00
# 15	39	0.305	5	0.340	0.1148	9.832E-01

Subject	Age (yrs)	Lb [all cases - in cd/m^2]	Lt - LED High Pos. 1 [steps]	Lt - LED High Pos. 1 [cd/m^2]	(Lt - Lb)/Lb - LED High Pos. 1	Lp [program output - arb. Units] - LED High Pos. 1
# 1	61	0.305	7	0.360	0.1803	6.999E+00
# 2	28	0.305	7	0.360	0.1803	4.034E+00
# 3	53	0.305	9	0.400	0.3115	5.664E+00
# 4	25	0.305	8	0.380	0.2459	3.984E+00
# 5	27	0.305	11	0.462	0.5148	4.016E+00
# 6	53	0.305	5	0.34	0.1148	5.664E+00
# 7	45	0.305	9	0.400	0.3115	4.815E+00
# 8	68	0.305	14	0.588	0.9279	8.687E+00
# 9	53	0.305	10	0.420	0.3770	5.664E+00
# 10	60	0.305	12	0.504	0.6525	6.800E+00
# 11	52	0.305	12	0.504	0.6525	5.535E+00
# 12	29	0.305	9	0.400	0.3115	4.055E+00
# 13	71	0.305	20	1.080	2.5410	9.590E+00
# 14	71	0.305	17	0.810	1.6557	9.590E+00
# 15	39	0.305	8	0.380	0.2459	4.415E+00

Subject	Age (yrs)	Lb [all cases - in cd/m^2]	Lt - LED Low Pos. 2 [steps]	Lt - LED Low Pos. 2 [cd/m^2]	(Lt - Lb)/Lb - LED Low Pos. 2	Lp [program output - arb. Units] - LED Low Pos. 2
# 1	61	0.305	4	0.330	0.0820	2.118E-01
# 2	28	0.305	4	0.330	0.0820	1.267E-01
# 3	53	0.305	4	0.330	0.0820	1.735E-01
# 4	25	0.305	3	0.320	0.0492	1.253E-01
# 5	27	0.305	5	0.340	0.1148	1.262E-01
# 6	53	0.305	3	0.320	0.0492	1.735E-01
# 7	45	0.305	4	0.330	0.0820	1.491E-01
# 8	68	0.305	5	0.340	0.1148	2.602E-01
# 9	53	0.305	5	0.340	0.1148	1.735E-01
# 10	60	0.305	4	0.330	0.0820	2.061E-01
# 11	52	0.305	5	0.340	0.1148	1.698E-01
# 12	29	0.305	5	0.340	0.1148	1.273E-01
# 13	71	0.305	9	0.400	0.3115	2.861E-01
# 14	71	0.305	7	0.360	0.1803	2.861E-01
# 15	39	0.305	4	0.330	0.0820	1.377E-01

Subject	Age (yrs)	Lb [all cases - in cd/m^2]	Lt - LED Med Pos. 2 [steps]	Lt - LED Med Pos. 2 [cd/m^2]	(Lt - Lb)/Lb - LED Med Pos. 2	Lp [program output - arb. Units] - LED Med Pos. 2
# 1	61	0.305	6	0.350	0.1475	5.165E+00
# 2	28	0.305	6	0.350	0.1475	3.091E+00
# 3	53	0.305	7	0.360	0.1803	4.232E+00
# 4	25	0.305	6	0.350	0.1475	3.056E+00
# 5	27	0.305	7	0.360	0.1803	3.078E+00
# 6	53	0.305	6	0.350	0.1475	4.232E+00
# 7	45	0.305	7	0.360	0.1803	3.638E+00
# 8	68	0.305	15	0.630	1.0656	6.346E+00
# 9	53	0.305	8	0.380	0.2459	4.232E+00
# 10	60	0.305	9	0.400	0.3115	5.026E+00
# 11	52	0.305	10	0.420	0.3770	4.141E+00
# 12	29	0.305	9	0.400	0.3115	3.106E+00
# 13	71	0.305	19	0.990	2.2459	6.978E+00
# 14	71	0.305	16	0.720	1.3607	6.978E+00
# 15	39	0.305	7	0.360	0.1803	3.358E+00

Subject	Age (yrs)	Lb [all cases - in cd/m^2]	Lt - LED High Pos. 2 [steps]	Lt - LED High Pos. 2 [cd/m^2]	(Lt - Lb)/Lb - LED High Pos. 2	Lp [program output - arb. Units] - LED High Pos. 2
# 1	61	0.305	13	0.546	0.7902	2.965E+01
# 2	28	0.305	10	0.420	0.3770	1.775E+01
# 3	53	0.305	11	0.462	0.5148	2.429E+01
# 4	25	0.305	12	0.504	0.6525	1.755E+01
# 5	27	0.305	14	0.588	0.9279	1.768E+01
# 6	53	0.305	8	0.380	0.2459	2.429E+01
# 7	45	0.305	13	0.546	0.7902	2.089E+01
# 8	68	0.305	20	1.080	2.5410	3.642E+01
# 9	53	0.305	13	0.546	0.7902	2.429E+01
# 10	60	0.305	16	0.720	1.3607	2.885E+01
# 11	52	0.305	14	0.588	0.9279	2.377E+01
# 12	29	0.305	18	0.900	1.9508	1.784E+01
# 13	71	0.305	31	3.360	10.0164	4.004E+01
# 14	71	0.305	25	1.960	5.4262	4.004E+01
# 15	39	0.305	14	0.588	0.9279	1.928E+01

Subject	Age (yrs)	Lb [all cases - in cd/m^2]	Lt - LED Low Pos. 3c [steps]	Lt - LED Low Pos. 3c [cd/m^2]	(Lt - Lb)/Lb - LED Low Pos. 3c	Lp [program output - arb. Units] - LED Low Pos. 3c
# 1	61	0.305	7	0.360	0.1803	2.927E+00
# 2	28	0.305	5	0.340	0.1148	1.993E+00
# 3	53	0.305	5	0.340	0.1148	2.507E+00
# 4	25	0.305	4	0.330	0.0820	1.978E+00
# 5	27	0.305	6	0.350	0.1475	1.987E+00
# 6	53	0.305	4	0.330	0.0820	2.507E+00
# 7	45	0.305	7	0.360	0.1803	2.239E+00
# 8	68	0.305	9	0.400	0.3115	3.458E+00
# 9	53	0.305	7	0.360	0.1803	2.507E+00
# 10	60	0.305	9	0.400	0.3115	2.864E+00
# 11	52	0.305	6	0.350	0.1475	2.466E+00
# 12	29	0.305	8	0.380	0.2459	2.000E+00
# 13	71	0.305	15	0.630	1.0656	3.742E+00
# 14	71	0.305	10	0.420	0.3770	3.742E+00
# 15	39	0.305	6	0.350	0.1475	2.113E+00

Subject	Age (yrs)	Lb [all cases - in cd/m^2]	Lt - LED Med Pos. 3c [steps]	Lt - LED Med Pos. 3c [cd/m^2]	(Lt - Lb)/Lb - LED Med Pos. 3c	Lp [program output - arb. Units] - LED Med Pos. 3c
# 1	61	0.305	14	0.588	0.9279	6.804E+01
# 2	28	0.305	14	0.588	0.9279	4.633E+01
# 3	53	0.305	12	0.504	0.6525	5.827E+01
# 4	25	0.305	17	0.810	1.6557	4.596E+01
# 5	27	0.305	18	0.900	1.9508	4.619E+01
# 6	53	0.305	11	0.462	0.5148	5.827E+01
# 7	45	0.305	18	0.900	1.9508	5.205E+01
# 8	68	0.305	29	2.880	8.4426	8.047E+01
# 9	53	0.305	11	0.462	0.5148	5.827E+01
# 10	60	0.305	22	1.380	3.5246	6.659E+01
# 11	52	0.305	20	1.080	2.5410	5.732E+01
# 12	29	0.305	19	0.990	2.2459	4.648E+01
# 13	71	0.305	39	5.324	16.4557	8.702E+01
# 14	71	0.305	24	1.750	4.7377	8.702E+01
# 15	39	0.305	16	0.720	1.3607	4.912E+01

Subject	Age (yrs)	Lb [all cases - in cd/m^2]	Lt - LED High Pos. 3c [steps]	Lt - LED High Pos. 3c [cd/m^2]	(Lt - Lb)/Lb - LED High Pos. 3c	Lp [program output - arb. Units] - LED High Pos. 3c
# 1	61	0.305	26	2.190	6.1803	4.158E+02
# 2	28	0.305	22	1.380	3.5246	2.833E+02
# 3	53	0.305	17	0.810	1.6557	3.562E+02
# 4	25	0.305	34	4.034	12.2262	2.811E+02
# 5	27	0.305	28	2.690	7.8197	2.825E+02
# 6	53	0.305	22	1.380	3.5246	3.562E+02
# 7	45	0.305	37	4.792	14.7115	3.182E+02
# 8	68	0.305	36	4.526	13.8393	4.912E+02
# 9	53	0.305	27	2.440	7.0000	3.562E+02
# 10	60	0.305	35	4.260	12.9672	4.069E+02
# 11	52	0.305	29	2.880	8.4426	3.504E+02
# 12	29	0.305	29	2.880	8.4426	2.843E+02
# 13	71	0.305	88	29.500	95.7213	5.316E+02
# 14	71	0.305	86	28.100	91.1311	5.316E+02
# 15	39	0.305	30	3.130	9.2623	3.004E+02

Subject	Age (yrs)	Lb [all cases - in cd/m^2]	Lt - LED High Pos. Alpha [steps]	Lt - LED High Pos. Alpha [cd/m^2]	(Lt - Lb)/Lb - LED High Pos. Alpha	Lp [program output - arb. Units] - LED High Pos. Alpha
# 1	61	0.305	20	1.080	2.541	8.644E+01
# 7	45	0.305	18	0.900	1.951	6.271E+01
# 15	39	0.305	19	0.990	2.246	5.836E+01

Subject	Age (yrs)	Lb [all cases - in cd/m^2]	Lt - LED High Pos. Beta [steps]	Lt - LED High Pos. Beta [cd/m^2]	(Lt - Lb)/Lb - LED High Pos. Beta	Lp [program output - arb. Units] - LED High Pos. Beta
# 1	61	0.305	21	1.220	3.000	1.523E+02
# 7	45	0.305	20	1.080	2.541	1.126E+02
# 15	39	0.305	21	1.220	3.000	1.053E+02

Appendix H: Matlab Program for Discomfort Glare Analysis Method 1

```matlab
% This is the "final" version of the discomfort glare scoring program that
% uses the Baer formula (the previous version was "BabyBaer.m").

clear all

indir = 'D:\\Corrected_Glare_Data\\Discomfort Glare\\Discomfort Scenes\\Final
Scene + LED\\';
outdir = 'D:\\Corrected_Glare_Data\\Discomfort Glare\\Discomfort
Scenes\\Final Scene + LED\\DeBoer Scores\\';
% Specify output file. ONE ONLY CHANGES "High" BELOW AND "H" IN fin TO
% RERUN FOR LOW AND MEDIUM.
fout = sprintf('HighLumScores.txt');
outfile = strcat(outdir,fout);
datout = sprintf(outfile);
fid = fopen(datout,'at');

% BEGIN A BIG DOUBLE LOOP. (Runs over various input files) *********
for m = 1:3
    for n = 1:3


% Start by reading in the name of the file that represents the LED + Scene,
% 1020 x 1020 luminance matrix.
fin = sprintf('H_Y_Pos%d_S%d.txt',m,n);
infile = strcat(indir,fin); % String concatenation.
datin = sprintf(infile);    % DOUBLE-CHECK THAT THIS IS NECESSARY
% Load the working matrix and give it a name.
W = load(datin,'-ascii');
% Turn the square matrix into a vector or list of numbers with "reshape".
% (Call the list "L".) This allows the search for a single maximum value.
L = reshape(W,1,1020*1020);
% Find the biggest entry.
tops = max(L);
clear L;

% We find a contour that acts as a bounding perimeter for the glare
% source(s). The *single-value* contour is based on a lower bound for the
% glare source luminance; the lower bound is a fraction of the maximum
% luminance. That fraction varies with the maximum value.
if (tops >= 10^5)
    perc = 0.005;
elseif ((tops >= 5*10^4) && (tops < 10^5))
    perc = 0.01;
elseif ((tops >= 2*10^4) && (tops < 5*10^4))
    perc = 0.02;
elseif ((tops >= 10^4) && (tops < 2*10^4))
    perc = 0.05;
elseif (tops < 10^4)
    disp('Glare unlikely. Quitting program.');
    quit;
else
    disp('Something wrong with program--quitting.');
    quit;
end
```

```matlab
lb = perc*tops;
vc = [lb lb]; % Method for a *single* contour value.
vc = ceil(vc); % Turn the value into an integer.

% Plot the straight image.
figure(1);
imagesc(W) % Stay in color.
colormap('default')

% Dropping "flipped" matrix (uses "flipud") for contour overlay used in
% "PreBabyBaer.m". Here we just plot the contours and the bounding
% rectangle. This also gives us the all important contour matrix C.
figure(2)
[C, h] = contour(W,vc);
clabel(C,h);
hold on; % Put in the bounding rectangle below; thus leave figure on "hold".

% Having learned in "PreBabyBaer.m" that, despite having only a single real
% glare source, one doesn't necessarily get just one actual contour. Stray
% (scattered) light can give, say, single pixels of high value nowhere near
% the actual glare source. A single high value pixel would be surrounded by
% at most 8 "contour pixels". Thus we go through the contour matrix and
% keep the largest contour. The contour plot will keep us from making a
% mistake.
uplim = length(C); % C is a 2 x "uplim" matrix.
index = 1;
indxbg = 1;
cval = C(1,1); % This is just the value vc chosen above.
npts = C(2,1); % This is the number of points in the 1st (and so far
               % only) contour.
% While loop (to the end of the rows of C) to find the contour with the
% most points. The number "index" represents the column number for
% the information regarding a given contour--see 'Remarks' under "contourc"
% in Matlab help for detailed information.
while (uplim > (index + npts))
    index = index + npts + 1;
    if (C(2,index) >= npts)
        indxbg = index;         % Store index of biggest contour.
    end;
    npts = C(2,index);
end;

cval = C(1,indxbg); % Should be value vc as above since there is only one
                    % contour value.
npts = C(2,indxbg); % This is now the number of points in the biggest
                    % countour.

% Put the points (coordinates) from this biggest contour into a matrix D.
% We take from C both rows (hence 1:2) but only the columns starting with
% one more than the index of the biggest contour (i.e. the first data point
% of that contour) through indxbg + C(2,indxbg). For example, if there were
% 59 points in the largest contour whose index was at column 7 then
% npts = C(2,7) = 59 and we take columns 8 (= 7 + 1) through 66 (= 7 + 59)
% --*inclusive* [66 - 8 + 1 = 59].
D = C(1:2,(indxbg + 1):(indxbg + npts));
```

```
% Figure out the max and min coordinates of a bounding rectangle for the
% contour.  The "ceiling" & "floor" operations give
xtop = ceil(max(D(1,:)));
xbot = floor(min(D(1,:)));
ytop = ceil(max(D(2,:)));
ybot = floor(min(D(2,:)));

% Make lines out of these to draw in the bounding rectangle.
xc = [xbot xtop xtop xbot xbot];
yc = [ytop ytop ybot ybot ytop];
hold on;
plot(xc,yc,'m'); % The 'm' makes the box magenta.
hold off; % This keeps the figure from "accumulating" after every loop.

% Now do two nested loops, "integrating" over the bounding rectangle. By
% "integrating", we mean the following. Test all pixels in the bounding
% rectangle to see if their values (matrix entries) are >= the lower bound.
% If no then disregard them. If yes, then:
% 1) Add their solid angle contributions up to get the total solid angle of
% the glare source.
% 2) Add up their luminance values along with the number of qualifying
% pixels (entries) in order to compute the average luminance of the source.
% 3) Add up the entries weighted by position in order to compute the
% centroid ("center of mass") coordinates of the luminance.
%
% Zero out the counters:
validpts = 0;
solang = 0;
totlum = 0;
centroid = [0 0];
%
% Begin loops. Note the ever present (row, col) vs. (x, y) problem. These
% ordered pairs are different when deciding standard coordinates vs matrix
% position. Rows increase downward and are the first coordinate in the
% pair. (Also they always start with 1--i.e. 1st row). The corresponding
% standard coordinate is y, but it is the second coordinate in its pair and
% increases upward. (Also it can start with zero but does not here.) A
% similar thing holds for x and column number. Here we are ok on direction
% of increase since the contour plot flips the ordinate scale automatically
% (hence the need for "flipud" to overlap images and contour *visually*).
% Also the center of the square matrix is what we reference (crosshairs)
% for our angle calculations and it is symmetrical relative to upper/lower.
% THE ONLY THING WE HAVE TO BE CAREFUL OF HERE IS THAT COL = X AND ROW = Y
% AND MATLAB (AND MOST MATRIX BOOKS) HAVE THE ENTRIES REFERED TO BY (ROW,
% COLUMN).
for col = xbot:xtop
    for row = ybot:ytop
        if W(row,col) > lb
            validpts = validpts + 1;
            totlum = totlum + W(row,col);
            centroid(1) = centroid(1) + row*W(row,col);
            centroid(2) = centroid(2) + col*W(row,col);
            % Solid angle calculation follows. Get corner coordinates of a
            % *single* pixel in standard form. Then use my m-file function
            % "SolidAngle".
            xl = col - 0.5 - 510.5; % xl is "x lesser".
```

```matlab
            xg = col + 0.5 - 510.5; % xg is "x greater".
            yl = 1021 - row - 0.5 - 510.5;
            yg = 1021 - row + 0.5 - 510.5;
            solang = solang + SolidAngle(xl,xg,yl,yg,1.4871271e+003);
        end
    end
end
% Do the computations for these quantities.
centroid = centroid/totlum; % "Center of Mass (Lum.)"
disp('Currently working on ');
fin
disp('The average luminance of the glare source is ');
avglum = totlum/validpts
disp('Number of points in glare source is ');
validpts
disp('Solid Angle is ');
solang


% METHOD FOR BACKGROUND LUMINANCE.  NOTE THIS HAS CHANGED FROM THE PREVIOUS
% INCARNATION!  The background luminance is now found from the average
% luminance in a rectangular box that basically encompasses the road ahead
% in the headlights. The size and location of the box is basically a
% judgement call.
lumsum = 0;
for i = 550:650
    for j = 475:650
        lumsum = lumsum + W(i,j);
    end
end
disp('The background luminance is ');
backlum = lumsum/(101*176)   % The divisor is (end row - start row + 1)*
                             % (end col. - start col. + 1).


% With photometric components in hand, write them to the file for each
% trial condition (i.e. run through the big double loop).  Given the
% centroid numbers the angle (eccentricity) can be computed using a
% crosshair center of (row = 510.5, col = 510.5).  This will be done
% outside of this program in Excel.

% Append results to output file.  Results will then be used in a
% multi-linear regression analysis to get GM (DeBoer Score)coefficients and
% hence GM (Glare Index) exponents.
fprintf(fid,'%s %d %.4e %.4e %.4e %.4f
%.4f\n',fin,validpts,avglum,solang,backlum,centroid(1),centroid(2));

% Clear *almost* all variables for the next round of the loop. NOTE THAT
% "KEEP" IS *NOT* A STANDARD MATLAB FUNCTION BUT AN M-FILE THAT SOME HELPFUL
% PERSON WROTE.
keep indir datout fid m n;



% END THE BIG DOUBLE LOOP. **********
    end
end
```

```
fclose('all');
```

Appendix I: Matlab Program for Discomfort Glare Analysis Method 2

```matlab
%{
%Process4
%}
home ; clc ; clear all ; close all ;
format compact
pause(.01)


%*******************************************************************************
******************
% Set Directories for Input and Output Files
%*******************************************************************************
******************
Dir           = 'D:\From Jays Computer\Headlight Glare\Jays Matlab Files\';
cd(Dir)
InputDir      = 'D:\Corrected_Glare_Data\Discomfort Glare\Discomfort
Scenes\Final Scene + LED\';
OutputDir     = 'D:\From Jays Computer\Headlight Glare\Jays Matlab
Files\Output_from_new_pgm\';
InputFileName = [strcat(InputDir,'H_X_Pos3_S3.txt') ;
                 strcat(InputDir,'H_Y_Pos3_S3.txt') ;
                 strcat(InputDir,'H_Z_Pos3_S3.txt')];
%*******************************************************************************
*************
% Initialize Parameters
%*******************************************************************************
*************
InitialPlots      = 0 ;
PlotFilterResult  = 0 ;
PlotFinalResult   = 1 ;
SaveWorkspace     = 1 ;
HPix              = 1020;
WPix              = 1020;
dW                = round(2*tan(.5*pi/180)/(6.72437e-4));     %~26;
dH                = dW;


MonCSF =
[0.7692;0.9155;0.9993;1.0000;0.9169;0.7713;0.5952;0.4212;0.2734;0.1626;0.0888
;0.0440];
RGCSF  =
[1.0000;0.9171;0.8114;0.6823;0.5341;0.3778;0.2315;0.1158;0.0435;0.0109;0.0015
;0.0001];
BYCSF  =
[1.0000;0.9185;0.8145;0.6872;0.5403;0.3846;0.2378;0.1205;0.0461;0.0118;0.0017
;0.0001];


FilterFreq = 2.^[-1:.5:4.5]    ; FreqEnd = length(FilterFreq) ;
ang        = pi/6.*[0:1:6]      ; AngEnd  = length(ang)          ;

% FilterFreq = 2.^[-1:1:1]        ; FreqEnd = length(FilterFreq) ;
% ang        = pi/2.*[0:1:2]      ; AngEnd  = length(ang)          ;



pool       = 4                 ; rho      = 3*sqrt(log(2))/pi  ;
Count      = 0                 ; dtsum    = 0                  ;
```

```
set(0,'units','inches')
ScreenSizeInch=get(0,'screensize');
set(0,'units','pixels')
ScreenSizePix=get(0,'screensize') ; SW=ScreenSizePix(3) ;
SH=ScreenSizePix(4);
PixperInch=ScreenSizePix(1,3:4)./ScreenSizeInch(1,3:4);


%**************************************************************************
*************
% Import Scene Data
%**************************************************************************
*************
InputFile       = fopen(InputFileName(1,:));
TristimX        = textscan(InputFile,'%f','headerlines',0);
TristimX        = cell2mat(TristimX);
fclose(InputFile);
TristimX        = reshape(TristimX,HPix,WPix);
TristimX        = TristimX';
Index           = find(TristimX<0);
TristimX(Index) = 0;

InputFile       = fopen(InputFileName(2,:));
TristimY        = textscan(InputFile,'%f','headerlines',0);
TristimY        = cell2mat(TristimY);
fclose(InputFile);
TristimY        = reshape(TristimY,HPix,WPix);
TristimY        = TristimY';
Index           = find(TristimY<0);
TristimY(Index) = 0;

InputFile       = fopen(InputFileName(3,:));
TristimZ        = textscan(InputFile,'%f','headerlines',0);
TristimZ        = cell2mat(TristimZ);
fclose(InputFile);
TristimZ        = reshape(TristimZ,HPix,WPix);
TristimZ        = TristimZ';
Index           = find(TristimZ<0);
TristimZ(Index) = 0;

R               =  3.240790 * TristimX -1.537150 * TristimY -0.498535 *
TristimZ;
G               = -0.969256 * TristimX +1.875992 * TristimY +0.041556 *
TristimZ;
B               =  0.055648 * TristimX -0.204043 * TristimY +1.057311 *
TristimZ;
Scene(:,:,1)    =  R;
Scene(:,:,2)    =  G;
Scene(:,:,3)    =  B;
Scene           = double(Scene);
Index           = find(Scene<0);
Scene(Index)    = 0;


%**************************************************************************
*************
% Create and Plot (If Desired) Black/White, Red/Green, and Blue/Yellow Sub-
Images
```

```
%*************************************************************************
*************
LumMatrix = TristimY;
MonMatrix = (Scene(:,:,1)+Scene(:,:,2)+Scene(:,:,3))/3.;
RGMatrix  =  Scene(:,:,1)-Scene(:,:,2);
BYMatrix  = (Scene(:,:,1)+Scene(:,:,2)-2*Scene(:,:,3));

if InitialPlots==1
  Status=PlotInitial(Scene,SH,SW,0,OutputDir);
end


%*************************************************************************
*************
% Create Filtered Sub-Images
%*************************************************************************
*************
Filter=1*dW;
FilterGridx=[round(-Filter/2):round(Filter/2)]'/round(Filter/2);
FilterGridy=FilterGridx;
[FilterX, FilterY] = meshgrid(FilterGridx,FilterGridy);

% HPix          = HPix-length(FilterGridx)+1
% WPix          = WPix-length(FilterGridy)+1  ;
LumPoolImage = zeros(HPix,WPix) ;
MonPoolImage = zeros(HPix,WPix) ;
RGPoolImage  = zeros(HPix,WPix) ;
BYPoolImage  = zeros(HPix,WPix) ;

disp(sprintf('Beginning First of %3i Convolutions at
%s',AngEnd*FreqEnd,datestr(now,14)));
for iang = 1:AngEnd
  Xrot =  FilterX*cos(ang(iang)) + FilterY*sin(ang(iang));
  Yrot = -FilterX*sin(ang(iang)) + FilterY*cos(ang(iang));
  for ifreq = 1:FreqEnd
    t0       = clock;
    Count    = Count+1;
    lambda   = rho/(FilterFreq(ifreq)/dW);
    Filter   = zeros(length(FilterGridy),length(FilterGridx));
    Filter   = exp(-(Xrot.^2 + Yrot.^2)/(lambda.^2));
    Filter   = Filter.*cos(2*pi*(FilterFreq(ifreq)/dW)*Xrot);
    Filter   = round(Filter);

    LumConvResult = conv2(LumMatrix,Filter,'same');
    MonConvResult = conv2(MonMatrix,Filter,'same');
    RGConvResult  = conv2( RGMatrix,Filter,'same');
    BYConvResult  = conv2( BYMatrix,Filter,'same');

    LumPoolImage  = LumPoolImage+MonCSF(ifreq)*(LumConvResult.^pool);
    MonPoolImage  = MonPoolImage+MonCSF(ifreq)*(MonConvResult.^pool);
    RGPoolImage   = RGPoolImage +RGCSF(ifreq) *(RGConvResult .^pool);
    BYPoolImage   = BYPoolImage +BYCSF(ifreq) *(BYConvResult .^pool);

    dt(Count)=etime(clock,t0);
    dtsum=dtsum+dt(Count);
    DT=dtsum/Count;
    ToGo=(AngEnd*FreqEnd-Count)*DT;
```

```
    Now=now;
    Line1=sprintf('Convolution %3i%3i: Iteration %3i of %3i; dt=%3i:%5.2f
min:sec;  ',...

iang,ifreq,Count,AngEnd*FreqEnd,floor(dt(Count)/60),rem(dt(Count),60));
    Line2=sprintf('DT=%3i:%5.2f; Completion in %3i:%5.2f or at %s',...
                  floor(DT/60),rem(DT,60),floor(ToGo/60),rem(ToGo,60),...
                  datestr(now+ToGo/(24*3600),14));
    disp([Line1 Line2]);
  end
end
disp(sprintf('Convolutions completed at %s',datestr(now,14)))


%******************************************************************************
*************
% Construct Final Pooled Images
%******************************************************************************
*************
LumFinalResult   = LumPoolImage.^(1/pool);
LumOverallAvgInt = sum(sum(LumFinalResult))/(WPix*HPix);
MonFinalResult   = MonPoolImage.^(1/pool);
MonOverallAvgInt = sum(sum(MonFinalResult))/(WPix*HPix);
RGFinalResult    = RGPoolImage.^(1/pool);
RGOverallAvgInt  = sum(sum(RGFinalResult))/(WPix*HPix);
BYFinalResult    = BYPoolImage.^(1/pool);
BYOverallAvgInt  = sum(sum(BYFinalResult))/(WPix*HPix);
RGBFinalResult   = (MonFinalResult+RGFinalResult+BYFinalResult)/3;


%******************************************************************************
*************
% Plot Filtered Sub-Images (If Desired)
%******************************************************************************
*************
if PlotFilterResult==1

Status=PlotFiltered(MonFinalResult,RGFinalResult,BYFinalResult,SH,SW,HPix,WPi
x,0,OutputDir);
end


%******************************************************************************
*************
% Locate Most Conspicuous Elements
%******************************************************************************
*************
disp(sprintf('Locating most conspicuous elements'))
for i=1:HPix
  for j=1:WPix
    LumCSR(i,j)  = LumFinalResult(i,j) / LumOverallAvgInt;
    MonCSR(i,j)  = MonFinalResult(i,j) / MonOverallAvgInt;
    RGCSR(i,j)   = RGFinalResult(i,j)  / RGOverallAvgInt;
    BYCSR(i,j)   = BYFinalResult(i,j)  / BYOverallAvgInt;
  end
end
OverallCSR       = (MonCSR+RGCSR+BYCSR)/3;
RGBResult        =  ConspicElements(5,OverallCSR,HPix,WPix);
RGBC             =  RGBResult{1};
RGBContours      =  RGBResult{2};
```

```matlab
RGBIndex          =  RGBResult{3};
LumResult         =  ConspicElements(5,LumCSR,HPix,WPix);
LumC              =  LumResult{1};
LumContours       =  LumResult{2};
LumIndex          =  LumResult{3};
YStimResult       =  ConspicElements(5,TristimY,HPix,WPix);
YStimC            =  YStimResult{1};
YStimContours     =  YStimResult{2};
YStimIndex        =  YStimResult{3};


%*****************************************************************************
*************
% Combine Most Conspicuous & Most Luminous Elements with a Logical AND
%*****************************************************************************
*************
disp(sprintf('Combining most conspicuous & most luminous elements'))
clear RGBLumIndex
RGBIndexSize      =  size(RGBIndex);
LumIndexSize      =  size(LumIndex);
for i=1:RGBIndexSize(2)
  k=0;
  for j=1:length(RGBIndex{i})
    for ii=1:LumIndexSize(2)
      for jj=1:length(LumIndex{ii})
        if RGBIndex{i}(j)==LumIndex{ii}(jj)
          k=k+1;
          RGBLumIndex{i}(k,1)=RGBIndex{i}(j);
        end
      end
    end
  end
end
for i=length(RGBLumIndex):-1:1
  if isempty(RGBLumIndex{i})
    RGBLumIndex(i)=[];
  end
end

RGBLum=zeros(HPix,WPix);
for i=1:length(RGBLumIndex)
  [Row{i},Col{i}]=ind2sub([HPix,WPix],RGBLumIndex{i});
  RGBLum(Row{i},Col{i})=LumFinalResult(Row{i},Col{i});
end


%*****************************************************************************
*************
% Compute Discomfort Glare Index
%*****************************************************************************
*************
disp(sprintf('Computing discomfort glare index'))
clear p Omega G
s     = 510/.342934;
Lu    = mean(mean(LumFinalResult));
Glare = zeros(length(RGBLumIndex),1);
HorDisFactor = [0 .5 1 1.5 2 2.5 3];
VerDisFactor = [0 .5 1 1.5 2];
P            = [1.    0.492 0.226 0.128 0.081 0.061 0.057;
```

```
                0.123 0.119 0.065 0.043 0.029 0.026 0.023;
                0.019 0.026 0.019 0.016 0.014 0.011 0.011;
                0.008 0.008 0.008 0.008 0.008 0.006 0.006;
                0.    0.    0.003 0.003 0.003 0.003 0.003];


for i = 1:length(RGBLumIndex)
  for j = 1:length(Row{i})
    a = Col{i}(j)-WPix/2+.5;
    b = a+1;
    c = Row{i}(j)-HPix/2+.5;;
    d = c+1;

    Num1 = (b/s)*(d/s);
    Num2 = (a/s)*(c/s);
    Num3 = (a/s)*(d/s);
    Num4 = (b/s)*(c/s);

    Den1 = sqrt((b/s)^2 + 1 + (d/s)^2);
    Den2 = sqrt((a/s)^2 + 1 + (c/s)^2);
    Den3 = sqrt((a/s)^2 + 1 + (d/s)^2);
    Den4 = sqrt((b/s)^2 + 1 + (c/s)^2);

    Omega{i}(j,1) =   atan2(Num1,Den1) + atan2(Num2,Den2) ...
                    - atan2(Num3,Den3) - atan2(Num4,Den4);
    XR            =   abs(a/s);
    YR            =   abs(b/s);
    if XR > HorDisFactor(end) || YR > VerDisFactor(end)
      p{i}(j,1) = 0;
    else
      p{i}(j,1) = interp2(HorDisFactor,VerDisFactor,P,XR,YR,'linear');
    end
    Glare(i,1)  = Glare(i,1) + (p{i}(j,1) *
LumFinalResult(Row{i}(j),Col{i}(j)))^1.6 * Omega{i}(j,1)^.8;
  end
  Glare(i,1)    = 2*Glare(i,1)/Lu;
  Result(i,1:3) = [mean(Row{i}) mean(Col{i}) Glare(i)];
end

Result=sortrows(Result,1);
for i=1:length(RGBLumIndex)
  disp(sprintf('Glare(%3.0f, %3.0f) =
%8.2f',mean(Row{i}),mean(Col{i}),Glare(i)));
end

if SaveWorkspace==1
  save (strcat(InputFileName(1,1:end-4),'.mat'),'Glare')  % Changed "-6" to
"-4". Kent 12/04/08
end

%**************************************************************************
*************
% Plot Final Result (If Desired)
%**************************************************************************
*************
if PlotFinalResult==1
```

```
Status=PlotFinal(Scene,RGBFinalResult,LumFinalResult,SH,SW,YStimC,YStimContou
rs,RGBC,...
                    RGBContours,LumC,LumContours,RGBLum);
end

% [Omega{1}(1:10) Omega{2}(1:10) Omega{3}(1:10) ]
% RGBLumIndex
% [RGBIndex{1}(1:10) RGBIndex{2}(1:10) RGBIndex{3}(1:10)]
% [LumIndex{1}(1:10) LumIndex{2}(1:10) LumIndex{3}(1:10)  LumIndex{4}(1:10)]
% [RGBLumIndex{1}(1:10) RGBLumIndex{2}(1:10) RGBLumIndex{3}(1:10)]
```

Appendix J: Position Factor for Discomfort Glare Analysis Method 2

ENERGYPLUS™

EnergyPlus
Engineering Reference

The Reference to EnergyPlus Calculations

(in case you want or need to know)

Date: April 23, 2005

Luminance of Shaded Window

The luminance of a shaded window is determined at the same time that the transmitted flux is calculated. It is given by

$$L_{sh} = \frac{1}{\pi} \int_{\theta_{min}}^{\theta_{max}} \int_{\pi/2-\phi_w}^{\pi/2} L(\theta,\phi) T(\beta) \cos\beta \cos\phi \, d\theta \, d\phi$$

Daylight Discomfort Glare

The discomfort glare at a reference point due to luminance contrast between a window and the interior surfaces surrounding the window is given by [Hopkinson, 1970] and [Hopkinson, 1972]:

$$G = \frac{L_w^{1.6} \Omega^{0.8}}{L_b + 0.07 \omega^{0.5} L_w}$$

where

G = discomfort glare constant

L_w = average luminance of the window as seen from the reference point

Ω = solid angle subtended by window, modified to take direction of occupant view into account

L_b = luminance of the background area surrounding the window

By dividing the window into N_x by N_y rectangular elements, as is done for calculating the direct component of interior illuminance, we have

$$L_w = \frac{\sum_{j=1}^{N_y} \sum_{i=1}^{N_x} L_w(i,j)}{N_x N_y}$$

where $L_w(i,j)$ is the luminance of element (i,j) as seen from the reference point.
Similarly,

$$\omega = \sum_{j=1}^{N_y} \sum_{i=1}^{N_x} d\omega(i,j)$$

where $d\omega(i,j)$ is the solid angle subtended by element (i,j) with respect to the reference point.

The modified solid angle is

$$\Omega = \sum_{j=1}^{N_y} \sum_{i=1}^{N_x} d\omega(i,j) p(x_R, y_R)$$

where p is a "position factor" [Petherbridge & Longmore, 1954] that accounts for the decrease in visual excitation as the luminous element moves away from the line of sight. This factor depends on the horizontal and vertical displacement ratios, x_R and y_R (Figure 53), given by

$$x_R(i,j) = \frac{\left| A^2 - (YD)^2 \right|^{1/2}}{RR}$$

$$y_R(i,j) = \left| YD / RR \right|$$

where

$$RR = D(\hat{R}_{ray} \cdot \hat{v}_{view})$$

$$A^2 = D^2 - (RR)^2$$

$$YD = R_{win}(3) - R_{ref}(3)$$
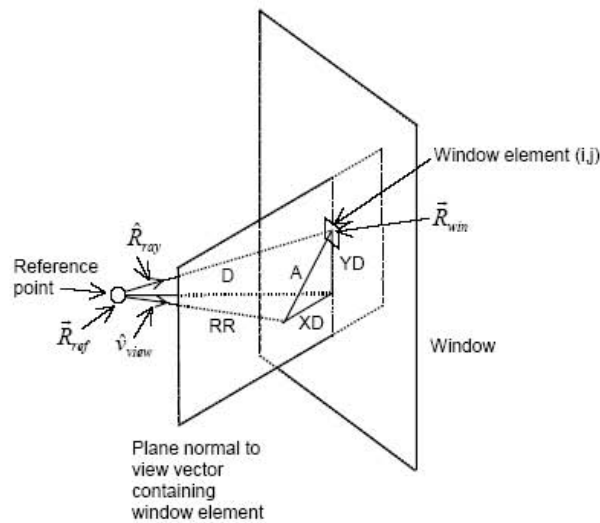
Figure 53. Geometry for calculation of displacement ratios used in the glare formula.

The factor p can be obtained from graphs given in [Petherbridge & Longmore, 1954] or it can be calculated from tabulated values of p_H, the Hopkinson position factor [Hopkinson, 1966], since $p = p_H^{1.25}$. The values resulting from the latter approach are given in Table 22. Interpolation of this table is used in EnergyPlus to evaluate p at intermediate values of x_R and y_R.

Table 22. Position factor for glare calculation

| | | x_R: Horizontal Displacement Factor | | | | | | | |
		0	0.5	1.0	1.5	2.0	2.5	3.0	>3.0
y_R: Vertical Displacement Factor	0	1.00	0.492	0.226	0.128	0.081	0.061	0.057	0
	0.5	0.123	0.119	0.065	0.043	0.029	0.026	0.023	0
	1.0	0.019	0.026	0.019	0.016	0.014	0.011	0.011	0
	1.5	0.008	0.008	0.008	0.008	0.008	0.006	0.006	0

	2.0	0	0	0.003	0.003	0.003	0.003	0.003	0
	>2.0	0	0	0	0	0	0	0	0

The background luminance is

$$L_b = E_b \rho_b$$

where ρ_b is approximated by the average interior surface reflectance of the entire room and

$$E_b = \max(E_r, E_s)$$

where E_r is the total internally-reflected component of daylight illuminance produced by all the windows in the room and E_s is the illuminance set point at the reference point at which glare is being calculated. A precise calculation of E_b is not required since the glare index (see next section) is logarithmic. A factor of two variation in E_b generally produces a change of only 0.5 to 1.0 in the glare index.

Glare Index

The net daylight glare at a reference point due to all of the windows in a room is expressed in terms of a *glare index* given by

$$G_I = 10 \log_{10} \sum_{i=1}^{\substack{\text{number of} \\ \text{windows}}} G_i$$

where G_i is the glare constant at the reference point due to the ith window

Time-Step Daylighting Calculation

Overview

A daylighting calculation is performed each time step that the sun is up for each zone that has one or two daylighting reference points specified. The exterior horizontal illuminance from the sun and sky is determined from solar irradiance data from the weather file. The interior illuminance at each reference point is found for each window by interpolating the daylight illuminance factors for the current sun position, then, for sky-related interior illuminance, multiplying by the exterior horizontal illuminance from the appropriate sky types that time step, and, for sun-related interior illuminance, multiplying by the exterior horizontal solar illuminance that time step. By summation, the net illuminance and glare due to all of the windows in a zone are found. If glare control has been specified window shading (by movable shading devices or switchable glazing) is deployed to reduce glare. Finally the illuminance at each reference point for the final window and shade configuration is used by the lighting control system simulation to determine the electric lighting power required to meet the illuminance set point at each reference point.

Table 23. Variables in Time-Step Calculations

Mathematical variable	Description	Units	FORTRAN variable
$S_{norm,dir}$	Direct normal solar irradiance	W/m^2	BeamSolarRad
$S_{h,dif}$	Exterior diffuse horizontal solar irradiance	W/m^2	SDIFH, DifSolarRad

Appendix K: Discomfort Glare Raw Data Tables

SCENE		scene 1 - photo 007								
POSITION		position 1 - outer			position 2 - middle			position 3 - inner		
INTENSITY		low	medium	high	low	medium	high	low	medium	high
Subject	Age (yrs)									
# 1	61	7.0	5.0	3.0	6.5	4.0	2.5	6.0	3.0	2.0
# 2	28	8.0	5.0	2.0	7.0	4.0	2.0	7.0	3.0	1.0
# 3	53	8.0	4.0	3.0	8.0	5.0	2.0	7.0	6.0	3.0
# 4	25	6.0	4.0	2.0	7.0	5.0	3.0	7.0	4.0	2.5
# 5	27	7.0	5.0	3.0	8.0	4.0	2.0	7.0	3.0	1.1
# 6	53	8.0	3.0	2.0	8.0	4.0	2.0	7.0	3.0	2.0
# 7	45	7.5	5.0	3.5	7.5	5.0	3.0	7.0	4.0	3.0
# 8	68	9.0	3.0	2.0	9.0	7.0	3.0	8.0	4.0	1.0
# 9	53	7.0	3.0	2.0	6.0	4.0	3.0	6.0	4.0	2.0
# 10	60	4.0	2.5	1.8	6.0	3.0	2.0	5.0	3.0	1.6
# 11	52	8.0	7.0	5.0	8.0	7.0	4.5	8.0	5.0	3.0
# 12	29	9.0	6.0	3.4	9.0	4.7	2.7	6.7	3.5	1.3
# 13	71	7.0	5.0	3.0	9.0	6.0	5.0	7.0	4.0	3.0
# 14	71	9.0	7.0	4.0	9.0	5.0	3.0	8.0	4.0	1.5
# 15	39	**This subject did not participate in *discomfort* glare experiments.**								
# 16	54	8.0	5.0	3.5	8.0	5.0	3.0	7.0	4.0	2.0
the average of the col.:		7.5	4.6	2.9	7.7	4.8	2.8	6.9	3.8	2.0
the standard dev. of the col.:		1.3	1.4	0.9	1.0	1.1	0.9	0.8	0.8	0.8

SCENE		scene 2 - photo 018								
POSITION		position 1 - outer			position 2 - middle			position 3 - inner		
INTENSITY		low	medium	high	low	medium	high	low	medium	high
Subject	Age (yrs)									
# 1	61	7.0	5.0	4.0	7.0	5.0	3.0	6.0	3.5	2.0
# 2	28	9.0	5.0	2.0	8.0	4.0	2.0	7.0	3.0	1.0
# 3	53	8.0	7.0	4.0	8.0	7.0	3.0	7.0	4.0	2.0
# 4	25	8.0	5.0	3.0	7.5	5.5	3.0	7.0	5.0	2.0
# 5	27	8.0	4.0	2.0	8.0	3.0	1.8	6.5	3.0	1.4
# 6	53	8.0	5.0	3.0	8.0	4.0	3.0	7.0	4.0	2.0
# 7	45	8.0	5.0	4.0	8.0	5.0	3.5	6.5	3.0	2.0
# 8	68	9.0	5.0	2.0	9.0	8.0	3.0	9.0	6.0	2.0
# 9	53	5.0	4.0	2.0	7.0	5.0	2.0	6.0	4.0	2.0
# 10	60	6.5	4.5	2.3	6.5	3.0	2.3	6.0	2.0	1.0
# 11	52	8.0	6.0	4.0	8.0	7.0	5.0	7.0	4.0	3.0
# 12	29	9.0	5.0	3.9	8.8	4.2	2.1	6.8	3.6	1.1
# 13	71	9.0	5.0	3.0	9.0	6.0	5.0	7.0	4.0	2.0
# 14	71	9.0	7.0	3.0	9.0	5.0	2.0	8.0	4.0	2.0
# 15	39	**This subject did not participate in *discomfort* glare experiments.**								
# 16	54	8.5	6.0	5.0	8.0	6.0	5.0	8.0	4.0	2.0
the average of the col.:		8.0	5.2	3.1	8.0	5.2	3.0	7.0	3.8	1.8
the standard dev. of the col.:		1.1	0.9	1.0	0.8	1.4	1.1	0.8	0.9	0.5

SCENE		scene 3 - photo 027								
POSITION		position 1 - outer			position 2 - middle			position 3 - inner		
INTENSITY		low	medium	high	low	medium	high	low	medium	high
Subject	Age (yrs)									
# 1	61	7.0	4.0	1.0	5.0	3.5	2.0	5.0	3.0	1.5
# 2	28	7.0	5.0	3.0	7.0	4.0	2.0	7.0	3.0	1.0
# 3	53	8.0	4.0	3.0	7.5	5.0	2.0	8.0	4.0	2.0
# 4	25	8.0	6.0	3.5	7.5	5.2	2.2	6.5	4.0	1.9
# 5	27	7.0	4.0	1.8	8.0	4.0	1.5	7.0	3.0	1.1
# 6	53	7.0	3.0	2.0	7.0	4.0	2.0	7.0	4.0	1.5
# 7	45	8.0	5.0	4.0	7.0	5.0	3.5	7.0	4.5	2.5
# 8	68	9.0	6.0	2.0	9.0	5.0	2.0	9.0	5.0	1.0
# 9	53	5.0	4.0	3.0	6.0	4.0	3.0	6.0	4.0	2.0
# 10	60	7.0	5.0	2.5	7.0	3.0	1.5	6.0	2.0	1.0
# 11	52	8.0	6.0	5.0	8.0	7.0	4.0	8.0	5.0	2.0
# 12	29	8.5	4.8	3.0	6.5	3.5	1.3	5.0	2.9	1.0
# 13	71	9.0	7.0	5.0	9.0	5.0	3.0	6.0	3.0	1.0
# 14	71	8.0	4.0	2.0	9.0	5.0	2.0	8.0	4.0	1.0
# 15	39	**This subject did not participate in *discomfort* glare experiments.**								
# 16	54	8.0	6.0	5.0	8.0	5.0	3.0	7.0	3.0	2.0
the average of the col.:		7.6	4.9	3.1	7.4	4.5	2.3	6.8	3.6	1.5
the standard dev. of the col.:		1.0	1.1	1.3	1.1	1.0	0.8	1.1	0.9	0.5

Appendix L: Glare Meter Tool – Condensed Instructions for Use

As noted in the body of this report, the Glare Meter Tool, while very successful at measuring glare, is not yet a robust instrument that is ready for field deployment. Too much time-consuming human intervention is required. Advent of a new generation of imaging photometers with increased dynamic range, and additional development work in software could likely alleviate this burden, but such work will require expertise in image-processing and pattern recognition.

Since the Glare Meter Tool is not at the "point and shoot and look at the dial" stage, we will not attempt to provide a completely detailed set of instructions. Rather, the steps listed below will broadly outline the algorithms and methods used and we refer the reader to appendices H and I for the specific computer programs we used.

Implementation:

- Using the Radiant Imaging digital imaging photometer, the roadway scene *without the glare source present* should be imaged. This means generating a luminance data file of the scene. Depending on the algorithm to be employed, tristimulus data files may also be needed. The center of the photometer's image (crosshairs) should be focused on where a driver will be looking in that situation (e.g. directly down the road on a straight highway).
- Without moving the photometer (ideally it should be mounted on a tripod or steady base) perform the same operation as was just done but now with the (static) glare source present. One must take care to set the exposure so as to avoid saturation of the CCD image sensor. Ideally, one image would preserve both the details of the scene and the intense glare source, but dynamic range limitations of the photometer prevent this, and thus two separate exposures are required. As a result, only static scenes can be analyzed.
- Combine the two images from the previous steps, and isolate the glare sources; what this means is that all scatter from the luminance image of the glare source (owing to the imperfect optics of the instrument itself) should be removed to the extent practicable. This is where further software development would really matter. Humans can look at a representation (false color image) of a luminance image and easily differentiate the glare sources from scatter in the photometer optics (most of the time anyway). It is much harder to program a computer to perform this task.
- Use the photometer data to get the background luminance. This will be necessary for both *discomfort* <u>and</u> *disability* glare measurements. Just what area is used for the background luminance can be a little subjective (see the body of the report for details). It is usually an area on the roadway directly in front of the driver's vehicle.
- For *discomfort* calculations use a computer program that implements the Glare Index of equation (12) (Method 1) or the Baer Glare Index (Method 2, equation (14)). These are similar in nature and both require the calculation of glare luminance, glare centroids (hence angle or position) and solid angle, in addition to the background luminance found in the previous step. Doing these calculations requires the software to "identify" or delineate the glare source. This is essentially an exercise in pattern recognition and could perhaps be done at the same time as glare source isolation if that step becomes automated. The software needn't be tied to any particular language. Our

- implementations used MATLAB. These are shown in appendix H (Method 1) and appendix I (Method 2).

- With a Glare Index in hand (which may combine the effects of multiple sources), one simply divides it by the necessary constant (Method 1—see equation (12); Method 2— see equation (14) and Table 6). One then takes the common logarithm (base 10) of that result and multiplies by the negative of the exponential scale factor (4 for Method 1; 2.67 for Method 2). This yields the Glare Mark (*GM*), otherwise known as the De Boer number.

- For *disability* glare calculations one needs to implement equation (6) from the disability section. This requires as an input the luminance image file of the glare source(s) *after* the sources have been isolated as described above. It also requires an input of the age of the observer/driver. The age or range of ages used would depend on the particular scenario and would have to be assessed beforehand by traffic authorities (i.e. does one plan on an average driving age or an older age where disability glare can be worse than for younger drivers?).

- In addition, transportation authorities or traffic engineers would have to specify the contrast thresholds or threshold luminance needed for certain situations and what constant "c" (contrast threshold constant) and constant "k" (proportionality constant) would be used in the calculation (see the section on disability glare in this report for details). With these specified, the veiling luminance (equation (7)) and threshold luminance (equation (9)) could be calculated from the results of the previous step and the background luminance.

These steps comprise the essence of the algorithms to compute both disability and discomfort glare. The reader can see that disability glare measurement doesn't give a simple "score" like discomfort glare, and involves more work for roadway engineers, but it is generally thought to have greater importance for traffic safety.

One potential pitfall that was not mentioned in the main body of this report is "undetected saturation", an unfortunate characteristic of our particular instrument. Our Radiant Imaging PR-1613F-2 video photometer with its *ProMetric* operational software warns the user when the image is saturating, but only some of the time. If the luminance "image" is *heavily* saturated then the software invariably gives a warning, and the bitmap image of the luminance shows obvious "blooming" or "bleeding" of the pixels. The data from such a run is then discarded.

However, if the luminance image is only *slightly* saturated, then *a software warning does not inevitably follow,* and the accompanying bitmap image *may not show "blooming".* Thus the operator of the photometer may not realize that saturation has, in fact, occurred. This happened to the VDL staff during this set of experiments, and was discovered as a result of certain repeat measurements that were made with different neutral density settings and exposure time settings. The result was a different measured value for the LED luminance under exactly the same conditions. Obviously this should not occur. If this were to happen during measurements of glare sources, then a consequence would be underestimated glare luminances and inflated De Boer numbers. We do not know if this "undetected saturation" is idiosyncratic to our particular instrument. Therefore, with any model of photometer, the operator should carefully run tests to gain familiarity with the instrument so that he can avoid this phenomenon.